uOttawa

L'Université canadienne
Canada's university

FACULTÉ DES ÉTUDES SUPÉRIEURES ET POSTOCTORALES

uOttawa

L'Université canadienne
Canada's university

FACULTY OF GRADUATE AND POSDOCTORAL STUDIES

Andrea Michelle Ramsay
AUTEUR DE LA THÈSE / AUTHOR OF THESIS

M.A.Sc. (Civil Engineering)
GRADE / DEGREE

Engineering
FACULTÉ, ÉCOLE, DÉPARTEMENT / FACULTY, SCHOOL, DEPARTMENT

The Impact of Climate Change on the Flood Frequency Distributions: A Case Study of the Kemptville Creek Watershed

TITRE DE LA THÈSE / TITLE OF THESIS

Ioan Nistor
DIRECTEUR (DIRECTRICE) DE LA THÈSE / THESIS SUPERVISOR

Ousmane Seidou
CO-DIRECTEUR (CO-DIRECTRICE) DE LA THÈSE / THESIS CO-SUPERVISOR

Paul Simms

Colin Rennie

Majid Mohammadian

Gary W. Slater
Le Doyen de la Faculté des études supérieures et postdoctorales / Dean of the Faculty of Graduate and Postdoctoral Studies

THE IMPACT OF CLIMATE CHANGE ON FLOOD FREQUENCY DISTRIBUTIONS: A CASE STUDY OF THE KEMPTVILLE CREEK WATERSHED

by

Andrea Ramsay

A thesis

submitted under the supervision of

Dr. Ioan Nistor

Dr. Ousmane Seidou

In fulfillment of the

requirements for the degree of

Master of Applied Science

in

Civil Engineering

uOttawa

Department of Civil Engineering

University of Ottawa

Ottawa, Canada

K1N 6N5

Your file Votre référence
ISBN: 978-0-494-79675-7
Our file Notre référence
ISBN: 978-0-494-79675-7

ABSTRACT

Distributions of future extreme hydrologic events represent a major concern in the context of climate change and its potential impacts. The accurate inference of their probability distribution for a given period (present or future) is crucial for the safe and economic design of a range of engineering works, from hydraulic structures such as dam spillways and bridges, to flow routing infrastructure such as culverts, stormwater ponds and channels.

These distributions are likely to evolve with climate change and the development of methods to estimate possible impacts on extreme event distributions has become a key area of study. In this study the impact of climate change on flood frequency distributions is ascertained through a combination of physical modeling and statistical analysis. This approach utilizes two of the most valuable tools in the field; general circulation models (GCMs) and non-stationary extreme value analysis, and seeks to capitalize on the strengths of established methods while limiting the number of unnecessary assumptions.

ACKNOWLEDGEMENTS

I would like to express my gratitude to Dr. Ousmane Seidou and Dr. Ioan Nistor for their generous support and guidance over the course my studies. They have been a tremendous resource for me and their dedication to the field has been inspiring.

I also wish to acknowledge the Rideau Valley Conservation Authority (RVCA) for the significant work they undertake in monitoring and modeling the regional watersheds. They generously provided us with a copy of their calibrated HEC-RAS model for use in this project.

Finally I would like to acknowledge all of the support I have received from my friends and family throughout the course of compiling this thesis. Much of my ability to complete this work has been a direct result of their kind contributions.

TABLE OF CONTENTS

List of Figures

LIST OF TABLES

LIST OF SYMBOLS

μ	location parameter
α	scale parameter
κ	The shape parameter
GEV	Generalized Extreme Value distribution
FGEV	GEV cumulative distribution function
D	Days
QD	highest average stream flow observed within a varying set number of days
t	time (in years)
a, b, c, d	constants
d	data
Mk	model being compared
Mr	model being used as a reference
Bkr	normalized Bayes Factor
T-year	return periods for project
L	design lives of a given number of years
N	length of the MCMC run
Y	vector of observed data
O_t	daily precipitation occurrence,
R_t	precipitation amounts
p_{ij}	predictors

θ	empirical coefficient
β	model parameters
e_t	modeling error
z_t	normally distributed random number
n	number of predictors
S_e	standard error of estimate
b	model bias
T_t	daily temperature (maximum, minimum or mean)
γ	model parameter.
E	Nash-Sutcliffe model efficiency coefficient
R2	regression correlation coefficient
Tmax	maximum temperature
Tmin	minimum temperature
Tc	time of concentration
CN	SCS curve number

1 INTRODUCTION

Flood quantiles are defined in hydrology as high and low flows with a given probability of occurrence. Their probability distributions represent the main input of hydraulic structure design. Particularly for the case of high flows, the underestimation of their magnitude can result in unsafe structures with potentially catastrophic consequences, while their overestimation can unnecessarily drive up the cost of these structures. For these reasons there is a lot of interest in estimating how global warming may affect low and high flow distributions. While several methods have been proposed in the hydrological literature to estimate how these distributions may be altered under various global warming scenarios, all of these methods suffer from conceptual difficulties. Most of them rely on General Circulation Models (GCM) and Regional Circulation Models (RCM) to generate daily grid-averaged climate variables which are later downscaled (i.e transformed from grid scale to station scale) to the station level. While it is well recognized that GCMs and RCMs combined with statistical downscaling approaches are able to satisfactorily reproduce mean climate values (Gachon, et al. 2007), their ability to reproduce extreme events are not as satisfactory (Haylock, et al. 2006, Schmidli, et al. 2007). Non-stationary models have recently been proposed to account for a linear or a quadratic trend in some the parameters of extreme distributions (El Adlouni, et al. 2007, Leclerc and Ouarda 2007). The drawback of these approaches is that while the hypothesis of a linear or quadratic trend may hold for the near future, it is unrealistic for long-term projections as variables with increasing trends will increase to unreasonably high values and variables with decreasing trends will hit zero after some time.

This study proposes a combined approach to estimate the impact of climate change on flood quantiles. It avoids direct use of daily simulated flows as it is well known that they are biased. The simulated flows are averaged on the timescale where they are more reliable, and the distribution of the maximum daily flow is described by a non-stationary distribution where the parameters are linked to aggregated simulated flows. Global warming induced changes in the averaged river flow are then estimated by forcing a rainfall-runoff model with downscaled GCM outputs. Once future averaged flows are obtained, the parameters of future peak flows

distributions can be estimated, and T-year floods calculated. Future extreme flow events are then routed using a hydraulic river model to identify the impact on water levels and floodplain extent. The results are then used to determine what impact climate change has on the risk associated with the safe functioning of various hydraulic structures as well as the future inundation levels of buildings located within the watersheds floodplain.

1.1 Significance of the Study

Gauging the influence of climate change on peak flow distributions is an important and complicated issue which in past studies has been approached in many ways. Knowledge of peak flows is necessary in many applications, including the design and operation of hydraulic structures and the delineation of regulatory floodplains. The current practice is to describe peak flows with stationary flood frequency distributions. The frequency distributions used to design hydraulic structures are calibrated by regulatory bodies and engineering consultants based on data observed over the past several decades. An important assumption of stationary frequency analysis is that the data are trend free. Trends in observed flow, however, are becoming more and more reported in hydro-climatic literature, suggesting that future flow values may stray from the past observed patterns. Therefore, existing probability distributions will become invalid, risky, or suboptimal to use. This is not just an issue for structures being built in the future. Existing hydraulic structures which were designed with an assumed stationary risk of failure based on the exceedance probability of the selected design flow will also be impacted as the risk associated with a given peak flow event may very well fluctuate in the future. In order to quantify how these risks will evolve, regional climate change impact assessment studies are required.

The novel aspects of this study come from how the non-stationarity induced climate change will be incorporated into the extreme value analysis of future peak flow events. In order to achieve this we require the use of four elements commonly used in climatology and flow modeling:

- GCM data, downscaled to improve regional variability
- A hydrologic rainfall-runoff model capable of assessing a watersheds response to climate forcing

- A non-stationary probability distribution capable of describing maximum daily flows given a time-averaged simulated flow.
- A hydraulic flood routing model.

While many studies have been conducted utilizing one or more of these elements at the same time, the use of all these methods in conjunction has yet to be examined.

1.2 Study Objectives

The purpose of the current study is to assess how climate change will impact flood frequency distributions within the Kemptville Creek. This approach involves the use of several deterministic physically based models in conjunction with a probabilistic extreme value probability distribution. These hydrologic and hydraulic models will be used to define the processes and operation of watershed itself along with the watercourse through which the peak flows will be routed. The main objectives of this study are as follows;

1. to determine how best to capture the non-stationarity that climate change imposes on flood frequency distributions
2. to determine how to best utilize existing techniques to reduce modeling error and assumptions required on the part of the modeller,
3. to improve the reliability and reproducibility of climate change predictions, and
4. to analyze what impacts climate change may have on a local watershed and, eventually, its infrastructure.

1.3 Scope of the Study

The current study deals with catchment level assessments as to impacts of climate change as defined by climate models on peak flow distributions. As conditions can vary from catchment to catchment, the results of this study should only be considered valid for the watershed in which it was conducted. This study uses the data obtained from the following sources:

- Coupled General Circulation Model 3.1 (CGCM3.1) run with the Special Report on Emission Scenarios (SRES) Scenario A2 results, spanning from 1970 to 2100
- National Centre for Environmental Prediction (NCEP) reanalysis data
- Flow data obtained through hydrometric data (HYDAT) for the Kemptville Creek gauging station
- Environment Canada climate station data obtained through Canadian Daily Climate Data (CDCD) for the Kemptville area
- U.S. Geological Survey (USGS) Global Land Cover Characterization database
- Soil Properties map produced by the Food and Agricultural Organization (FAO) Land and Water Digital Media Series
- NASA Shuttle Radar Topographic Mission (SRTM) 90 meter resolution survey mapping

1.4 Organization of Dissertation

The present thesis has been organized into six main sections. This first section introduces the topic of this study, provides justification, and outlines the key objectives. The second section covers a review of the current state of climate change and climate change modeling. It also includes a review of the four key elements of this study as well as background information on the programs/functions selected to model these elements including how they have been applied elsewhere in the area of climate change impact studies. The third section outlines the proposed methodology of this study. It highlights the novelty of our approach as well as describing in detail how each of the elements has been dealt with. The fourth section discusses the application of our proposed methodology to the selected study area and covers the set up and calibration of the various models used in the study. The fifth section details the results of the study. The sixth section highlights the implication of the results as well as assesses if the study objectives have been met. The seventh and eighth section will conclude the study and recommend future areas for further research.

2 LITERATURE REVIEW

2.1 Introduction

Water is a fundamental part of life on Earth. It is relied upon around the world everyday for drinking, agriculture, basic sanitation, power generation, transportation, and recreation. Its importance extends beyond human life to the endless wildlife and entire ecosystems which is dependent on it. It is one of the most important natural resources we have and the power that it can wield from the destructive force of flood waters to the devastating force of drought is almost unmatched. Stewardship of this resource is key to ensuring that potential risks be mitigated and that the resource is preserved for future generations. This literature review will provide insight as to the current and possible future state of extreme flows (both low and high) and what impacts could result if current trends remain unchanged.

2.2 Climate Change

According to the 4th Climate Change Assessment Synthesis Report published in 2007 by Intergovernmental Panel on Climate Change (IPCC), climate change is driven by alterations to the global energy balance. These alterations are caused by changes to atmospheric concentrations of greenhouse gases, GHGs (namely carbon dioxide (CO_2), methane (CH_4), nitrous oxide (N_2O), halocarbons), and aerosols, land cover, and solar radiation. Since 1750 the concentration of GHGs has been increasing and this is believed to be caused by the use of fossil fuels and agricultural by-products. It has been estimated using a linear trend that between 1906 and 2005 the global Earth surface temperature increased by approximately 0.74°C. The IPCC has concluded that it is very likely that the observed warming over the last 50 years has been due to the increase of anthropogenic GHGs.

Not all regions will react to a change in climate the same way, however. For example mean annual precipitation has increased over last century in regions located between 30°N and 85°N but decreases have been observed in the past few decades in regions located between 10°N and 30°N. And yet at the same time increases in vapour pressure caused by the warming effect have possibly led to heavier individual precipitation events even in regions where the total

precipitation has decreased. Clearly the issue of the assessing the impacts of climate change is a complex one, both in terms of trying to quantifying the possible risks and impacts as well attempting to identifying the best ways to mitigate these risks.

2.3 Impacts of Climate Change

Though there is truly a wide variety of methods for estimating the possible impacts of climate change together with a wide variety of results, there appears to be a general consensus formed about certain impacts which most climate models seem to agree upon. As this study will mainly focus on the impacts of climate change on stream flow and extreme flood events, the following sections provide a summary of the current consensus on the possible impacts of climate change on these events.

2.3.1 Global Impact of Climate Change on River Flow

It is widely believed that as the climate gets warmer, the frequency of flood and drought events will increase (IPCC: Kundzewicz, et al. 2007b). Examining the direct impact of climate change on river flow can be challenging as it can be difficult to extract significant trends in the data (Kundzewicz et al. 2005, Barredo 2009, Merz 2010). This may be caused by a variety of factors, including difficulty in reproducing catchment scale processes and often more significantly, by the limitations imposed due to the lack of data or even the quality of observed data used in the analysis. The quality of the data can be impacted by the collection method, length of collection time, and by human impact on the flow measurement regime itself. Significant changes in precipitation can be easier to detect, and similarly the changes in runoff rates. Figure 1 presents the estimated change in runoff for the period of 2090-2099 relative to the period of 1980-1999. In this figure, compiled by the IPCC (IPCC, Contribution of Working Groups I, II and III to the Fourth Assessment Report of the Intergovernmental Panel on Climate Change 2007a) based on the results of 12 climate models using the SRES A1B scenario, the hatched areas represent results of 90% agreement between the 12 models examined as to the sign of the change. The white areas represent where fewer than 66% of the models agreed on the sign of the change. We can see from this figure that runoff rates in the Northern Hemisphere, especially northern Canada and northern Russia, are expected to increase from 20% to 40+%. Regions surrounding the

Mediterranean Ocean conversely are expected to become increasingly arid with runoff rates decreasing by 10% to 40+%.

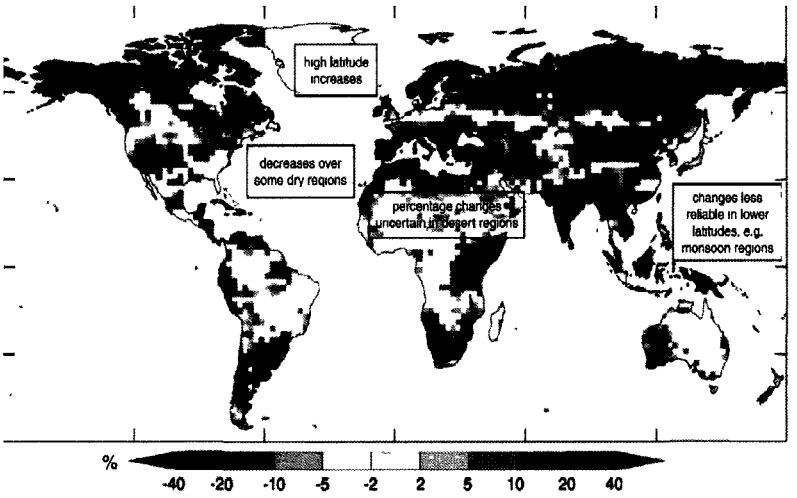

Figure 1: Change in global runoff trends by 2100, (IPCC 2007a)

However even with an expected trend in runoff rates established, with so many potential factors affecting the relationship between runoff volume and extreme flow events a direct correlation cannot be drawn from these results as to the future potential for increasing peak flows in various regions. For this level of analysis regional studies need to be conducted.

2.3.2 *Regional Impacts*

It is believed with very high confidence that climate change will have a significant impact on North America due to the numerous demands already placed on water resources (IPCC 2008). Some of the changes currently anticipated for North America under a changing climate (IPCC 2008, Kling 2003, IJC 2006) include:

- lower duration and extent of snow cover,
- widespread thawing of permafrost,
- increased frequency of heavy precipitation,
- increased water temperature in lakes by 0.1 – 1.5 C, and
- decreased storage levels in the Great Lakes.

In Canada, increases in precipitation of up 20% in the summer and 30% in the winter have been projected based on the A1B climate changes scenario established by IPCC (IPCC, Contribution of

Working Groups I, II and III to the Fourth Assessment Report of the Intergovernmental Panel on Climate Change 2007a). Projections also indicate that even larger changes will be observed in precipitation extremes. Coupled with this is the fact that the general warming trend will also very likely lead to an earlier snow melt, leading to earlier spring peak flow events and lower summer flows in some regions.

In 2007, NRCAN released their key findings on the potential impacts of climate change on the province of Ontario. Some of these key findings have been summarized below (NRCAN: Lemmen 2007).

2.3.2.1 Impact on water resources

Due to anticipated decreases in water levels throughout the Great Lakes, water shortages are expected through the southern areas of the province. Increased peak flood events could also lead to greater risks of ice jams and flooding.

2.3.2.2 Impact on health

A warmer climate can adversely impact health through means such as prolonged heat waves, smog conditions, and outbreaks of water-borne diseases due to increased bouts of extreme precipitation. It is estimated that deaths due to heat related causes could double by 2050 and deaths due to air quality could increase by 15 – 20%.

2.3.2.3 Impact on Infrastructure

Beyond the direct impact to hydraulic structures that could result due to increased peak flow events, impacts on water treatments plants, delivery systems, and transportation systems such as canals and locks can also be anticipated.

2.3.2.4 Impact on ecosystems

Wetlands and other sensitive ecosystems can be dramatically impacted by shifts in temperature and precipitation. Not only can the sustainably of these areas be impacted but their effectiveness in terms of pollutant removal can also be reduced. Changes in fish species, variance in aquatic

life, and the health of arctic animals residing around the Hudson Bay area such as polar bears and seals are also anticipated to be impacted.

The Great Lakes and St. Lawrence Basin regions have been the focus on many climate change studies due to the large population that are reliant upon them for water supply and industry (IJC 2006, GCRIO 2002, Kling 2003). As seen in Figure 2, the frequency of heavy rainfall events within the Great Lakes Region is expected to almost double over the next 100 years, with even the more conservative future emission scenarios predicting increases in rate of occurrence of for these heavy rainfall events.

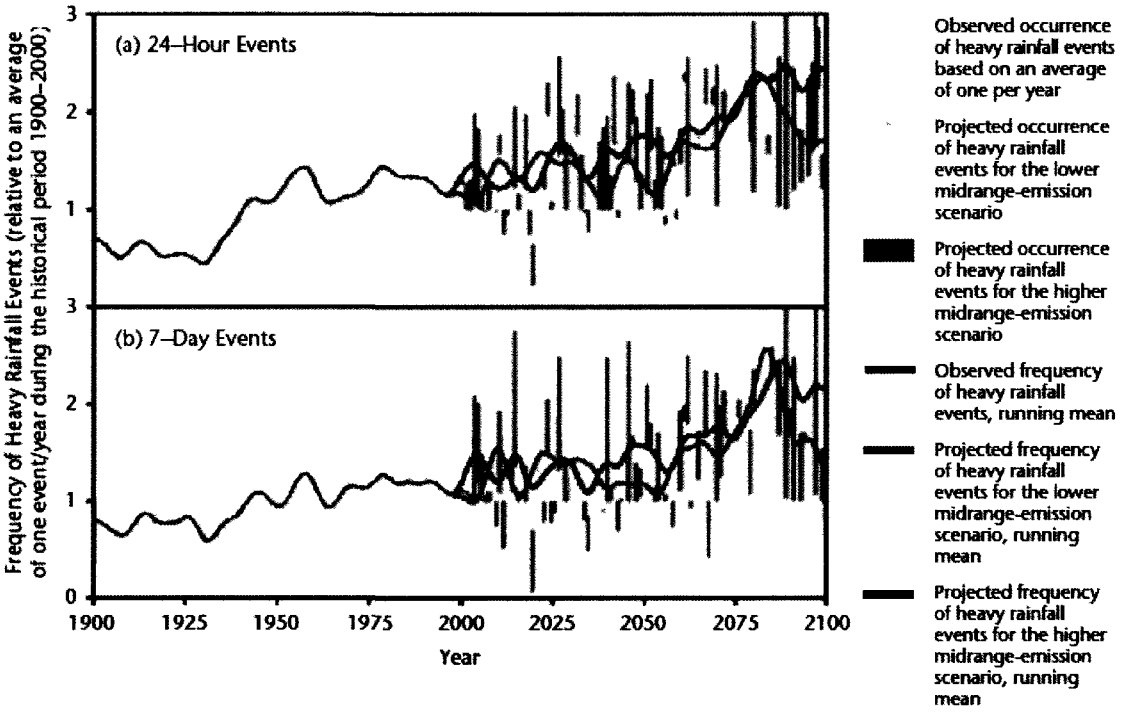

Figure 2: Future Trends in Heavy Rainfall Events in the Great Lakes Region, Kling 2003, from Wuebbles and Hayhoe 2003

Many assessments for the region have projected that lower mean water levels in lakes and other bodies of water are likely towards the end of the century due to decreased supply (Kling 2003, IJC 2006). This reduction in water level could lead to large economic losses for the region, particularly be means of reduced hydropower generating capacity in the range of $437-660 million/yr (Ouranos 2004).

2.4 Climate Change Modeling

A shift in climate, whether as a result of natural climatic cycles or as a result of external forcing, can have a major impact on the balance of the hydrologic cycle. There are many ways in which studies have attempted to estimate if and how the climate is changing and to what extent it may change in the future and what impacts it may have on stream flows. Sharif et al, 2010, attempted to link extreme flow events to large scale climate indices. Thodson 2006 and Somura 2009 used rainfall-runoff models together with RCM outputs to assess the watershed's response to climate change scenarios. Crisci et al 2002 applied precipitation trends detected in observed data to a GEV probability distribution to assess the trend in extreme rainfall events. These methods have examined a wide range of possible future scenarios and models and they all include an inherent amount of uncertainty. Many studies examining a change in climate from a physically based perspective start their analysis from results of large scale climate models used to assess the impact of different future scenarios on global climate called general circulation models, or GCMs.

2.4.1 General Circulation Models

GCMs are complex multi-component models that generate daily or sub-daily grid-averaged climate variables over the surface of the earth. These models are generally developed and maintained by government agencies within various countries. The CGM developed in Canada is the CGCM3.1, the third generation coupled global climate model produced by Environment Canada through the Canadian Centre for Climate Modelling and Analysis (CCCma). This updated model includes improved process for modeling the coupled (atmospheric and ocean) interaction. The T63 version of the model has a spatial resolution of roughly 2.8 degrees latitude/longitude and has 31 vertical levels. While developed in Canada it has been used in many climate change studies and remains a popular GCM worldwide (IPCC 2007a, GCRIO 2002).

2.4.1.1 Climate change scenarios

GCMs are run with various climate change emission scenarios which make projections as to how GHGs might respond to certain social, economical, and environmental trends in the future. A

popular family of scenarios are those proposed by the Intergovernmental Panel on Climate Change in the Special Report on Emission Scenarios (SRES) in 2000 (IPCC 2000). They proposed four climate change storylines for analysis, each resulting from a different potential future. These scenarios are characterized as follows:

A1 This scenario examines a rapid economic growth with its main focus on material production. Here global populations are peaking mid-century to around 9 billion and then slowly declining. Rapid migration is observed towards more efficient technologies, and the entire global community is acting together to address climate change. In recent years this option has been expanded to included options where fossil fuels are still used prevalently in society (A1FI), one where greener fuels are used (A1T), and a third where both fuels are used (A1B).

A2 This scenario examines a slow growing economy, an ever increasing population, and a splintered regional approach to addressing climate change.

B1 As in A1, this scenario family examines a rapid economic growth, population peaking mid-century to around 9 billion and then slowly declining. However in this scenario it is assumed that the economy will center less on material production and more on service and information technology and therefore will be more ecologically centered then A1.

B2 This scenario family examines intermediate economic development, an ever increasing population, and a regional approach towards sustainability.

These story lines correspond to GHG emissions as illustrated in Figure 3. The grey area in this figure represents the 80th percentile interval of scenarios published since the release of the initial SRES scenarios.

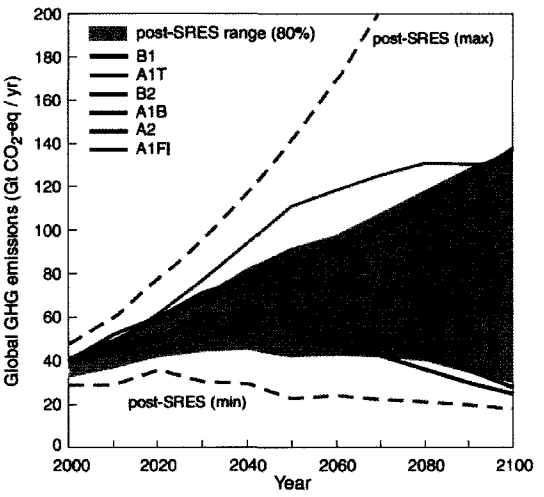

Figure 3: Future Implications of SRES Emission Scenarios, (IPCC 2007a)

The impacts of these emission scenarios have been analysed using a range of climate models and the resulting changes in temperature and sea level rise under each scenario has been determined, as presented in Figure 4. Here we see that is likely that the A1FI scenario in which the economy is driven by materials manufacturing and fossil fuels are still prevalent will result in the greatest temperature and sea level increase, followed by the A2 scenario. The B1 scenario will likely result in the smallest rise.

Case	Temperature change (°C at 2090-2099 relative to 1980-1999)[1]		Sea level rise (m at 2090-2099 relative to 1980-1999)
	Best estimate	*Likely* range	Model-based range excluding future rapid dynamical changes in ice flow
Constant year 2000 concentrations[2]	0.6	0.3 – 0.9	Not available
B1 scenario	1.8	1.1 – 2.9	0.18 – 0.38
A1T scenario	2.4	1.4 – 3.8	0.20 – 0.45
B2 scenario	2.4	1.4 – 3.8	0.20 – 0.43
A1B scenario	2.8	1.7 – 4.4	0.21 – 0.48
A2 scenario	3.4	2.0 – 5.4	0.23 – 0.51
A1FI scenario	4.0	2.4 – 6.4	0.26 – 0.59

Figure 4: Potential Changes Resulting from SRES Scenarios from IPCC 2007a

2.4.1.2 Reanalysis

In 1996 the National Centre for Environmental Prediction (NCEP) and the National Center for Atmospheric Research (NCAR) collaborated on a project to provide 40 years (1957-1996) of "reanalysis" on observed data from various atmospheric variables generally used in climate modeling. Effectively they wanted to use a frozen forecasting model to assimilate 40 years of

observed global data with a global Climate Data Assimilation System (CDAS), the outputs of which they could later use to calibrate GCM outputs. The model would then be used to assimilate future observations as they became available. The data were obtained from various sources (ships, satellites, aircraft, etc.) at a range locations and altitudes (Kalnay et al. 1996; Kistler et al. 2001)

In 1997 it was suggested that as regional data assimilation systems (RDAS) would be better then global CDAS as they could better capture regional variabilities that was often not captured by GCMs. In 2004 NCEP released the North American Regional Reanalysis (NARR) Regional Climate Data Assimilation systems (R-CDAS) model to the research community. The NARR model operates at a 32 km / 45 layer resolution and presently covers the time period for 1979 to present day. This regional model is able to produce higher quality assessment of land hydrology and land-atmosphere interaction. The boundary conditions for the NARR model are currently provided by NCEP/DOE Global Reanalysis as outlined in Kanamistu, et al. 2002. The NARR model is also able to better address precipitation variability then a global climate data reanalysis model, which makes it a much more attractive model for flood frequency modeling (Mesinger, at al. 2006, Masoud, et al. 2007)

2.5 Downscaling

Due to the coarse scale inherent with GCM output, new techniques needed to be developed to apply their results to specific geographic locations (IPCC 2007b). The practice of relating these large scale generated climate variables to smaller and more useful scales is known as downscaling. The downscaling of global climate data allows for the influences of small scale locally observed trends and variability which is usually not captured in large scale models. Currently there is a wide range approaches taken to downscale climate data from quick and simple methods such the change factor method to more complex methods such as statistical downscaling or dynamic downscaling. Each of these approaches has its own drawbacks and benefits and are usually better suited to one application over another. While these downscaling methods can be fairly simple to implement, the innate flaw in these methods is that they operate

under the assumption that whatever empirical relationships are found between the global and local climate will remain valid in the future when in reality there is no way to verify this.

Wilby and Wigley (1997) established the four basic groups of statistical downscaling techniques: regression analysis, weather patterning, stochastic weather generators, and limited area climate models. Statistical downscaling is the process of relating certain global predictor variables to local predictant variables. Wilby, et al. (2004) compared the strength and weaknesses of the three main statistical downscaling techniques. This comparison is presented in Table 1.

Table 1 Comparison of statistical downscaling methods, (Wilby 2004)

Method	Strengths	Weaknesses
Weather typing (e.g. analogue method, hybrid approaches, fuzzy classification, self orfanizing maps, Monte Carlo methods).	• Yields physically interpretable linkages to surface climate • Versatile (e.g., can be applied to surface climate, air quality, flooding, erosion, etc.) • Compositing for analysis of extreme events	• Required additional task of weather classification • Circulation-based schemes can be insensitive to future climate forcing • May not capture intra-type variations in surface climate
Weather generators (e.g. Markov chains, stochastic models, spell length methods, storm arrival times, mixture modelling).	• Production of large ensembles for uncertainty analysis or long simulations for extremes • Spatial interpolation of model parameters using landscaping • Can generate sub-daily information	• Arbitrary adjustment of parameters for future climate • Unanticipated effects to secondary variables of changing precipitation parameters
Regression methods (e.g. linear regression, neural networks, canonical correlation analysis, kriging).	• Relatively straightforward to apply • Employs full range of available predictor variables • 'Off-the-shelf' solutions and software available	• Poor representation of observed variance • May assume linearity and/or normality of data • Poor representation of extreme events

For this study the regression based downscaling tool ASD was selected to downscale climate data due mainly to its ease of use and reliability. The core weakness of regression based

techniques stated in Wilby et al. 2004, namely that the method has a poor ability to reproduce observed variance or extreme events, will be addressed in this study though the application of a local rainfall-runoff model.

The results generated from different downscaling approaches can differ dramatically and as such results of downscaled GCM data may be subject to a great deal of error. It is important to correctly gage the local climate factors and properly assess how these factors relate to the GCM output. Even with this, the results of any downscaling approach should be scrutinized and used with caution.

2.5.1 ASD

ASD (Automated Statistical Downscaling) is a weather generator/regression based stochastic downscaling tool developed through collaboration between the Canadian Research Chair on the Estimation of Hydrometerological Variables, Pr. T. Ouarda, and the Adaptation and Impacts Research Division of Environment Canada, led by Dr. Philippe Gachon. It was developed and operates within the MATLAB environment and use the same equations as the popular SDSM (Statistical Downscaling Model) tool as presented in the Wilby 2002 paper.

ASD works by evaluating the relationships between the locally observed rainfall and temperature data and the outputs of GCMs and reanalysis data. For the downscaling of precipitation data, ASD first conditionally models the occurrence of rainfall events and then models the amount of rainfall that occurred, if any. (Hessami et al. 2007) Temperature is modeled under an unconditional relationship. Both rainfall and temperature are modeled deterministically and include a factor for model error which is assumed to follow a Gaussian distribution in the model.

Hessami et al. (2007) compared the ASD and SDSM models using the CGCM1 and HadCM3 CGM data with NCEP reanalysis data at 10 meteorological stations in eastern Canada. The study found that overall based on the root mean square error (RMSE)of the two methods, the ASD results were generally superior to the SDSM results in the majority of climatic and statistical indices that were examined. The study also found that neither model outperformed the other in the downscaling of precipitation. The study ultimately concluded that neither model was able to

perform well in every month or season and that the results can be subject to a large degree of uncertainty.

2.6 Rainfall-Runoff Models

In order to generate the future flow sequence to be applied to the probability distribution, a rainfall-runoff model will be used with the downscaled future climate. Rainfall-runoff models can be physically or statistically based and are usually parameterized and calibrated for a specific site. For this study the Soil and Water Assessment Tool (SWAT) was used to transform the climate data to daily stream flow data.

2.6.1 SWAT

SWAT is a watershed modeling tool that was developed in part to provide a reliable standardized method for which to conduct studies involving watershed management processes. The model is a continuous physically based model which can be run over long periods of time. While SWAT has many advantages, it has been found that like many rainfall-runoff models it performs poorly in reproducing extreme events. The reason for this is mainly due to the fact that these models are calibrated using mean flows and the nature of the parameters which define the model make it difficult for it to predict peak flows accurately. It is therefore not recommended to apply a flood frequency analysis directly to the results of a SWAT model.

SWAT was originally developed as a water quality and land management assessment tool but it has now been developed to a point where it can be used for a wide range of hydrologic modeling applications. In the literature one can find many examples of where SWAT has been used in climate change impacts assessments. Zhang, et al. (2007) used SWAT to analyse the impact of climate change on the Luohe River Basin. There, global climate data from A2 and B2 SRES scenarios were downscaled using the Kriging statistical downscaling method. The study concluded that by 2050 the mean stream flow would be approximately 10% greater in the spring and summer than at present. Similarly Githui, et al. 2008 used SWAT to analyse the impacts of climate change in western Kenya and Franczyk, et al. 2009 used the program to assess the impact of climate change and urbanization on changes in mean runoff depth in the Portland

metropolitan area in Oregon. Jha, et al. 2006 utilized a SWAT model combined with 6 difference GCMs to assess the regional sensitivity to climate change in the upper Mississippi River basin.

Some caution needs to be exercised when using rainfall-runoff models to predict a watershed reaction to climate change. Subcatchments can be affected by other by-products of climate change aside from just changes in temperature and precipitation. For example as CO_2 concentrations rise, vegetation will become increasingly dense and this could lead to increases in evapotranspiration rates (IPCC 2007b) that would not be reflected in the future rainfall-runoff model. Essentially, the potential inaccuracy of the approach is similar to that which would be seen in any transfer function applied to future time series; it can't be guaranteed that the watershed's current response to climatic forcing will hold in the future.

2.7 Extreme Event Distribution

The development of frequency analysis of extreme events has been motivated by the need to design systems (e.g. dams, flood protection systems, water supply system) able to safely handle the peak flow events while being economically viable. Due to the lack of knowledge about all of the generating mechanisms, extreme events are usually not well reproduced in physical models and are thus usually addressed using statistical methods.

The probability of occurrence of an event with a given magnitude is described by a probability density function, $f(x;\boldsymbol{\theta})$, where x is the magnitude of the event and is $\boldsymbol{\theta}$ the vector of parameters defining the distribution. Some common extreme value distributions are the Pearson type III, Log Pearson type III, log Normal, Gumbel, and Generalized Extreme Values (GEV) distributions. The GEV distribution is particularly popular due to its flexibility that allows it describe the typical distributions for a large array of hydrological variables.

The time scale of observed data used to calibrate the extreme value distribution can also be varied. Most studies choose to calibrate the parameters of a distribution from maximum or mean daily variables taken on a monthly or yearly scale, but others have examined the impacts of varying the time scale window. In Feng, et al. 2007, different time scales such as the 2-day and 10-day annual maximum precipitation were evaluated in order to attempt to best capture the impact of larger extreme events that extend beyond a single calendar day. Other studies (Ferro

and Porto 1999; Fowler and Kilsby 2003) have similarly explored the use of varying time scales. Comparing the impact of the varying time windows might help improve the fit of the distribution as it allows for more flexibility and may help to provide better correlation between mean flow and precipitation.

2.7.1 *Stationary extreme events distributions*

Traditional extreme event models assume that climate is stationary (i.e. $\boldsymbol{\theta}$ does not change with time). This assumption is the basis of a large body of literature and as well almost all established regulatory design storm calculations. Many studies highlighting the shortfalls of these models have been published (Leadbetter, et al., 1983; Douglas, et al., 2000). There are several reasons for $\boldsymbol{\theta}$ to change with time, such as changes in the response of a watershed to precipitation. These changes can be the result of land use changes like deforestation and urbanisation or even just the gradual erosion or deposition of certain classes of soil. While the use of stationary distributions may no longer be justified, these models are still used because; a) they are recommended by engineering design codes and they are the ones that practitioners are more familiar with, b) they are easier to use and understand, and c) currently there is no standard method to include climate change in the design process.

2.7.2 *Non-stationary extreme events distributions*

Non-stationary distributions are ones that allow the parameter vector to change over the length of the period analyzed. In most cases, the vector varies as a function of time and an assumption is made as to the form of this function takes with time (i.e. linear, quadratic, step-change, etc.). While it has been shown that these types of models are able to produce more accurate results than those obtained from stationary models, a great deal of uncertainty remains as how to capture best the relationship between the changing climate and meteorological events.

2.7.2.1 Bayesian Modeling

In 2000, Perreault et al attempted to develop a Bayesian model that could analyse a sudden change in the sequence of energy inflows at an unknown point in time. This method allowed for non-stationary trends to be incorporated through a single change in the mean and a single change in the variance of normal random variables. In their study several models were

examined and then weighted based on the likelihood of the model. However as Renard, et al. (2006) points out, the method proposed by Perreault cannot be applied directly to extreme values analysis because his study had assumed normality in the data. Thus Renard, et al. attempted to develop a Bayesian framework that could be applied to extreme events based on comparison models.

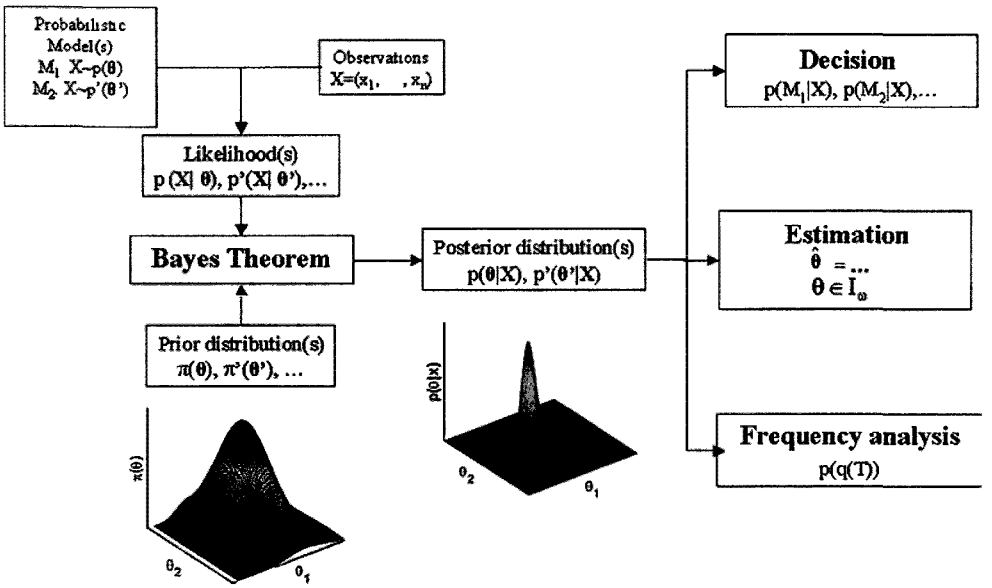

Figure 5: Application of Bayesian Theorem to Extreme Distributions (Source Renard, et al. 2006)

Their study examined a variety of probability density functions, including the GEV distribution, as well as a range of methods for parameter estimation including a stationary model as well as step-change and linear trend models to attempt to account for non-stationarity. The study used Bayes factors to compare the likelihood of the models examined and found that in general the non-stationary models performed better then the stationary ones. Bayes factors are powerful Bayeian tools for comparing two competing models. They provide a weighted comparison of the likelihood of each model given observed data. The study also noted that this proposed framework, as detailed in Figure 5, could be extended to other models with additional change possibilities, including the use of polynomials or covariables.

2.7.3 *Climate change and extreme events*

While the exact relationship between the climate change and peak flow in rivers remains largely uncertain, it has been demonstrated that should changes in climate arise, precipitation, snow

melt, and peak river flows distributions will be impacted (Marshall et al., 2008, IPCC 2007a, NRCAN 2007). Because of this, more reliable methods are needed to assess the risk that climate change to hydraulic structures and zones in watersheds which may be subject to flooding.

2.8 Flood Routing Models

Flood routing models are traditionally used to analyse the hydraulic characteristics of a waterway under a given flow event. They can be used to generate floodplain mapping, asses the flow profile along the length of a channel, and analys) the impacts of hydraulic structures on the flow regime. One of the most commonly used hydraulic routing software packages is HEC-RAS.

2.8.1 HEC-RAS

The HEC-RAS (Hydrologic Engineering Center's River Analysis System) software package is a one dimensional physically based river modeling tool developed by the U.S. Army Corps of Engineers.

While HEC-RAS has not been used as prominently for the specific application of analysing the impacts of future peak flow resulting from climate change, it has been regularly used in the past for dam breach studies and other flood frequency analysis applications (Gee and Brunner, 2005). Harvey and Mussetter, 2005, used HEC-RAS to attempt to determine if assumed relationships actually hold between bank full discharge, flood frequency, and effective discharge to sediment transport in rivers across the arid Southwestern US. They found that assumed relationships in fact do not hold and that site specific analysis is required. While these types of site specific studies can be laborious, they could be especially useful in the future as flow regimes change and such existing models could be used to assess the associated impacts

In 2007 the HEC-GeoRAS version of the software package was released which allows the user to extract channel cross-sections from Digital Elevation Models (DEMs) in a GIS interface and then allows the results of individual HEC-RAS runs to be export of back into the interface to be plotted along the DEM. This feature can be especially useful when dealing with multiple scenarios at once, such as was the case in the Benito, et al. (2003) study in which historical flood stages within the Tagus Basin in Central Spain were compared against computed water surface

profiles to analyse past flooding regimes. The study found that towards the end of the century flooding extremes were being caused by climate variations independently of the mechanisms producing the flood.

2.9 Impact of Climate Change on Hydraulic Structures

Assessing the impact of climate change on hydraulic structure is ultimately one of the main reasons for assessing the impact on future flood frequencies. The risk of failure associated with these structures has long been assumed to be constant, but as the frequency of extreme events is capable of varying in a changing climate, so too is the frequency of structural failure. Beyond the potential increased risk of failure, the operational characteristic of many of these hydraulic structures will ultimately change as well. Hydroelectric power generation potential, the allowable range of flow depth required to permit navigational though locks and waterways, flow depths and velocities over spillways all could be impacted by climate change. Previous studies analysing the impacts of climate change on hydraulic structures have produced mixed results.

In Graham, et al. 2007, the impact of climate change on the hydrology in Northern Europe was assessed. The ultimate goal of the study was to assess the impacts of the changing hydrologic cycle on hydroelectric generating potential in Northern Sweden. An ensemble of 15 climate change predictions were examined and it was concluded that the hydroelectric generating potential in the Lule River Basin could increase by 34% over current conditions.

In 2007, Sik, et al. and Kang, et al. conducted two studies examining the impacts of climate change on Yongdam Dam in Korea. The two studies utilized different sets of climate and precipitation models and the results of these models proved to be quite different. The studies used different GCMs with different scenarios, with the Sik, et al. study using a model created within the region and the Kang, et al. study using a more well known GCM. The emissions scenario used in both studies, however, dealt with the assumption of CO_2 concentrations doubling in the future. The results of the Sik, et al. study indicated that under a climate change scenario the annual rainfall in the area would decrease and that under a changing climate the region will experience longer periods of wet weather. Also while mean low flows will increase,

wet and normal flows will decrease. The Kang, et al. study found, however, that mean flow increased almost 40% and the maximum flow increased almost 125% from the time period of 1984-1993 to the period of 2010-2019. The study then concluded that as a result, the Yongdam Dam will become more vulnerable in the future. These studies are an example of the wide variance that can exist in climate change modeling.

In a 2009 publication by the Ouranos Consortium (Vescovi, et al.), the potential impacts of climate change on the dams in Quebec are examined. The publication highlights studies conducted at the Université du Québec's École de Technologie Supérieure (ETS) which suggested that spring floods will occur earlier and that the overall flood volumes will likely decrease in the future. It also points to a study conducted for the Ottawa River based on the results of four GCMs which suggests that the flows in the Ottawa River will decrease by 1% to 8% in the future. Decreases in mean flow however can still lead to a range of troublesome issues such as lower water quality and reductions in shipping capabilities in the Saint Lawrence Seaway.

Mareuill, et al. 2007 examined the possible impacts of climate change on the severity of floods in the Chateauguay River basin in Quebec. The study compared three GCMs and used a delta change approach to transform the temperature and precipitation along with a stochastic weather generator calibrated based on observed data. Using the climate change scenario B2, the study found that the results of two of the GCMs indicated a peak flow reduction in at least one season while the third model was not able to detect a statistically significant change of any kind. This model again highlights the large range of uncertainty that is inherent in climate change modeling.

While this is not the main focus of this study, it is worth mentioning that while climate change has the possibility to make a large impact on functioning of water resource systems, other factors such as population growth or land development may play as large of a role or larger depending on the location. Chang, et al. (2007) looked to assess the vulnerability of the Korean water resources system to both changes in climate and population. The study compared historical water use data with historical and projected future population data and variables such as

population, land cover, gross regional product for various city and provinces. The study found that the impacts of population growth outpaced the anticipated impacts of climate change.

3 METHODOLOGY

The method proposed in this study seeks to capitalize on the strengths of established methods while limiting the number of unnecessary assumptions that are required. Since GCMs tend to be more reliable when their outputs are averaged over a period longer than a day, the time averaged (over a D-days length period to be optimized) simulated flow are used to set the trend in the parameters of a non-stationary distribution. The method developed here takes advantages of the robustness of GCM outputs on larger time scales and the flexibility of non-stationary frequency analysis, while eliminating the need to set an arbitrary equation for the trend. The proposed method is applied in six steps:

(1) Daily outputs of the third generation Canadian Climate Model (scenario SRES A2) are downloaded from Environment Canada's website, and downscaled using ASD (Automated Downscaling Method) to produce one hundred equiprobable climate data sets of the present period, which are used to force the calibrated rainfall-runoff model (SWAT) and to further produce one hundred scenarios of daily flows.

(2) The Soil and Water Assessment Tool (SWAT) rainfall-runoff model is calibrated and validated based on observed data obtained for the Kemptville watershed.

(3) The daily flow scenarios are averaged and used to calculate annual maximum D-days flow for D=1 day to 20 days.

(4) For each value of D, the resulting time series of annual maximum D-days flow are utilized to calibrate a non-stationary probability distribution of maximum observed flows using simulated flows for the current period; the best value of D is selected using Bayes factors.

(5) The peak flows are routed through a hydraulic flood routing model (HEC-RAS) to determine what impacts they have on water levels and floodplain extent.

This process which includes a combination of physical modeling and statistical analysis has been summarized in Figure 6.

Figure 6: Methodology Outline

The most novel aspect of the study is the approach taken to incorporate the non-stationary trend of climate change into the prediction of future flood frequency distributions. Previous studies have examined the use of co-variants in climate change modeling (Wang, et al. 2004; Sankarasubramanian, et al. 2003) and have found this approach to produce superior results. This approach follows the one outlined in El Adlouni et al. (2008) in which the parameters incorporating the co-variant are estimated using Markcov Chain Monte Carlo (MCMC) approach.

3.1 Non-stationary GEV model

The GEV distribution is used in this study to examine the flood frequency of the maximum flow values. The cumulative distribution function of the GEV is defined in equation (1).

$$
\begin{aligned}
F_{GEV}(x) &= \exp\left[-\left(1-\frac{\kappa}{\alpha}(x-\mu)\right)^{1/\kappa}\right] && \kappa \neq 0 \\
x &= \left(1-\left(-\ln(F_{GEV}(x))\right)^{k}\right)\frac{\alpha}{\kappa}+\mu && \\
F_{GEV}(x) &= \exp\left[-\exp\left(-\frac{(x-\mu)}{\alpha}\right)\right] && \kappa = 0
\end{aligned}
\qquad (1)
$$

Usually the GEV distribution assumes the data to be independent, identically distributed, and thus stationary (Leclerc 2007). This study will examine the case outlined in El Adlouni, et al. (2007), where the location parameter, μ, and the scale parameter, α, are non-stationary (see equation (2)). The shape parameter, κ, is assumed to be stationary (Renard 2006, El Aldouni, et al. 2007).

$$F_{GEV}(x) = \exp\left[-\left(1-\frac{\kappa}{\alpha(X)}\left(x-\mu(X)\right)\right)^{1/\kappa}\right] \quad (2)$$

Where $x=\left(1-\left(-\ln(F_{GEV}(x))\right)^{k}\right)\frac{\alpha(X)}{\kappa}+\mu(X)$ and X is an external variable that modulates the parameters of the GEV distribution, i.e. mean flow, and k is a constant.

3.1.1 Parameter estimation

Several methods have been proposed in El Adlouni et al. (2007) to estimate the parameters of the non-stationary GEV model; the maximum likelihood (ML), the generalized maximum likelihood method (GML), and the Monte Carlo Markov Chain (MCMC) method. MCMC is a Bayesian statistical method able to sample the posterior probability distributions of the parameters of a given model and can be used instead of analytical methods when the formulas are too complex to be useful. In Bayesian statistics, the posterior distribution of a given quantity is the belief about its value inferred from observed data and prior knowledge. MCMC was preferred in this work because it can handle complex models and because the ML and GML require complex theoretical developments and suffers from some limitations related to the optimisation of a complex likelihood function over a changing support. The Metropolis-Hasting algorithm will be applied to construct the Markov Chain and the Geweke test was used to gauge the convergence of the MCMC.

3.1.1.1 Selection of the time window for calculation of the maximum D-day average flow

A certain time window will be used to average GCM output to make them more reliable. In order to account for peak flow events that extend beyond a single calendar day, the highest annual average stream flow observed within a varying set number of days, referred to as Q_D, will be used to modulate the parameters of the GEV distribution. When D is equal to 1, Q_D is the daily peak flow. Averaging is required because peak flows are usually poorly reproduced by rainfall-runoff models (i.e simulated Q_D has a better correlation to the observed peak flows than the daily simulated peak). One reason for that is the fact that these model are calibrated based on mean squared error, and to GCM outputs, as these models are generated on such coarse scales that local variability is not well captured. The concept of maximum D-days average flow is

illustrated below in Figure 7.

The specific number of days, D, within the time scale window will be optimized to generate parameters which maximize the likelihood of the GEV function. Extending the time window beyond a single day is anticipated to enable a better correlation between simulated flow and observed peak flows time series.

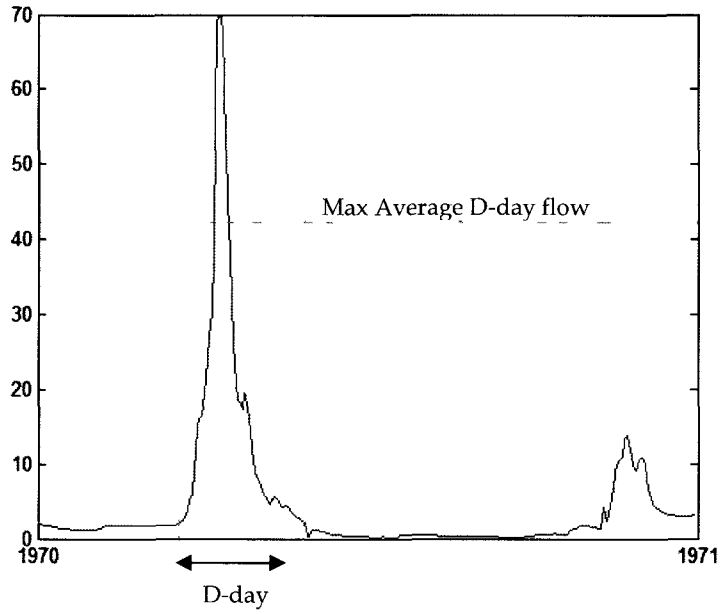

Figure 7: Definition of the maximum average D-days average flow

To facilitate comparison between the proposed models with varying time scale windows and more conventional approaches, 64 models were analyzed. These models, as listed in Table 2, include the proposed approach where one or more of the parameters varies with Q_D and more traditional approaches where one or both of the parameters vary linearly with time and a stationary model.

Table 2: Model Characteristics

Model description		Parameters equations
Stationary GEV model		$\mu(t)=a\,;\ \alpha(t)=c$
Only the scale parameter varying with time		$\mu(t)=a\,;\alpha(t)=c+d\times t$
Only the location parameter varying with time		$\mu(t)=a+b\times t\,;\alpha(t)=c$
The scale parameter and the location parameters vary with time		$\mu(t)=a+b\times t\,;\alpha(t)=c+d\times t$
Repeat for D=1 to D=20	Only the scale parameter varying with Q_D	$\mu(t)=a\,;\alpha(t)=c+d\times Q_D(t)$
	Only the location parameter varying with Q_D	$\mu(t)=a+b\times Q_D(t)\,;\alpha(t)=c$
	The scale parameter and the location parameters vary with Q_D	$\mu(t)=a+b\times Q_D(t)\,;$ $\alpha(t)=c+d\times Q_D(t)$

In the above table t represents the time (in years), and *a, b, c,* and *d* are constants.

3.1.1.2 Determination of the optimal value of D

Two types of climate data can be used to force the rainfall-runoff model for the current period: observation from climate stations, or downscaled outputs of GCMs for the current periods. Depending on whether observed climate data or downscaled climate is used, the value of D will change. The type of climate data used to calculate D and calibrate the non-stationary distribution has to be consistent in all applications.

When comparing the proposed model with more traditional models (stationary frequency analysis), the optimal value of D will be determined by calibrating the GEV distribution based on simulated flow data forced by observed climatic data for the period of 1970-2004. This approach has been applied to show that the proposed non-stationary model outperforms stationary peak flow models.

When climate change is the focus of the study, we have to keep in mind that only downscaled data are available beyond today. Therefore, the optimal value of D will be determined by calibrating the GEV distribution based on simulated flow data forced by downscaled GCM

outputs for the period of 1970-2004. The downscaled GCM outputs, however, produce 100 possible climate change scenarios. Therefore the results of the downscaled GCM outputs could be applied in one of three ways: 1) using the mean of the D-day flows calculated for each scenario, 2) using the median of the D-day flows calculated for each scenario, and 3) using the D-day flows calculated from the average of all the scenarios. The third option was found to provide distributions that best describe observed data and was therefore chosen. Through this method the future non-stationary GEV probability distributions can be established.

3.1.1.3 Model selection procedure

The normalized Bayes Factor, B_{kr} as presented in Min & Hense (2006), compares the posterior log likelihood of the data, d, of a given model, M_k, to that of another reference model, M_r. This relationship is described in equation (3).

$$B_{kr} = \frac{l(\mathbf{d}|M_k)}{l(\mathbf{d}|M_r)} \tag{3}$$

Bayes factors are an appealing way to compare competing models, but calculating $l(\mathbf{d}|M_k)$ can be quite difficult and in fact methods for its calculation are the subject of intense research in applied statistics. In this paper we chose to use one of the simplest methods of calculating Bayes factors from MCMC runs; using the harmonic mean of the posterior distribution n as proposed by Newton and Raftery (1994), defined in equation (4).

$$l(d|M_k) = \frac{1}{N}\left(\sum_{m=1}^{N}\frac{1}{f(Y|\theta_m)}\right) \tag{4}$$

Where N is the length of the MCMC run, $\mathbf{Y}$ is the vector of observed data, $\{\boldsymbol{\theta}_m, m = 1,..,N\}$ is the series of parameters vectors generated by the MCMC run.

The following scale presented in Table 3 is used to interpret the value of a Bayes factor B_{kr}.

Table 3: Interpretation of Bayes Factor

Bayes Factor	Interpretation
$B_{kr} < 1/10$	Strong evidence for M_r
$1/10 \le B_{kr} < 1/3$	Moderate evidence for M_r
$1/3 \le B_{kr} < 1$	Weak evidence for M_r
$1 \le B_{kr} < 3$	Weak evidence for M_k
$3 \le B_{kr} < 10$	Moderate evidence for M_k
$B_{kr} \ge 10$	Strong evidence for M_k

For our analysis, model M_k is considered to be the best if $B_{kr} \ge 1$.

Once the variation method of the parameters is optimized and the best model is selected it will then used to analyse flood events of various T-year return periods for project with design lives of a given number of years, L. These results are then compared to the results of the stationary model for the same given characteristics.

3.2 Downscaling of Climate Data

Due to the coarse scale of CGM outputs, they are not suitable for direct application to catchment scale hydrologic studies (Wilby, et al. 2002b) and they are not able to capture local inter-annual variability. In order to make use of the data obtained from the GCM output, the data will be transformed via the statistical downscaling tool ASD. ASD uses multiple linear regression (MLR) to relate CGM outputs to local climate variables. ASD works by first automatically determining which GCM parameters best define the relationship between the observed data and

the GCM outputs through the use of either stepwise regression or partial correlation. In this study ASD will be used to downscale both precipitation and temperature using stepwise regression.

The downscaling of precipitation data is carried out in two steps; first the probability of occurrence of an event is gauged and then conditionally on that occurrence the intensity of that event is assessed (see equation (5)).

$$O_t = \alpha_0 + \sum_{j=1}^{n} \alpha_j p_{ij}, R_t^{0.25} = \beta_0 + \sum_{j=1}^{n} \beta_j p_{ij} + e_t \tag{5}$$

Where O_t is the daily precipitation occurrence, n is number of predictors, R_t are daily precipitation amounts, p_{ij} are predictors, α and β are model parameters and e_t is the modeling error. Here the modeling error term is estimated using a Gaussian distribution:

$$e_t = \sqrt{\frac{VIF}{12}} z_t S_e + b \tag{6}$$

Where z_t is a normally distributed random number, S_e is the standard error of estimate, b *is* the model bias (0 when NCEP reanalysis data is used to calibrate ASD) and VIF is the variance inflation factor (12 when NCEP reanalysis data is used to calibrate ASD).

The downscaling of temperature data is carried out in single step as it is an unconditional parameter (see equation 7)).

$$T_t = \gamma_0 + \sum_{j=0}^{n} \gamma_t p_{ij} + e_t \tag{7}$$

Where T_t is the daily temperature (maximum, minimum or mean) and γ is the model parameter.

Once calibrated, the ASD equations can be used to generate a model space to sample from. This model space can generate endless possible time series of future data. More information on the operation of ASD can be found in (Hessami et al., 2008).

3.2.1 *Alterations made to ASD model*

The initial results of the ASD model proved to be unsuitable for this analysis. It was found that the results were well outside the range of expected values as well as physically unrealistic. For example the results would include maximum temperature values lower than minimum temperature values on the same day. It was decided therefore that attempts would be made to try to improve the downscaling algorithm. The alterations, as detailed in Seidou et al, 2010, are as follows:

3.2.1.1 Temperature downscaling

Originally ASD produced the minimum and maximum temperature series independent of each other and due to the random nature of z_i component in equation 6, the two series were completely uncorrelated. This was revised so that these two data series were generated simultaneously and a cross correlation was maintained between the two series.

3.2.1.2 Precipitation occurrence

The multiple linear regression algorithm used to decide the occurrence of rainfall was replaced with a classification and regression trees (CART) model. The model incorporates multiple explanatory variables to improve the results of the occurrence prediction.

3.2.1.3 Precipitation intensity

As seen in equation 5, ASD originally takes the fourth root of the rainfall amount, R_i, in an attempt to normalize the precipitation data. In this study the R_i variable will be normalized through the application of a Generalized Pareto probability distribution as it was found to best fit the monthly intensities when compared to other probability distributions. The results of the application of the Generalized Pareto distribution to monthly flow data are presented in Appendix D.

3.3 Rainfall-Runoff Modeling

In order to generate the future mean flow data series, the rainfall- runoff model SWAT was chosen. SWAT was developed by a team headed by Dr. Jeff Arnold of the US Department of Agriculture. It is a physically based continuous model that can be used with even limited information to analyse flow, sediment transport, and pollutant dispersal, and other hydrologic phenomena. Physical models are developed by linking together various process equations. These models are becoming increasingly popular in hydrologic modeling due to their versatility and applicability to many areas. They are also preferable over black box models such as ANN, especially in a catchment scale analysis such as the present one, because they produce results that are known to be physically possible. Also physical models can be used to analyse data sets beyond the bounds of the data used to calibrated them, which make them particularly attractive in a climate change modeling scenarios where one would likely expect to require the capability to analyse values beyond which have been observed at the site in the past.

For this study ArcSWAT Version 2009.93.4, a version of SWAT2009 operating through a GIS interface, was used. The program was operated through the ArcGIS 2009 software package. There are many benefits to using a GIS based model. Once a DEM of the study area is loaded into the program and an outlet point is selected (corresponding to either a gauging station or the outlet of the watershed), the software automatically analyses the terrain and delineated the contributing watershed and sub-catchments. Separate digital maps containing information about other major inputs such as soil and land use data can also be added to the model. These maps are presently readily available online and can be obtained through numerous government run and private sites. Similarly multiple temperature and precipitation monitoring sites can be incorporated into the model and the model can then associate different sub-catchments with different gauging stations depending on their proximity.

The operation of the SWAT model is conducted in three phases; calibration, validation, and future application. In the calibration phase, a sensitivity analysis is conducted on the model to determine which modeled parameters have the greatest influence on the results. These parameters can include the SCS curve number (CN) value, a imperical value which relates rainfall to runoff based on land type and condition, associate with each sub-catchment, the base

flow parameter, the channel hydraulic conductivity, or a range of other hydrologic and hydraulic variables.

Once the sensitivity analysis is completed the model can then be calibrated based on acceptable ranges for each of the parameters using the auto-calibration function built within the software program. The quality of the calibration is often gauged statistically using the Nash-Sutcliffe model efficiency (NSE) coefficient (E) and the regression correlation coefficient (R^2). See equations 8and 9 below from Legates and McCabe (1999):

$$E = 1.0 - \frac{\sum_{i=1}^{N} (O_i - P_i)^2}{\sum_{i=1}^{N} (O_i - \bar{O})^2}. \tag{8}$$

$$R^2 = \left\{ \frac{\sum_{i=1}^{N} (O_i - \bar{O})(P_i - \bar{P})}{\left[\sum_{i=1}^{N} (O_i - \bar{O})^2\right]^{0.5} \left[\sum_{i=1}^{N} (P_i - \bar{P})^2\right]^{0.5}} \right\}^2 \tag{9}$$

Where P_t is the modeled value, $\bar{P}$ is the average model value, O_t is the observed value, and $\bar{O}$ the average observed value.

The E coefficient can range from $-\infty$ to 1 and R^2 can range from 0 to 1, with values closer to 1 indicating a better fit for both models. Effectively the R^2 value represents the degree to which the variability in the observed data is explained, so a value of 0.80 would signify that 80% of the variability is explained. The E value represents the extent of the mean square error is represented by the variance in the observed data. Once the model has been calibrated, a validation run is completed for a separate time series and the R^2 and E coefficients of the output are determined. If it is found that the calibration and validation runs produce reasonable results the model can then be applied to future scenarios. As with most physically based models, however, the degree to which the model is able to reproduce accurately the watershed's behaviour is largely dependent on quality of the input.

A brief description of the foundation of the SWAT model has been provided in the following sections.

3.3.1 Model Components

SWAT is comprised of seven main physical process components; climate analysis, hydrology, pesticide/bacterial, erosion, land cover/plant growth, soil/land management practices, and channel/water body processes. As this study will focus mainly on the climate and hydrologic aspects of the model, a deeper analysis of these components has been given below.

3.3.1.1 Climate

The major climatic inputs for the SWAT model include precipitation, maximum/minimum air temperature, solar radiation, wind speed, and relative humidity. SWAT gives the user the option to enter some, all, or none of these inputs. When no inputs are given SWAT allows the user to select data from its own internal database of climatic data records from various locations around United States.

Precipitation is perhaps the most important climatic element in the modeling process, and, unfortunately, may be one of the hardest parameters to reproduce accurately. Studies have found that the typical rain gauge will have an error of 10% due to factors such as wind. Aspects such as this should always be kept in mind when analysing the results of any rainfall-runoff model.

3.3.1.2 Hydrology

SWAT allows the user to choose between the SCS curve number method and the Green-Ampt Mein-Larson excess rainfall method for the estimation of infiltration and runoff volume. Peak runoff rates are determined using the modified rational method with the time of concentrations taken as the sum of the overland flow time and the channel flow time, both calculated based on derivations of the Manning's equation. The time of concentration is the time at which runoff from the entire watershed has begun to reach the outlet. Potential evaportranspiration is calculated using the Penman-Monteith equation based on mean daily parameter values. Actual evaportranspiration is calculated based on canopy storage, transpiration, and soil sublimation potential.

Based on user inputs identifying the soil type covering various parts of the drainage area, the soil water is calculated based on the individual soil profiles contained within the model's

internal database. Based on the ratio of loam, sand, and clay with the soil, the model determines the field capacity of the soil, the available water capacity (or water available for plant life), and wilting point. The general hydraulic routing process used in the model follows the hillslope/ impoundment scheme presented in Figure 8.

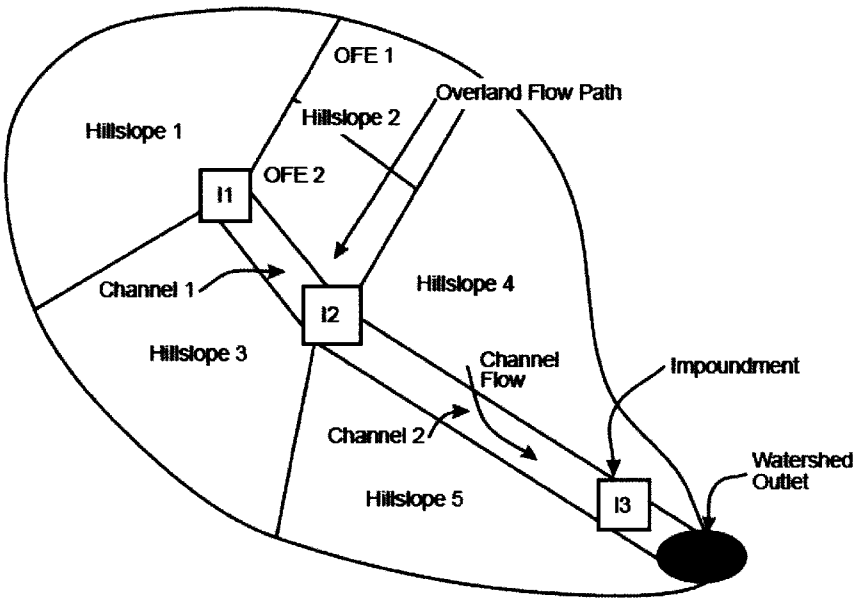

Figure 8: Rainfall-Runoff Model Schematic, Source: http://topsoil.nserl.purdue.edu/nserlweb/weppmain/docs/chap1.pdf

3.4 Flood Routing of Future Peak Flows

GeoHEC-RAS, a GIS extension of the HEC-RAS software package, was used to create a steady state flood routing model of the study area. Future peak flow events as determined by the non-stationary peak flow distribution will be applied to the model. The model then was used to generate water surface profiles and floodplain maps for a fictional engineering work of a given design life under design flow conditions.

The model used in this study was obtained from the Rideau Valley Conservation Authority (RVCA) (Ahmed and McGreath 2007; Ahmend, Soutar and Hardy 2009). In 2007 the RVCA began a project to develop a thorough and up-to-date flood plain map for the Kemptville Creek. Previous mapping initiatives involving portions of the Creek had been conducted 1972, 1983,

and most recently in 2003. The 2003 mapping focused mainly on the Rideau River and its confluence with the Creek. The 2007 model would use the downstream water levels established in the 2003 study as the boundary conditions for the Kemptville Creek model.

In preparation for the floodplain modeling, high resolution aerial photographs were taken of the Creek in the Winter of 2001. From these a Digital Terrain Model (DTM) was generated which would form the base of the floodplain model. Flow data collected for the study were taken from the same water survey location used in the study, 02LA006, however the RVCA model was based on 38 years of data as opposed to 35 years used in this present study.

The 37 bridges and culverts within the study area were incorporated in the model using physical data either collected for this study or taken from previous studies. The Oxford Mills Dam is located approximately 15 km upstream of the Creeks outlet and is the only control structured located in the Creek. It is a simple sluice gate dam which uses logs to raise or lower the upstream water level depending on the flow conditions. The RVCA model operated under the assumption that no logs would be in place during the peak flooding events and thus the dam would serve to control the upstream water level to the sill elevation of 95.26 meters.

In order to route the desired flood flows along the length of the Creek, the RVCA study conducted a single site flood frequency analysis. The results of several popular probability distributions were compared and based on visual inspection, it was found that the Three-Parameter Log Normal distribution provided the best fit to observed data and was therefore used in the analysis. The results of the flood frequency analysis were then interpolated to determine the flows at other nodal locations along the Creek using the method of area prorating as described in equation 10. These nodal points were selected based on confluence and catchment boundary locations.

$$Q2=(A2/A1)Q1 \tag{10}$$

As the present study was also centered around conducting a single site flood frequency analysis, the method of area prorating was used to generate flows for the HEC-RAS model.

The upstream boundary conditions for the model are established based on the water surface elevation in the Rideau River and the confluence of the Kemptville Creek. Based on a stage-discharge relationship established at this location, water surface elevations corresponding to various flow events were determined.

GeoHEC-RAS works by using a GIS software package such as ArcMap to generate cross sections from a DTM. These cross sections are then exported to the HEC-RAS program where water surface elevations can be generated from the flood flows inputed at various locations along the Creek. The results of the HEC-RAS model are then imported back into GIS where complete floodplain maps can be generated with the results. In the RVCA model, 276 cross sections were taken to define the Creek's geometry.

The RVCA GIS model also contained layers of additional information such as the locations of buildings and roadways. A copy of the model inputs and other data are provided in Appendix B.

4 MODEL APPLICATION

To assess the viability of the proposed methodology presented in the previous section, a regional climate change impact assessment was conducted. In the present study the methodology was applied to a largely agricultural watershed near Ottawa, Ontario, Canada.

4.1 Study Area

The Kemptville Creek watershed was the site selected for analysis in this study. The Kemptville Creek watershed is part of the larger Rideau River watershed and has a contributing area of approximately 409 km^2. The outflow from the watershed is monitored at the HYDAT station located at the terminus of the watershed (see Figure 9 and Figure 10). The average annual mean river flow taken from this station over the past 30 years ranged from 2.9 – 6.9 m^3/s. Observed flow and rainfall data are presented in Appendix A.

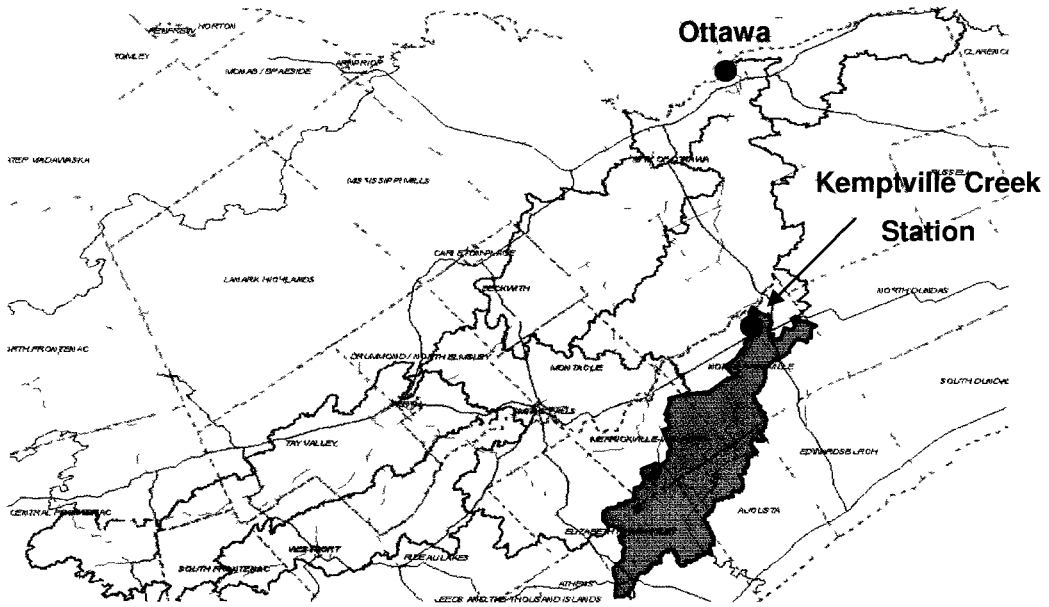

Figure 9: Kemptville Creek Watershed within the larger Rideau River Watershed

Figure 10: Kemptville Creek Immediately Downstream of Gauge Station

The average monthly flow was extracted from the site over the length of the study period from 1970 - 2004 is presented below in Figure 11. From this figure one can identify that the peak flow period for this catchment occurs during the spring thaw period of March – May.

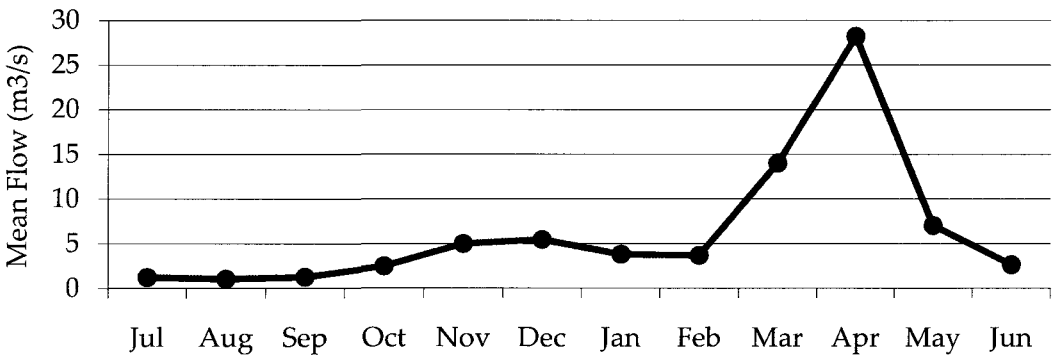

Figure 11: Average monthly flow from 1970-2004

4.1.1 Land Cover

The Kemptville Creek watershed is home to approximately 5,000 – 7,000 people and supports a diverse ecology of plants and animals. The catchment consists of 22% wetland, 45% forest, 31% agricultural, 1% settled land, and 1% water (See Figure 12). The proportion of the watershed dedicated to agriculture has decreased in the past few decades, with a reported decrease of 17% from 1981 to 2001. It is believed the reason for this decrease is due to changes in agricultural methods and increased woodland cover (RVCA, 2007).

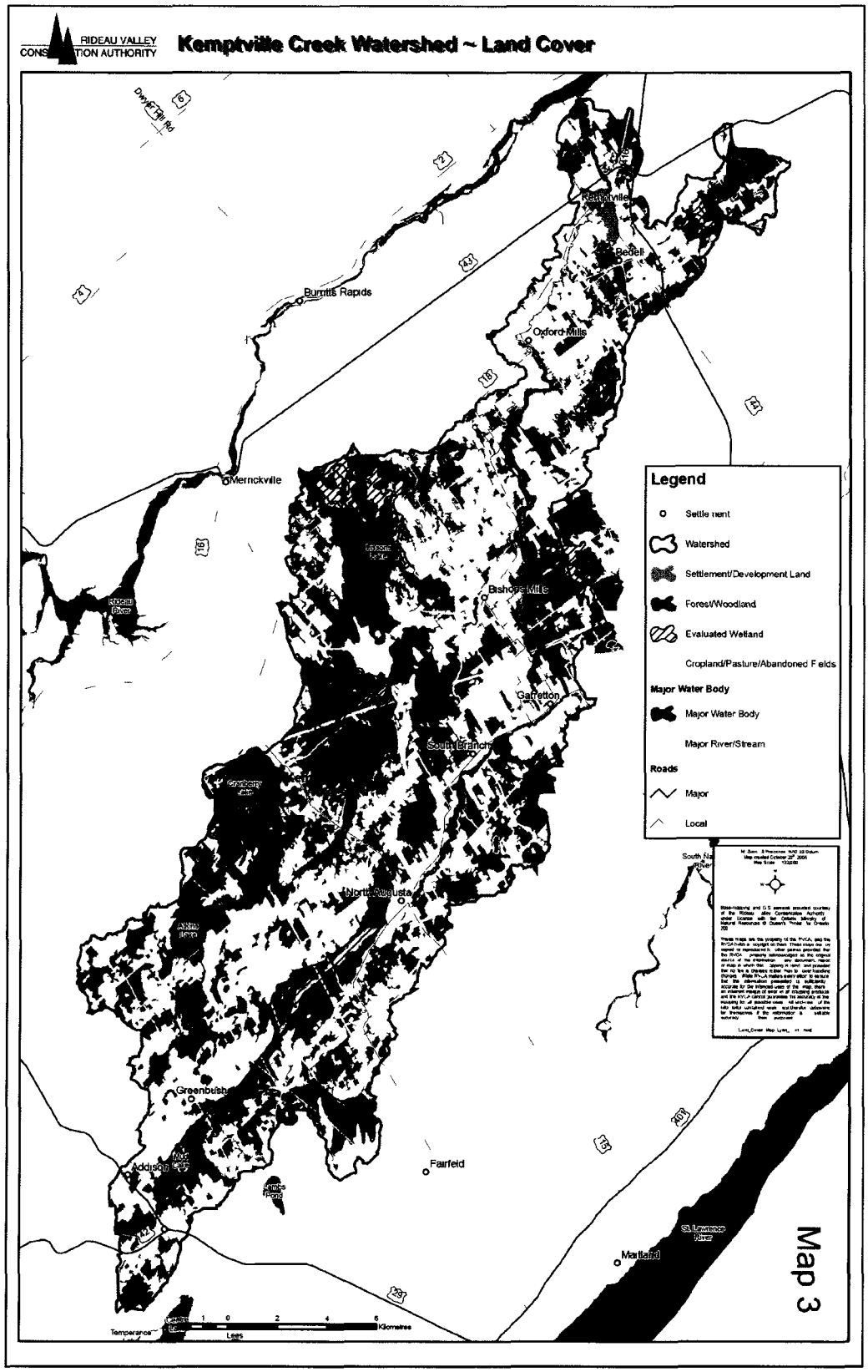

Figure 12: Kemptville Watershed Land Use (RVCA 2007)

4.1.1.1 Soil Data

Soil maps for the area were obtained from the CanSIS National Soil Database for the two counties in which the watershed resides, Leeds County and Grenville County. As seen in Figure 13, the dominant soil types in the area include Peat, Farmington (loam), Grenville (loam), Granby (sandy loam), and Muck. The presence of peat and muck, both poorly draining soils, is consistent with the high proportion of wetlands location throughout the watershed.

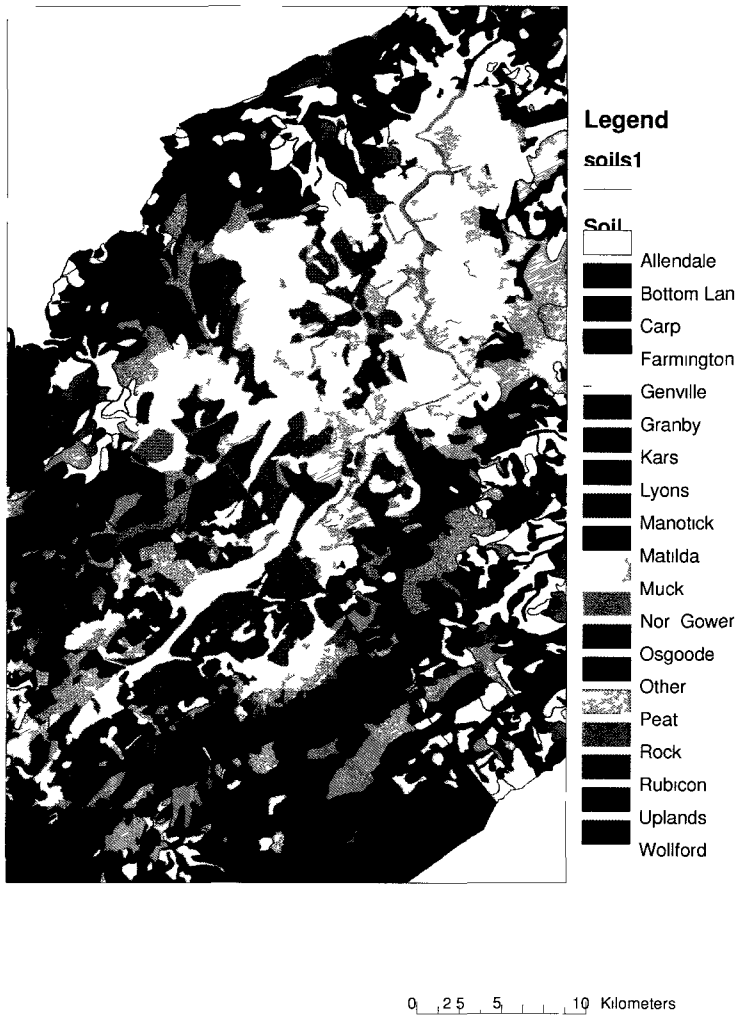

Figure 13: Kemptville Watershed Soil Use (Source: CanSIS National Soil Database)

4.1.1.2 Elevation Model

From a DEM of the watershed, presented in Figure 14, we can see that the upstream segments of the watershed have greater variations in height while the downstream regions are mainly flat. Overall the catchment has an average slope of 0.01 m/m.

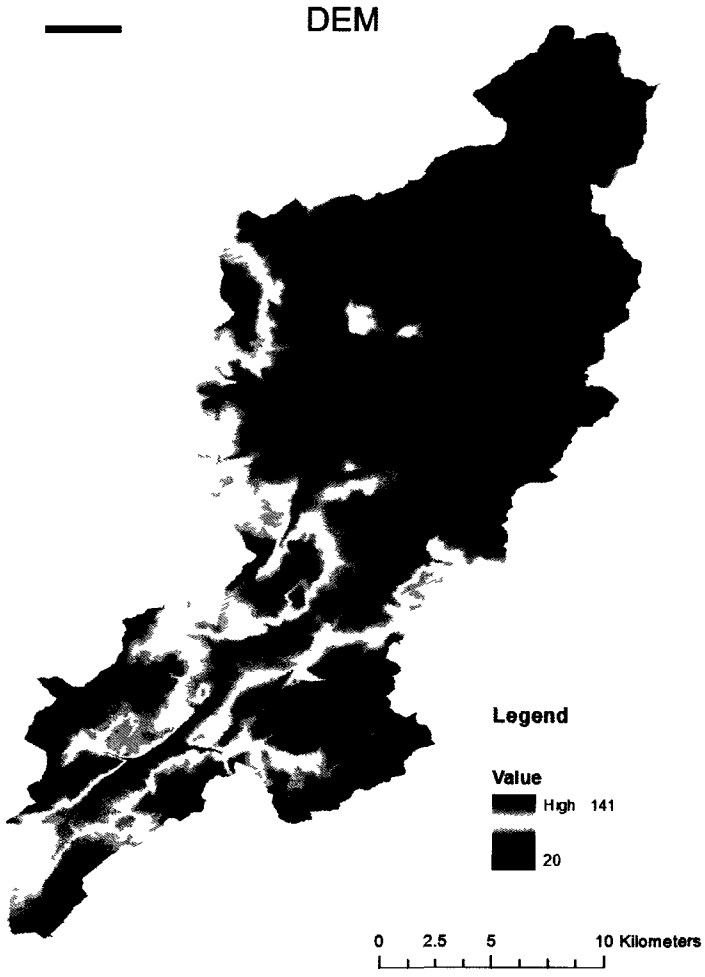

Figure 14: Kemptville Watershed DEM (Source: Canadian Digital Elevation Data, www.Geobase.ca)

4.1.2 Hydrology

Over years residents of the watershed have had various issues regarding local hydrology within the watershed. These include reports of poor drainage, high water levels, and even low water

levels at times. Many residents believe that these issues are related in part to the operation of the Oxford Mills Dam location approximately 5 km upstream of the Town of Kemptville. The Oxford Mills Dam, pictured in Figure 15 was constructed in 1959 and is operated by the Ministry of Natural Resources Canada. In an attempt to address complaints over what impact if any the dam was having on upstream water levels, the RVCA developed a Mike 11 model for the area. It was determined in a preliminary study that the dam was not impacting upstream water levels and that the possible cause was likely beaver activity and the expansion of the wetlands trapping runoff before it reached the Creek.

Figure 15: Oxford Mills Dam

4.1.3 Water Quality

The RVCA currently monitors the water quality of the Kemptville Creek through 14 sampling locations. Since 1995 2 E. coli sampling of different branches has shown that approximately 0% to 37% of tests exceeded the criteria of the Provincial Water Quality Objective of 100 counts per 100 ml of water. Total Kjeldahl Nitrogen levels, an indicator of the nitrogen loading in the Creek, remain high while Dissolved Oxygen concentrations remain low due to increasing plant growth creating a less than ideal atmosphere for the fish species residing in the Creek.

4.2 Downscaling of Climate Data

For this study, global climate data will be downscaled to the regional scale through the application of the ASD software package. Outputs from the third generation of the Canadian Circulation Model (CGCM3) were obtained from the Data Access Integration (DAI) website which is maintained by Environment Canada and The Global Environmental and Climate Change Centre (GEC3) out of Quebec, Canada. CGCM3 predictor data for the SRES A2 climate change scenario were obtained for the years of 1961-2000 and from 2001 – 2100 at grid box number 77X, 12Y located in the vicinity of the study area, as illustrated in Figure 16.

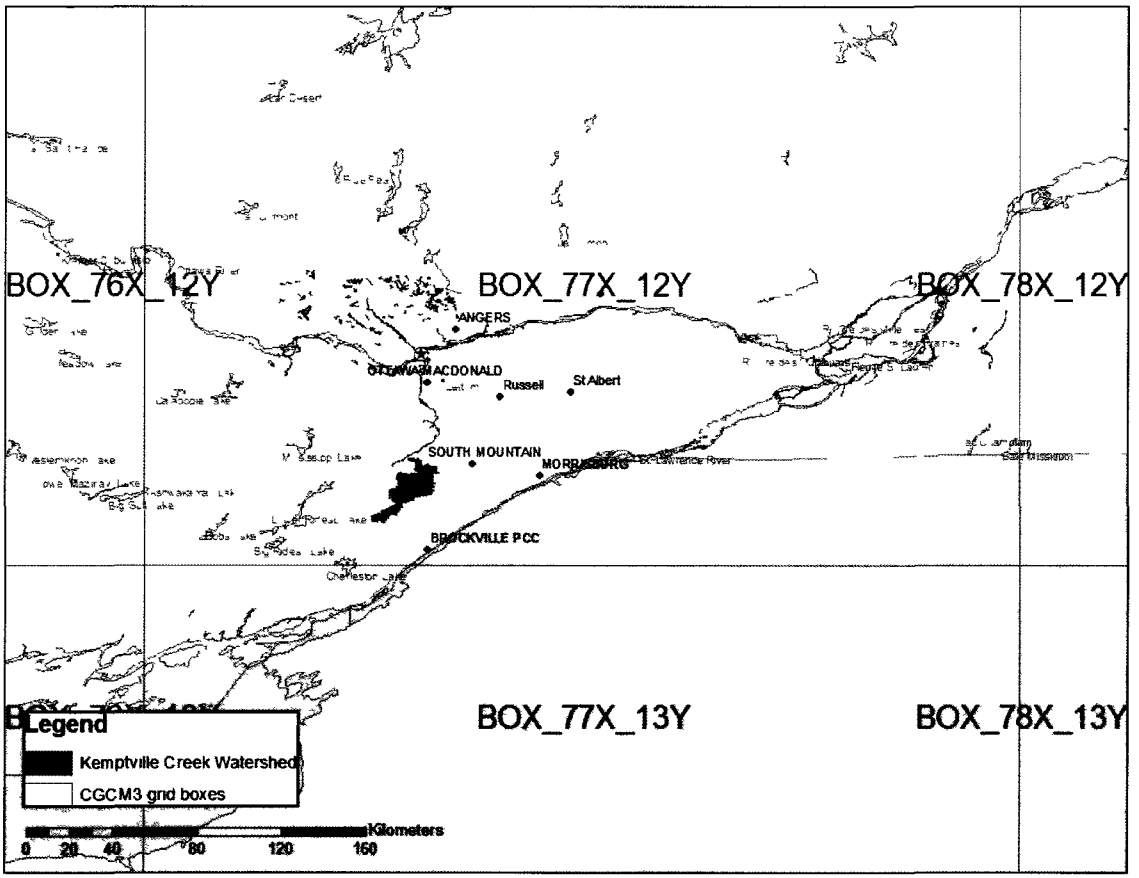

Figure 16: Kemptville Creek position with respect to CGCM3

NCEP predictors were also obtained from the DAI site at the same grid point for the period of 1961 – 2003. A comparison between the average annual NCEP precipitation, observed precipitation, and observed flow has been presented in Figure 17. From this figure we can see that while NCEP data generally follows a pattern similar to that of observed data, the magnitude

of the data is slightly off as the NCEP complied rainfall data appears to have a slightly higher bias. We can also see that the relationship between rainfall and flow is not necessarily clear, hence why establishing a direct relationship between flow and rainfall can prove difficult.

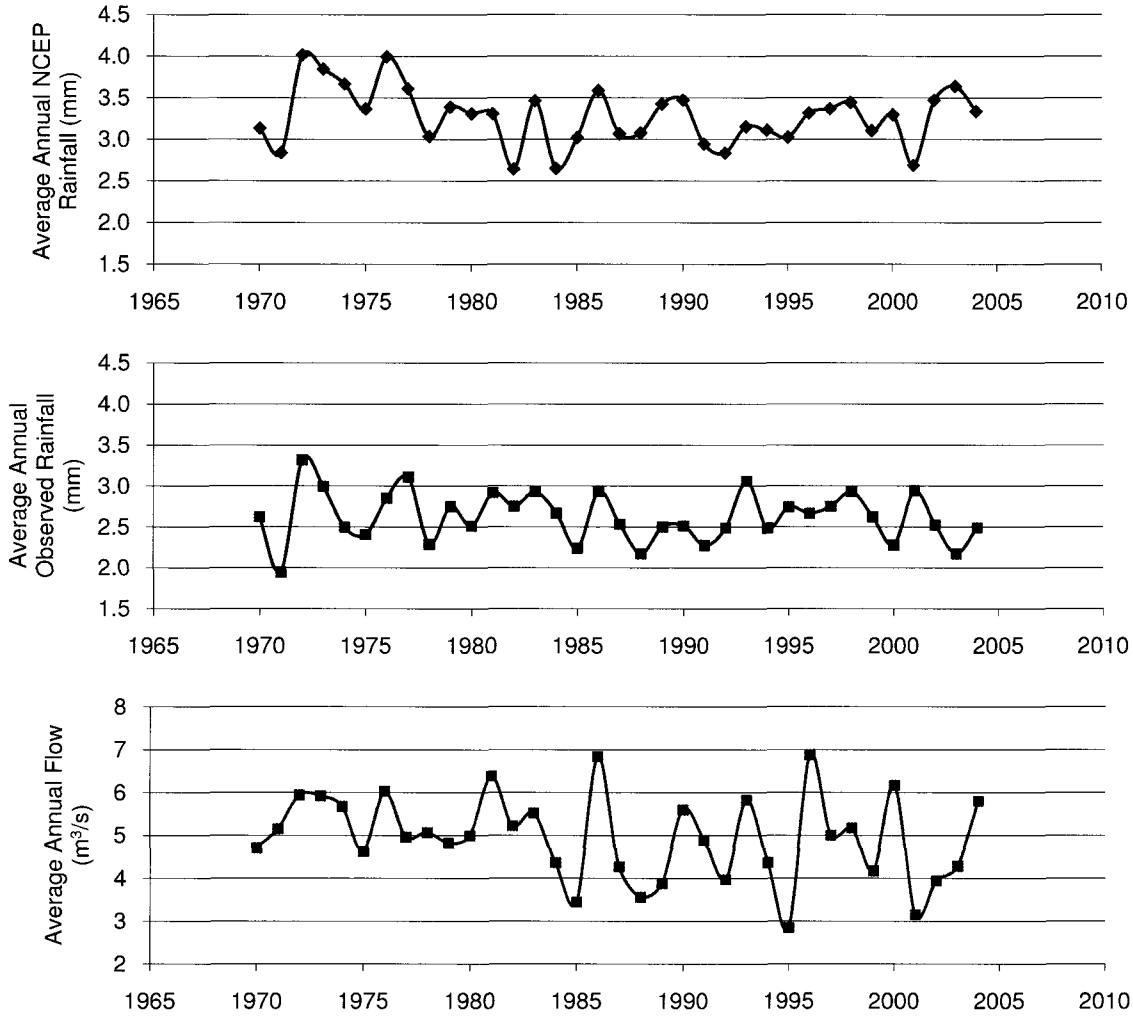

Figure 17: Comparison of Average Annual Precipitation and Flow

A list of the predictors that were obtained for the ASD model have been provided in Table 4 and a detailed description of select predictors has been provided in Table 5.

Table 4: List of available predictors

#	CGCM3.1	Type	NCEP	Type	Predictor Type	
1	c3a2mslpgl.dat	D	ncepmslpgl.dat	P	Mean sea level pressure	
2	c3a2p__fgl.dat	D**	ncepp__fgl.dat	Dg	1000hPa	Wind Speed
3	c3a2p__ugl.dat	D*	ncepp__ugl.dat	Dg	1000hPa	U-component
4	c3a2p__vgl.dat	D*	ncepp__vgl.dat	Dg	1000hPa	V-component
5	c3a2p__zgl.dat	D*	ncepp__zgl.dat	Dg	1000hPa	Vorticity
6	c3a2p_thgl.dat	D**	ncepp_thgl.dat	Dg	1000hPa	Wind Direction
7	c3a2p_zhgl.dat	D*	ncepp_zhgl.dat	Dg	1000hPa	Divergence
8	c3a2p5_fgl.dat	D**	ncepp5_fgl.dat	Dg	500hPa	Wind Speed
9	c3a2p5_ugl.dat	D*	ncepp5_ugl.dat	Dg	500hPa	U-component
10	c3a2p5_vgl.dat	D*	ncepp5_vgl.dat	Dg	500hPa	V-component
11	c3a2p5_zgl.dat	D*	ncepp5_zgl.dat	Dg	500hPa	Vorticity
12	c3a2p500gl.dat	D	ncepp500gl.dat	P	500hPa	Geopotential
13	c3a2p5thgl.dat	D**	ncepp5thgl.dat	Dg	500hPa	Wind Direction
14	c3a2p5zhgl.dat	D*	ncepp5zhgl.dat	Dg	500hPa	Divergence
15	c3a2p8_fgl.dat	D**	ncepp8_fgl.dat	Dg	850hPa	Wind Speed
16	c3a2p8_ugl.dat	D*	ncepp8_ugl.dat	Dg	850hPa	U-component
17	c3a2p8_vgl.dat	D*	ncepp8_vgl.dat	Dg	850hPa	V-component
18	c3a2p8_zgl.dat	D*	ncepp8_zgl.dat	Dg	850hPa	Vorticity
19	c3a2p850gl.dat	D	ncepp850gl.dat	P	850hPa	Geopotential
20	c3a2p8thgl.dat	D**	ncepp8thgl.dat	Dg	850hPa	Wind Direction
21	c3a2p8zhgl.dat	D*	ncepp8zhgl.dat	Dg	850hPa	Divergence
22	c3a2s500gl.dat	D	nceps500gl.dat	D*	500hPa	Specific Humidity
23	c3a2s850gl.dat	D	nceps850gl.dat	D*	850hPa	Specific Humidity
24	c3a2shumgl.dat	D	ncepshumgl.dat	D*	1000hPa	Specific Humidity
25	c3a2tempgl.dat	D*	nceptempgl.dat	D*	Temperature at 2m	

** Computed from U and V wind components

* Computed from the horizontal Geopotential gradient at corresponding level

Table 5: Predictor Description

PREDICTOR	UNIT	CGCM3.1 T47	NCEP/NCAR
Temperature at 2m (TEMP)	°C	Results of post-processing at CCCma (i.e. interpolated at 2m from the lowest model level)	Results of post-processing at NCEP/NCAR
Specific humidity at 2m	kg/kg		
Mean sea level pressure	Pa	Calculated from ln(Surface Pressure), TEMP, and Surface Geopotential, and then while archived at 6-hours daily averaged	
Specific humidity (SHUM)	kg/kg	Calculated from the model's humidity variable	Calculated from the reanalysis' (relative) humidity variable
Geopotential	m	Calculated from ln(Surface Pressure), TEMP and SHUM)	Results of post-processing at NCEP/NCAR
Vorticity	s^{-1}	Calculated from U and V wind components	Calculated from U and V wind components
Divergence	s^{-1}		
Zonal wind component (U)	m/s		
Meridional wind component (V)	m/s		
Wind speed	m/s	Calculated from U and V wind components	Calculated from U and V wind components
Wind direction	degrees from N		

A separate ASD model was developed for each of the three main SWAT inputs, maximum temperature (Tmax), minimum temperature (Tmin), and precipitation. These models were calibrated from the period of January 1, 1970 to December 31, 1984 and were validated for the period January 1, 1985 to December 31, 2000, as illustrated in Figure 18.

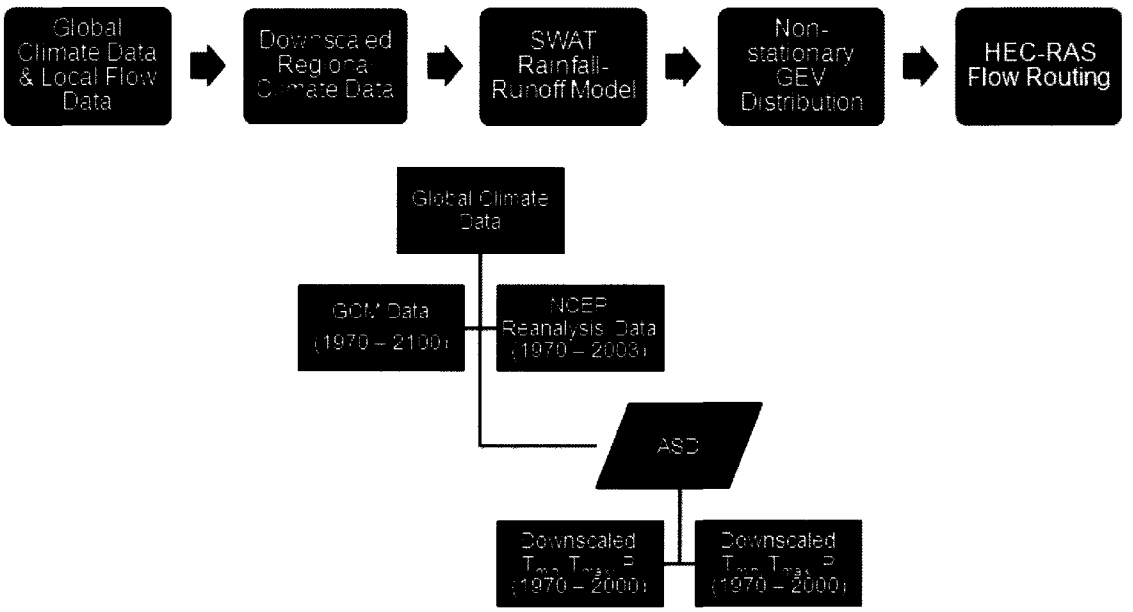

Figure 18: Application of ASD

Of the 24 Predictors available a maximum of five were used for analysis. These parameters were evaluated based on the stepwise selection method using a significance level of 0.05. The projected periods were from 2011 to 2040, 2041 to 2070, and 2071 to 2100. A total of 100 scenarios were generated for each projection.

4.3 Generation of Future Mean Flow Series with SWAT

The rainfall-runoff model SWAT was used to generate flow data series for the Kemptville Creek from the downscaled climate data. The following sections will detail the various inputs used to build and calibrate the model.

4.3.1 Model Inputs

The ArcSWAT model requires four basic inputs: a digital elevation map (DEM) of the area, land use information, soil type information, and local climate and flow data. Ideally, a DEM, digital land use map, and digital soil map are entered into ArcGIS as separate layers and using the information contained in each delineated sub-catchments the model can compute runoff rates over the entire surface of the watershed.

4.3.1.1 DEM

The DEM used in this analysis was taken from the NASA Shuttle Radar Topographic Mission (SRTM) 250 meter resolution re-sampled survey mapping obtained through the WaterBase organization website (WateBase 2010) which provides access to various SWAT compatible mapping sites.

Once the DEM was input into the SWAT model, an outlet location was chosen and the software delineated the watershed contributing to this outlet. For this analysis the location of the Kemptville Creek HYDAT station was chosen as the outlet for the watershed. Due to the course resolution of the DEM used in the model, the watershed that was delineated did not have the same extents as the one delineated by the RVCA. In order to overcome this, the area of the individual subcatchment used in the computations were manually adjusted so that the total area of the modeled watershed agreed with its actual size. A copy of the delineated DEM is presented in Figure 19.

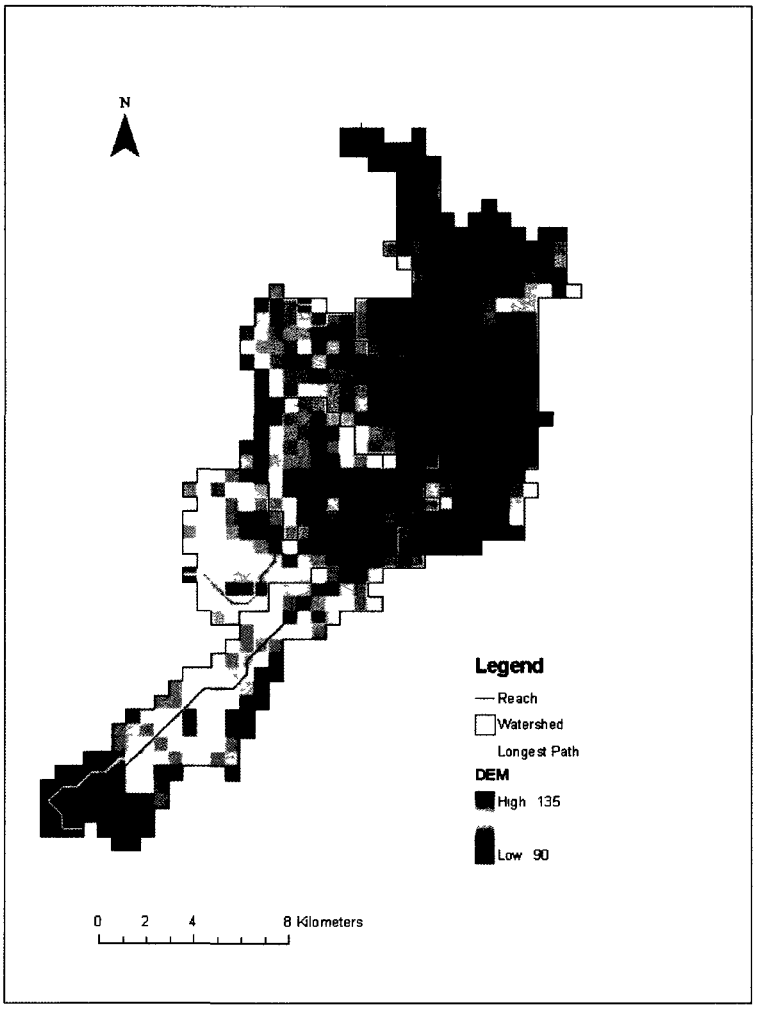

Figure 19: SWAT DEM

4.3.1.2 Flow and climate data

Mean monthly and daily flows were extracted from the HYDAT database of Environment Canada for station 02LA006 located at 44°59'39" latitude and 75°39'45" longitude near the terminus of the watershed (see Figure 20). This gauging station has over 35 years of uninterrupted flow gauging data from 1970 to the present day and meets the standards of the United Nation's World Meteorological Organization.

Daily precipitation, minimum temperature and maximum temperature were taken from the Environment Canada Station 6104025 located approximately 9 km east of the Kemptville

HYDAT gauge (see Figure 20). Data were available at this location from 1945 to the present day, but unfortunately the station was altered in 1996 so the data set is split into two time series.

In order to avoid any error that could be introduced as a result of the alteration of the climate gauging station, the period chosen in the study for the calibration and validation of the SWAT model was the 27 year period from 1970 to 1996.

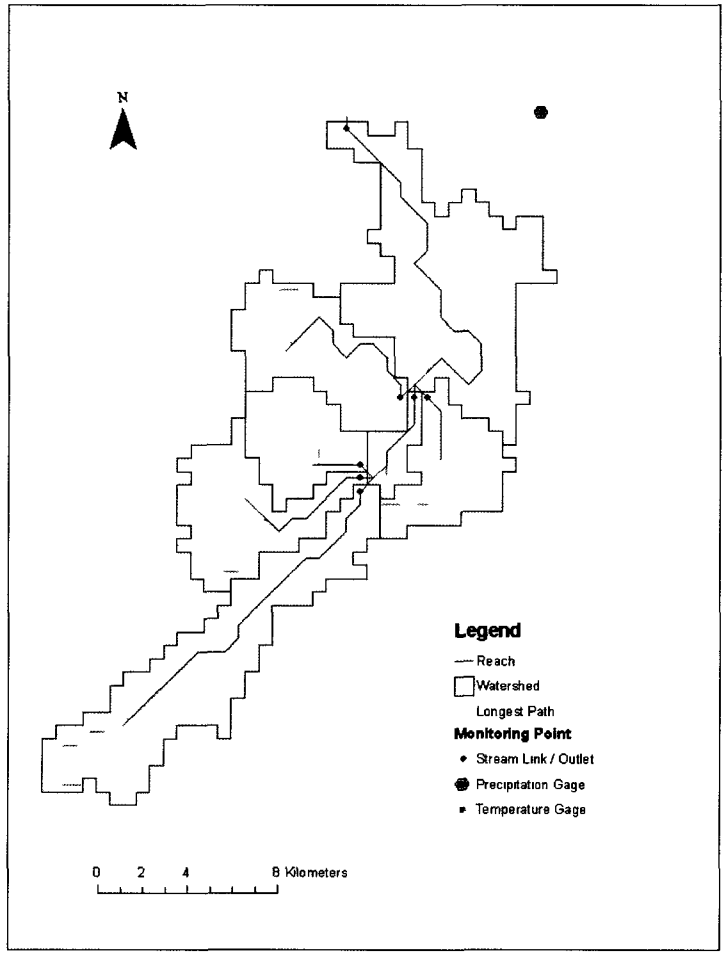

Figure 20: SWAT Gauging Stations

4.3.1.3 Soil Class and Land Use Data

The soil and land use data used in the model were also obtained through the WaterBase organization website (Waterbase 2010). The land use data were taken from USGS Global Land Cover Characterization database with a 1 km resolution. The soil data were taken from the

Digital Soil Map of the World and Derived Soil Properties map produced by the FAO Land and Water Digital Media Series in 2003 with a scale of 1:5,000,000. This soil map was of substantially lower resolution than the one presented in Figure 13, however the map from the FAO was compatible with SWATs internal database and as such data could be more readily extracted from it and applied to the model. A copy of the soil map used for the model is presented in Figure 21.

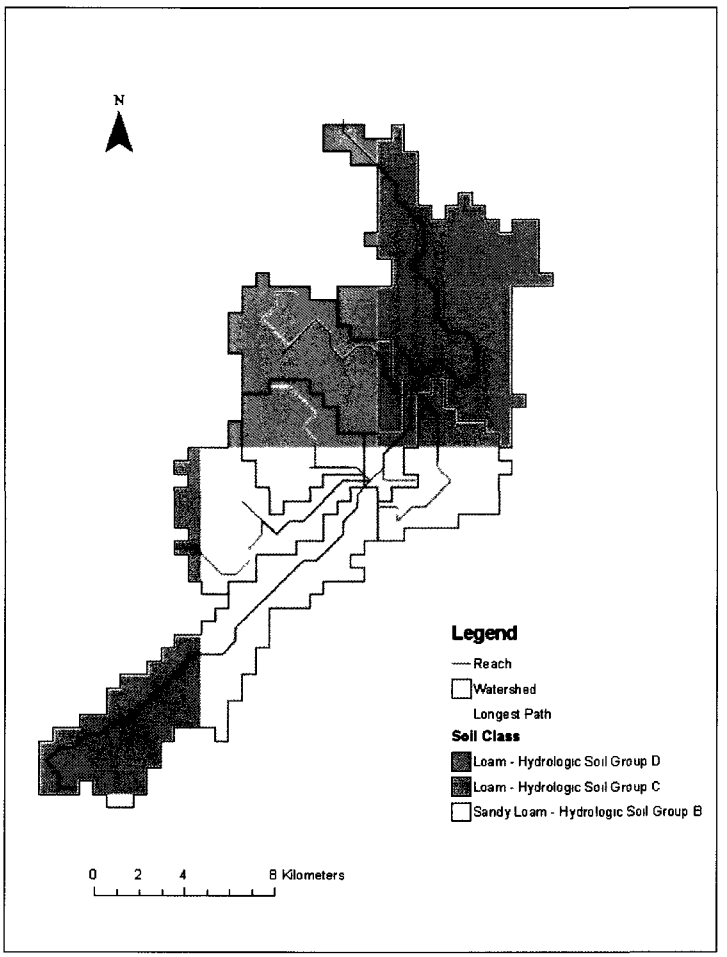

Figure 21: SWAT Soil Map

4.3.2 *Model Setup*

Once the input maps were entered into ArcGIS, a SWAT model was generated. The process has been illustrated in Figure 22.

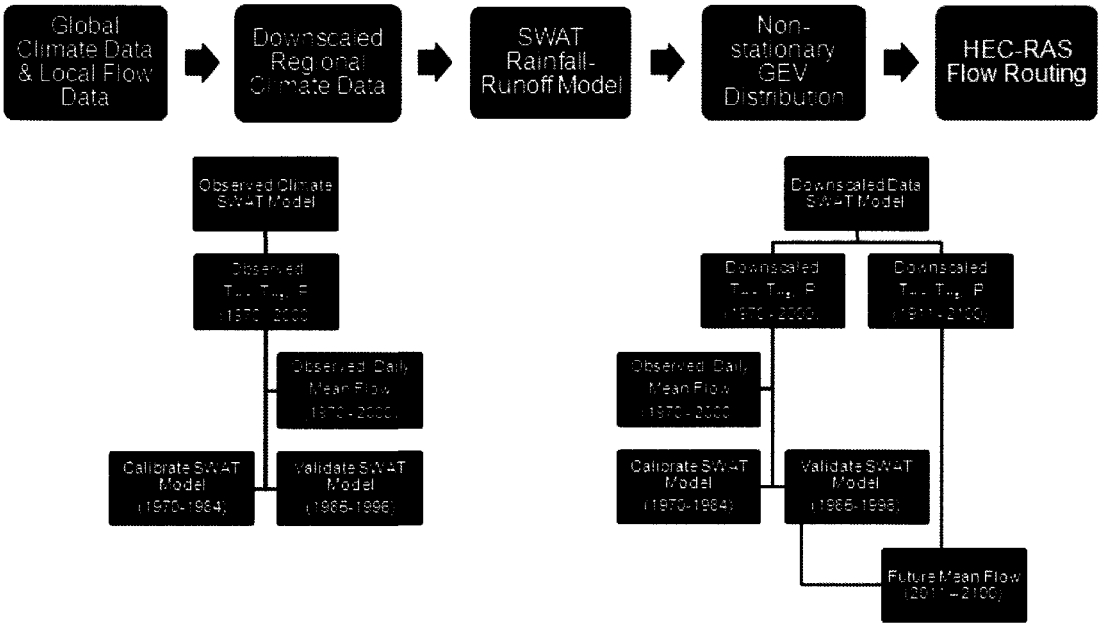

Figure 22: Application of SWAT Model

As seen in Figure 20, SWAT delineated the watershed into 6 subcatchments. The characteristics of these subcatchments, as determined by the SWAT model, have been presented below in Table 6. As mentioned previously, the actual area of the subcatchments has been edited to create a model that better represented the extent of the watershed contributing to the gauging station.

Table 6: Subcatchment Physical Characteristics

Subcatch.	Area (ha)	Latitude	Longitude	Min Elev (m)	Max Elev (m)	Avg Elev (m)	Slope (%)
1	11907	44.926	-75.685	90	117	99	0.38
2	5607	44.906	-75.754	100	123	109	0.41
3	3969	44.858	-75.681	97	115	106	0.42
4	3654	44.868	-75.761	104	130	109	0.50
5	1134	44.861	-75.711	98	115	108	0.36
6	5229	44.830	-75.779	102	125	109	0.34
7	10143	44.774	-75.812	104	135	116	0.37

From this table we can see that the overall slope of the modeled watershed is lower than that of the actual watershed. This is likely due to the fact that the steeper portions of the watershed located in the south were not captured by the delineation due to the coarse resolution of the DEM.

The SCS curve number method was selected for the estimation of infiltration and runoff volume in the model. The hydrologic modeling parameters determined by the SWAT model have been presented in Table 7 below. Overall these values appear to be consistent of what one would anticipate for the watershed given the actual land cover and soil characteristics.

Table 7: Subcatchment Hydrologic Characteristics

Subcatch.	Tc (hr)	Soil Group	CN (AMC II)
1	4.931	C	79.44
2	3.765	D	85.63
3	3.073	B	68.09
4	2.379	D	85.63
5	2.321	B	68.09
6	3.291	B	68.09
7	5.439	B	68.09

The hydraulic modeling parameters generated by the SWAT model are presented in Table 8.

Table 8: Main Channel Characteristics

Subcatch	Channel Length (km)	Channel Width (m)	Channel Depth (m)	Channel Slope (%)
1	18.98	34.4	1.16	0.06
2	9.61	10.33	0.52	0.07
3	3.8	8.39	0.45	0.10
4	2.95	7.99	0.44	0.03
5	4.95	22.26	0.87	0.08
6	7.32	9.9	0.51	0.03
7	16.75	14.74	0.66	0.07

4.3.3 Model Calibration

Once the setup was completed, a break in run was conducted where the uncalibrated model was put through an initial run of the calibration period. For this study the calibration period was taken between January 1, 1970 and December 31, 1984. These initial results were then subjected to a sensitivity analysis and auto-calibration procedure. The sensitivity analysis was conducted

for all parameters within the SWAT model that influence the flow results. SWAT then automatically ranked these parameters based on their level of influence and the top 10 parameters were chosen for calibration. The model was then calibrated using SWAT's auto-calibration tool against the mean monthly flow taken from the HYDAT gauging station. The selected parameters were allowed to vary within an acceptable range through thousands of model runs and the parameter values that produced the lowest variation between the modeled flow and the observed flows were selected. A list of the chosen parameters and their calibrated values is presented below in Table 9.

Table 9: Calibrated SWAT parameters

Variable	Description	Units	Allowable Range	Initial Estimate	Calibrated Value
Alpha_Bf	Baseflow alpha factor	days	0-1	0.048	0.586
Canmx	Maximum canopy storage	mm H2O	0-10	0-10	9.831
Ch_K2	Channel hydraulic conductivity k factor	mm/hr	0-150	0	148.550
Cn2	Initial SCS curve number (AMC II)		± 25%	66-77	68 - 85
Esco	Soil evaporation compensation factor		0-1	0.95	0.007
Gw_Delay	Groundwater delay time	days		31	40.973
Gw_Revap	Groundwater "revap" coefficient			0.02	0.056
Revapmn	Threshold aquifer depth for "revap" /percolation	mm H2O		1	0.001
Surlag	Surface runoff lag coefficient		0-10	0-10	0.650
Timp	Snowpack temperature lag factor		0-1	0.438	0.435

4.3.4 Model Validation

Once the model was fully calibrated a validation run of the model was completed. The validation period selected for this study was from the period January 1, 1985 to December 31, 1996. Figure 23 illustrates the results of the calibration and validation runs of the model compared to the observed flow.

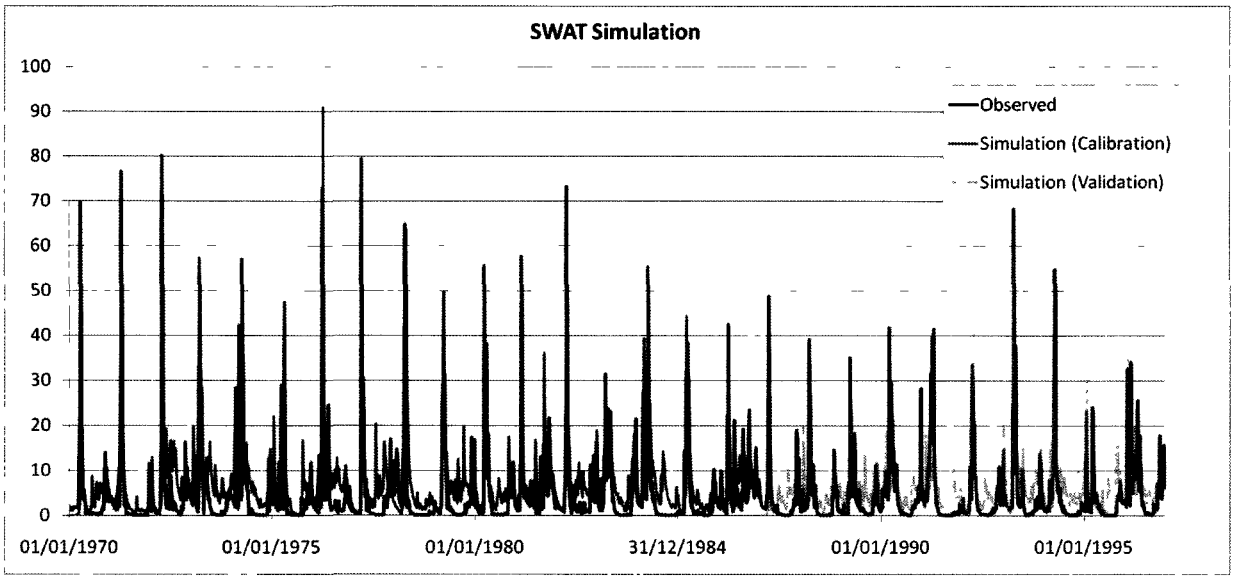

Figure 23: Observed and SWAT simulated flows for the calibration and validation periods

From this figure we can see that while the model is able to reasonably reproduce mean flow trends, it tends to generally underestimate peak flow events and underestimate low flows. Scatter plots of the calibration and validation time series have also been provided in Figure 24 and Figure 25.

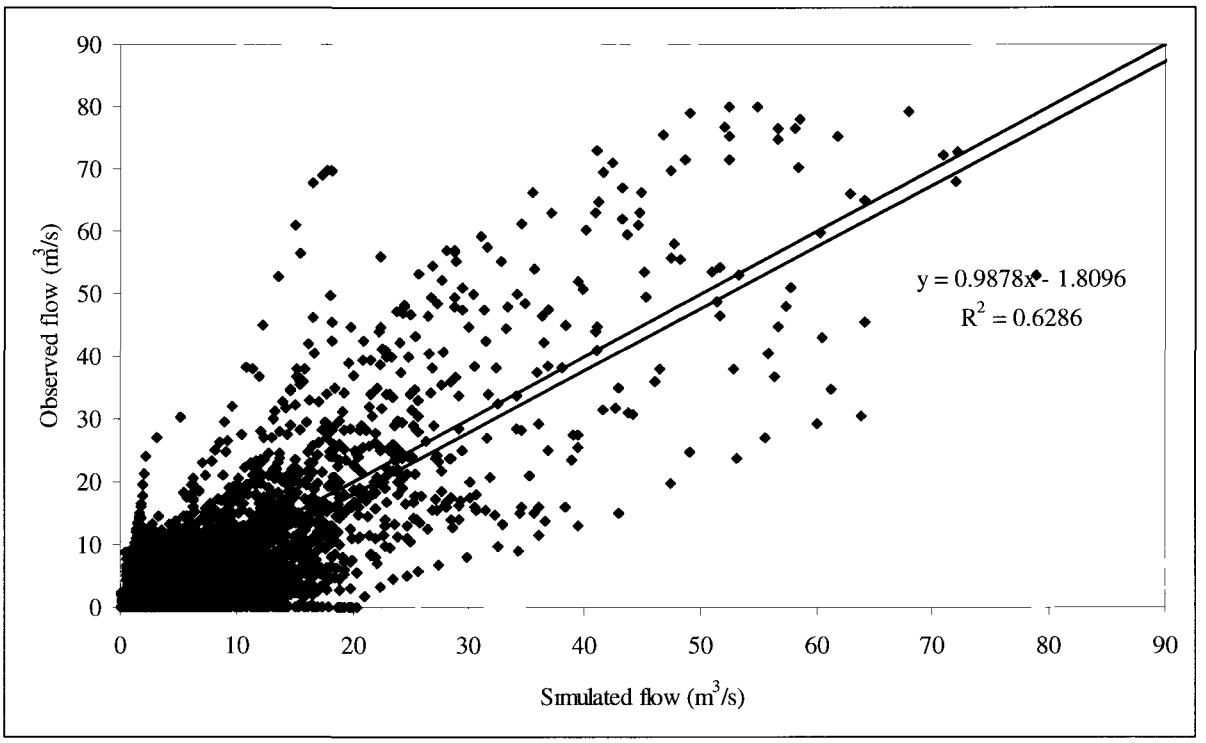

Figure 24: SWAT Calibration Scatter Plot

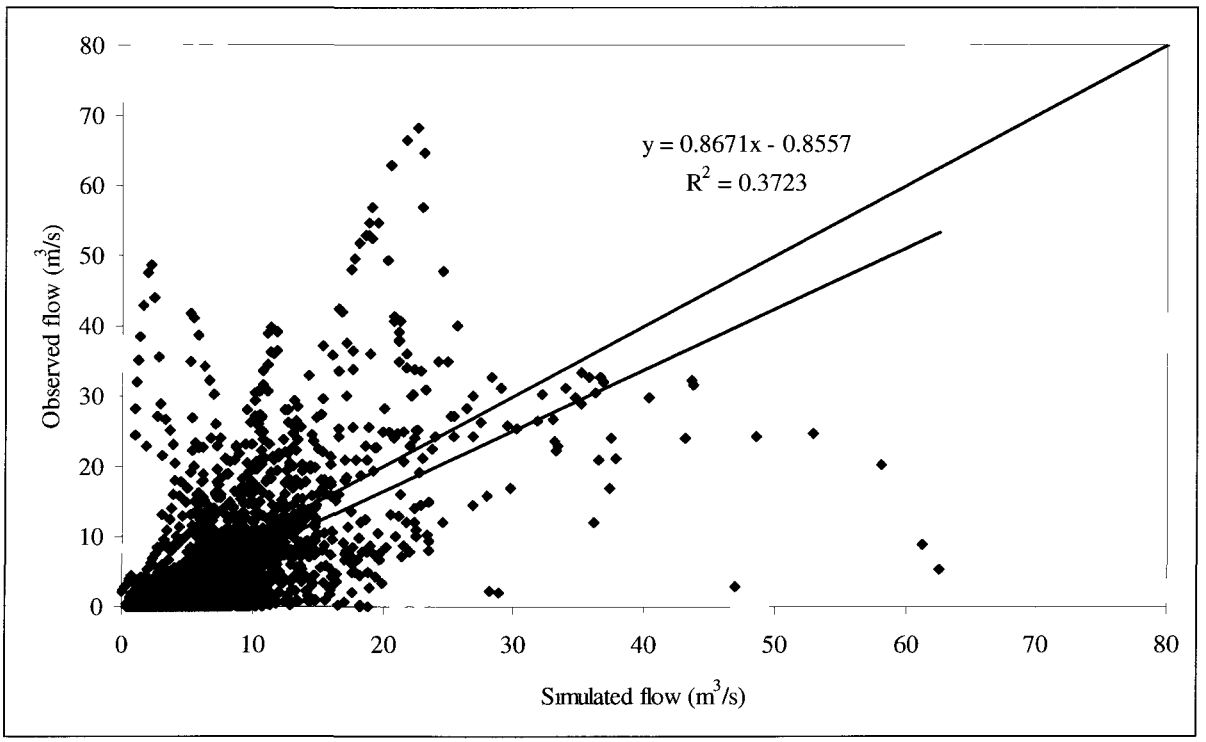

Figure 25: SWAT Validation Scatter Plot

The results of the calibration and validation runs of the SWAT model were analysed using the Nash-Sutcliffe model efficiency (NSE) coefficient (E) and the regression correlation coefficient (R^2). The model was analysed using both a daily and monthly time scale. The relative error (*Re*) between the observed flow and simulated flow was also calculated. A summary of this analysis has been presented below in Table 10. Detailed outputs for the calibration and validation runs can be found in Appendix B.

Table 10: SWAT model evaluation statistics

	Mean (m^3/s)					
Period	Obs.	Sim.	*Re*	Time Step	R^2	E
Calibration	5.32	7.22	-35.67%	Daily	0.79	0.59
				Monthly	0.84	0.62
Validation	4.64	6.34	-36.59%	Daily	0.61	0.32
				Monthly	0.77	0.49

Based on these results we see that overall the model was able to perform to an acceptable level and that the monthly model is able to perform better then the daily model, which is normally the case with such models. The relative error in both the calibration and validation runs of the model is relatively high, but that is not unusual in cases where the values being analysed are small as even small discrepancies between the two values can have a large impact.

The calibrated SWAT model was then used to determine future mean flow values. The 100 equiprobable ASD downscaled future climate scenarios were run though the model and 100 future mean flow series were generated. The mean daily flow of all the scenarios was then determined and it was this mean flow series which was applied to the calibrated GEV model.

4.4 Determining Future Flood Flows

In order to determine the future extreme flow values in the Creek, the flow sequence generated by the SWAT model was distributed using a calibrated non-stationary GEV probability distribution. This process has been outlined in Figure 26.

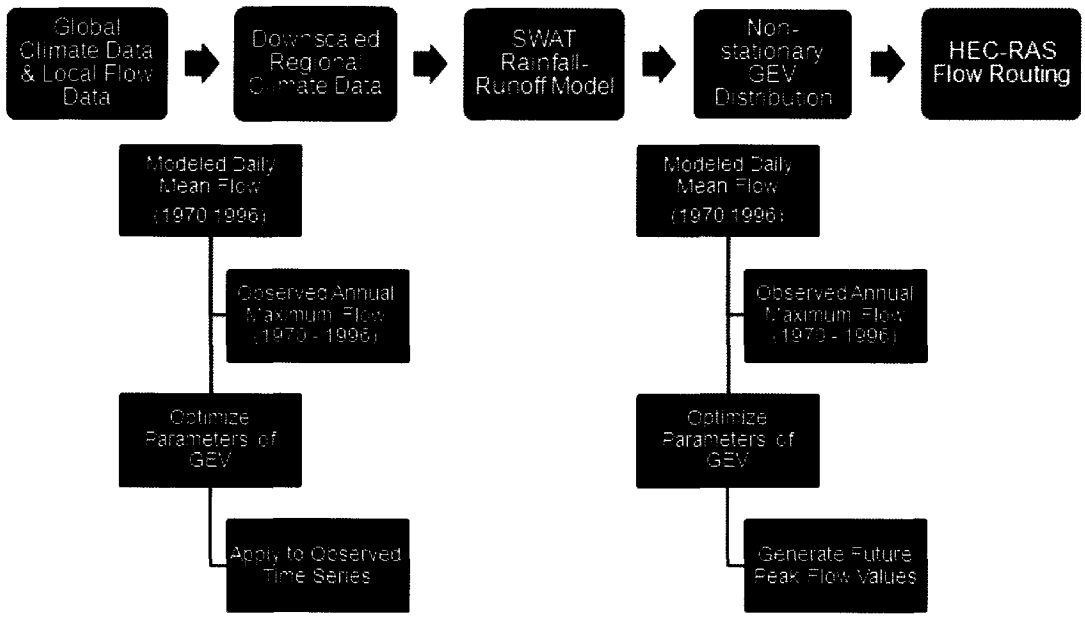

Figure 26: Application of GEV Model

In order to determine how to optimize best the parameters of GEV distribution under the non-stationary trend imposed by climate change, 64 models were analyzed. These models included traditional approaches to estimating stationary and non-stationary parameters as well as several in which the parameters were optimized as a function of the maximum annual mean flow over a set time scale window ranging from 1 to 20 days. The parameter models were compared and the optimal model was selected based on Bayes factors. The Bayes factors are an indication as to the likelihood of one model's ability to reproduce the observed maximum annual flow in the Creek over another.

As this study uses the GEV distribution for two separate applications, one to validate the methodology through application to the present time period and another to apply the methodology to the future time period, two GEV models were required. In the first model the parameters would be optimized so that the distribution was able to reproduce maximum annual flow values based on maximum average annual-day flow taken from SWAT simulated flow series forced by observed climate data. This distribution was used to analyze present peak flow distributions in the Creek. In the second model the parameters would be optimized so that the distribution was able to reproduce maximum annual flow values based on maximum average

annual-day flow taken from SWAT simulated flow series forced by downscaled GCM climate data. This distribution was used to determine the future peak flow distributions in the Creek.

4.5 Evaluating the Impacts of Future Flood Flows

As a Hec-GeoRAS model had already been compiled for the study area, in this study we will update the existing model with the revised peak flow values and assess the impacts of these flows in the upstream segments of the watershed. This process is outlined in Figure 27.

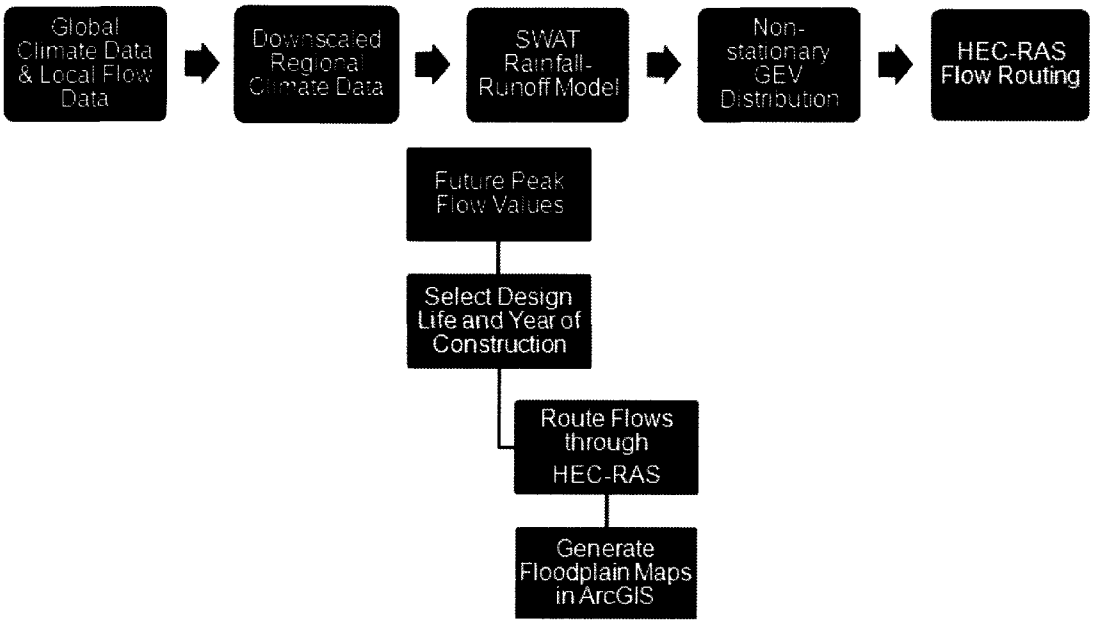

Figure 27: Application of Flow Routing

Similarly to the modeling process followed in the RVCA analysis, the future peak flows in this analysis were only determined at the location of the HYDAT gauge station. As was the case in the RVCA study, these flows were transposed to other locations along the length of the Creek through the process of area prorating. A map detailing the locations to which the flow was extrapolated has been provided in Figure 28.

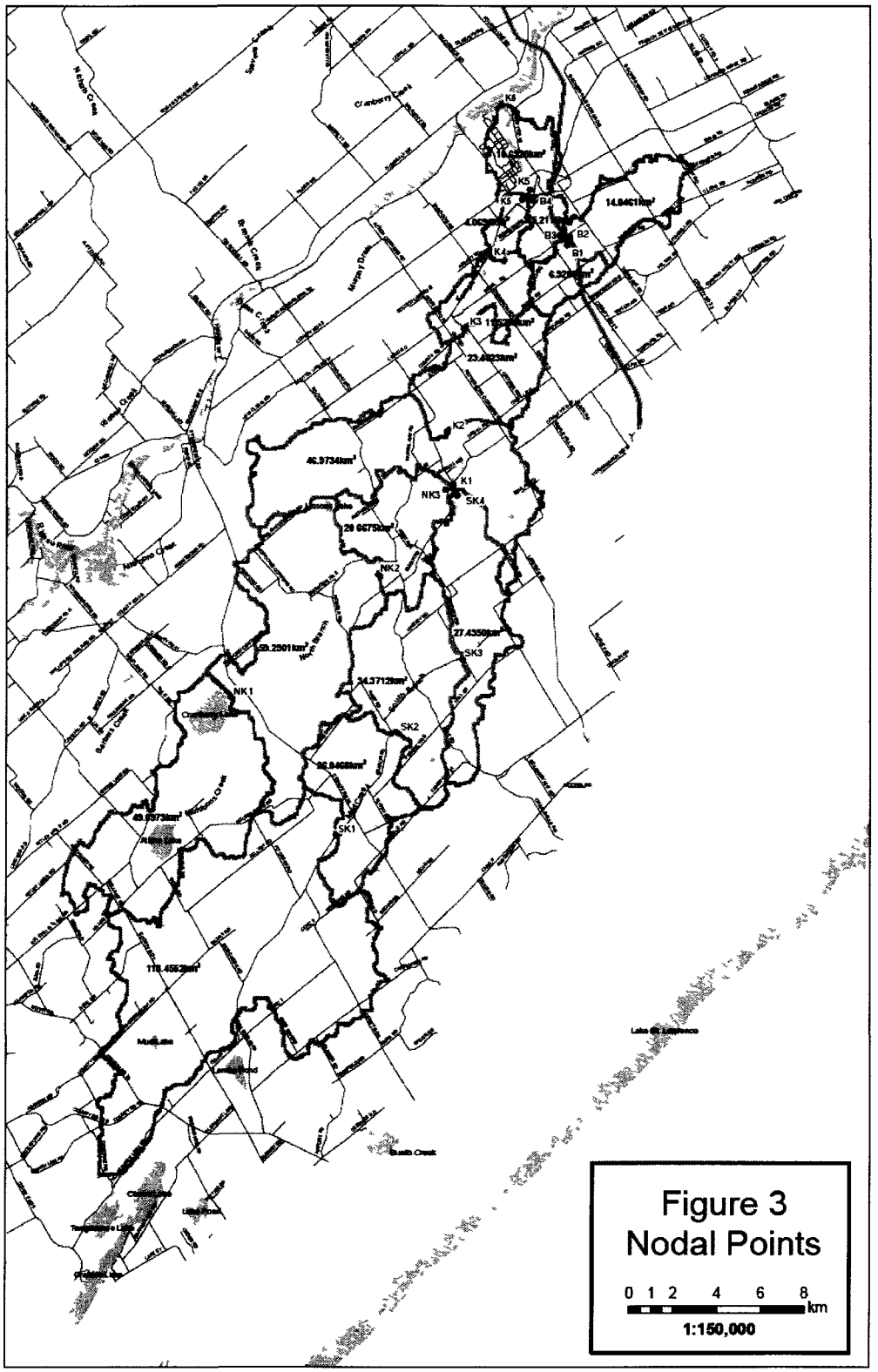

Figure 28: Kemptville Creek flow extrapolation locations (RVCA 2007)

4.5.1 *Sub-catchment Flow*

The upstream initial boundary conditions in the RVCA model were defined by the stage - discharge curve taken at the Kemptville Creek's confluence with the Rideau River. This curve, as presented in Figure 29, was extrapolated from the model and the relationship was applied to the flow data analysed in this study to obtain the initial boundary conditions.

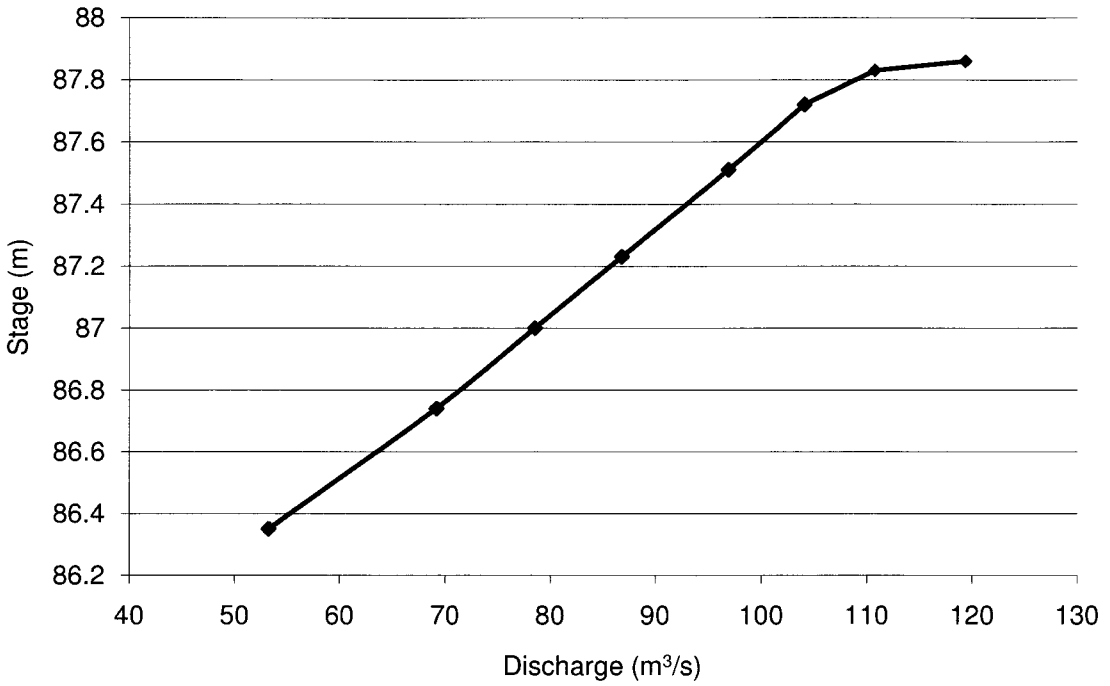

Figure 29: Stage-discharge curve of Kemptville Creek taken at the confluence of the Kemptville Creek and Rideau River

5 RESULTS

5.1 Downscaling of Climate Data

For this study the downscaling tool ASD was used to downscale GCM outputs to the catchment scale. Through the course of this study it was found that ASD was not producing results that were suitable for use. Figure 30 compares the simulated flow results of the SWAT model when it is run under observed climate data as well as ASD downscaled climate data. It shows the flow hydrographs generated by SWAT using 100 equiprobable synthetic future sets of climate data generated by ASD, along with mean of the these simulations, the observed flow hydrograph, and the flow hydrograph generated by SWAT using observed climate data. From this one can notice that the ASD driven flow data are underestimating peak flows and overestimating low flow values.

The modifications outlined in this study were applied to ASD and it was found that the model was better able to reproduce the inter-annual variability that was not captured by the original model. For example, the agreement between the observed and modeled rain days from the months of September to December in the revised model is far better than in the results produced by the original ASD model, as illustrated in Figures 31 and 32. From these figures we can see that the revised ASD model is better able to reproduce observed trends.

The impact of the revisions to ASD on the final flow results have been presented in Figure 33 and 34. Here the original ASD model and the revised version are compared through the use of box plots of the simulated peaks, and minimum, maximum, mean, and median peak flow versus observed peak flows and flows simulated with observed climate. From the box plots we can see that the variability in peak flow of the revised ASD model is much greater than that of the original model. The comparison of the ASD driven flows to observed peak flows and observed climate driven peak flows in Figure 33: Characteristics of peak flows obtained with ASD downscaled climate data sets, 1970-2001. Upper panel: box plots of simulated peaks; middle panel: minimum, maximum, mean and median peak flow versus observed peak flows; lower panel: minimum, maximum, mean and median peak flow versus peak flows simulated with observed climate. highlights that the original ASD model produced mean flow sequences that showed little variation and actually projected that means

flows will be lower towards the end of the century. The results of the revised ASD model presented in Figure 34 appears to be much better at reflecting the trends in the observed flow data and indicates an increase in mean flow towards the end of the century.

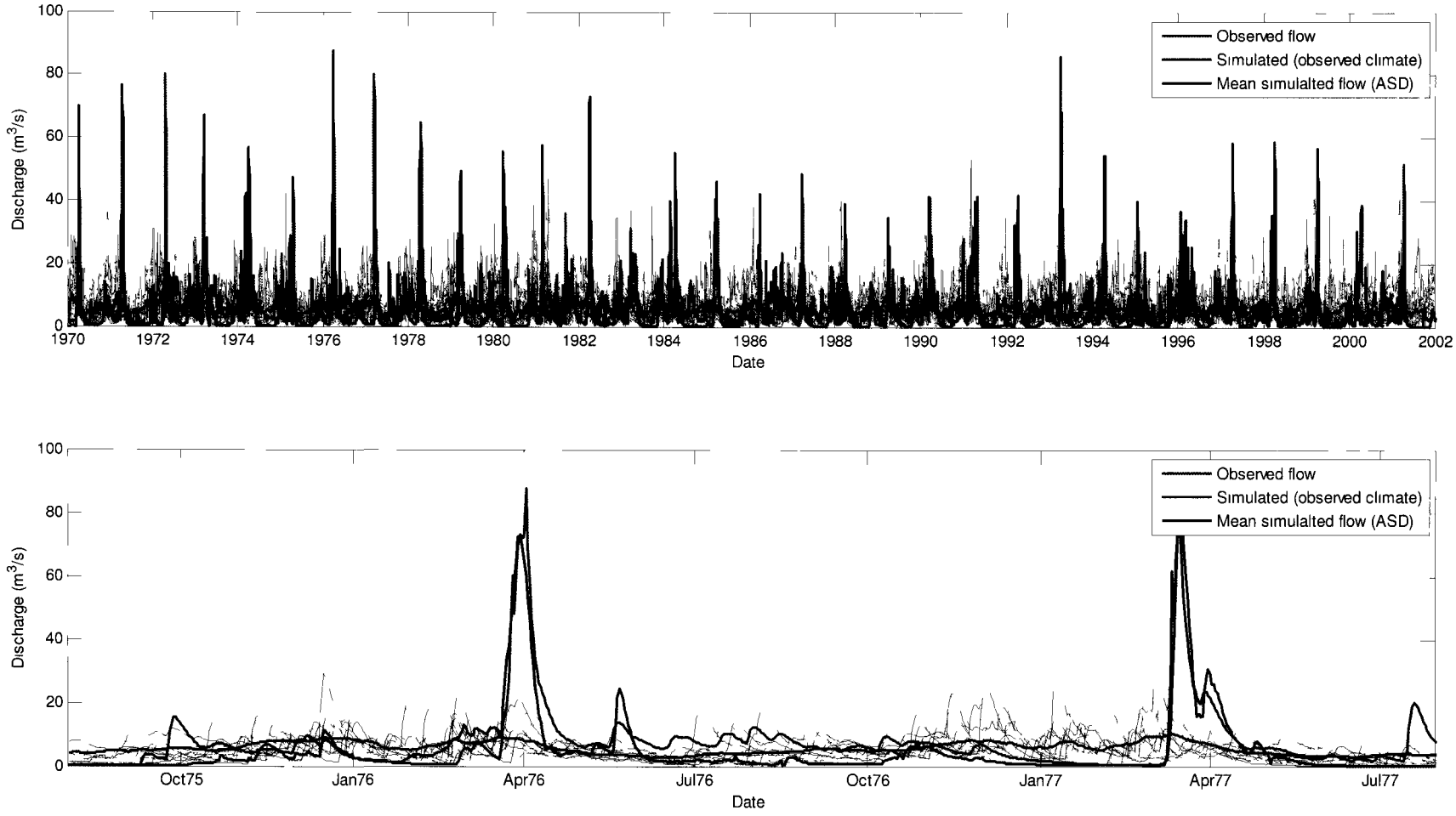

Figure 30: Hydrographs obtained with downscaled climate data sets. upper panel: 1970-2001; lower panel: 1975-1976. The thin lines represent the SWAT hydrographs resulting from the 100 synthetic ASD generated series of climate data while the thicker lines represent the observed flow, the SWAT hydrographs driven by observed climate, and the mean of the 100 ASD driven hydrographs, as outlined in the legend.

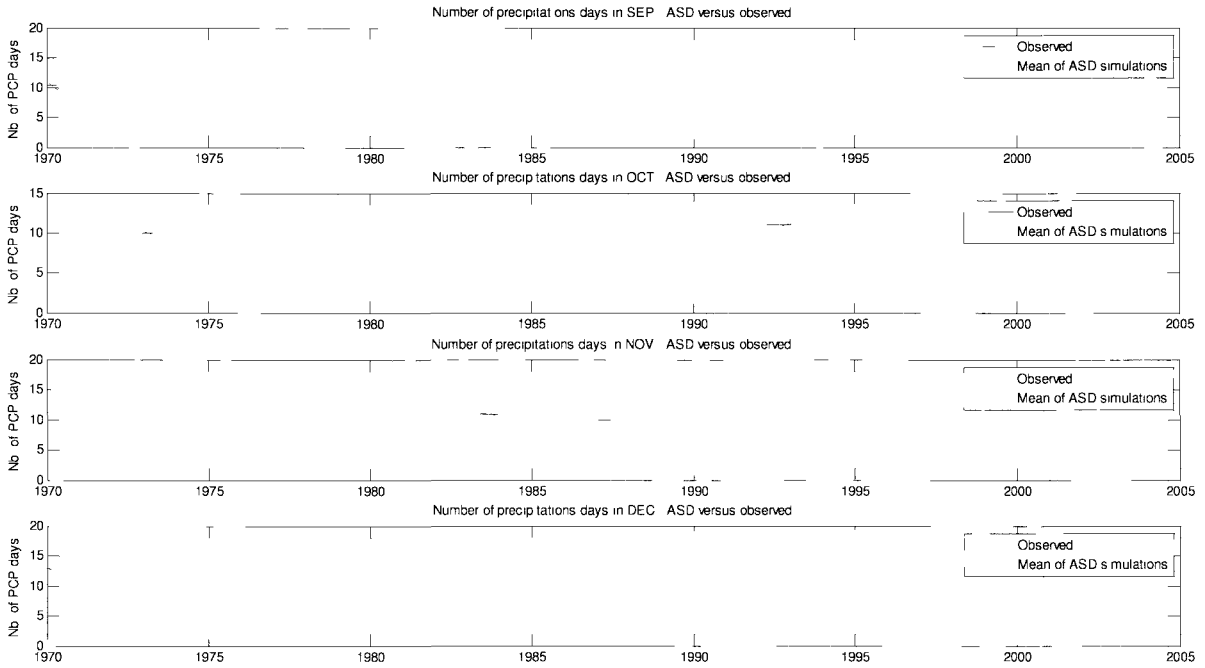

Figure 31: Average number of rain days in ASD generated scenarios versus observed number of rain days, September to December.

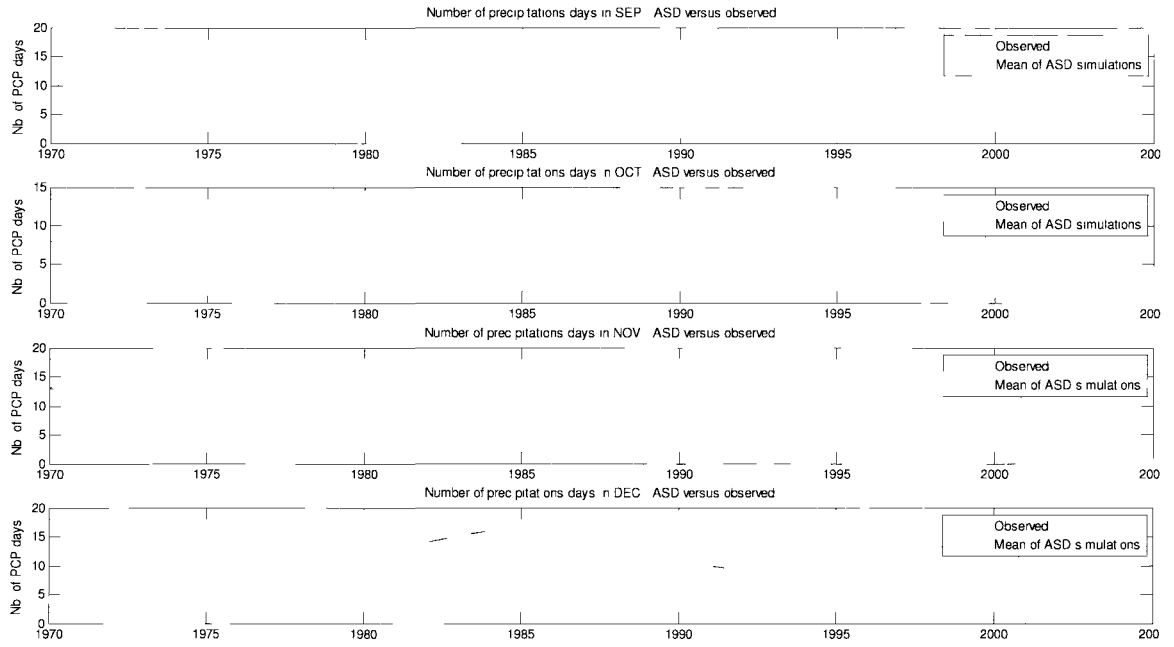

Figure 32: Average number of rain days in revised ASD generated scenarios versus observed number of rain days, September to December.

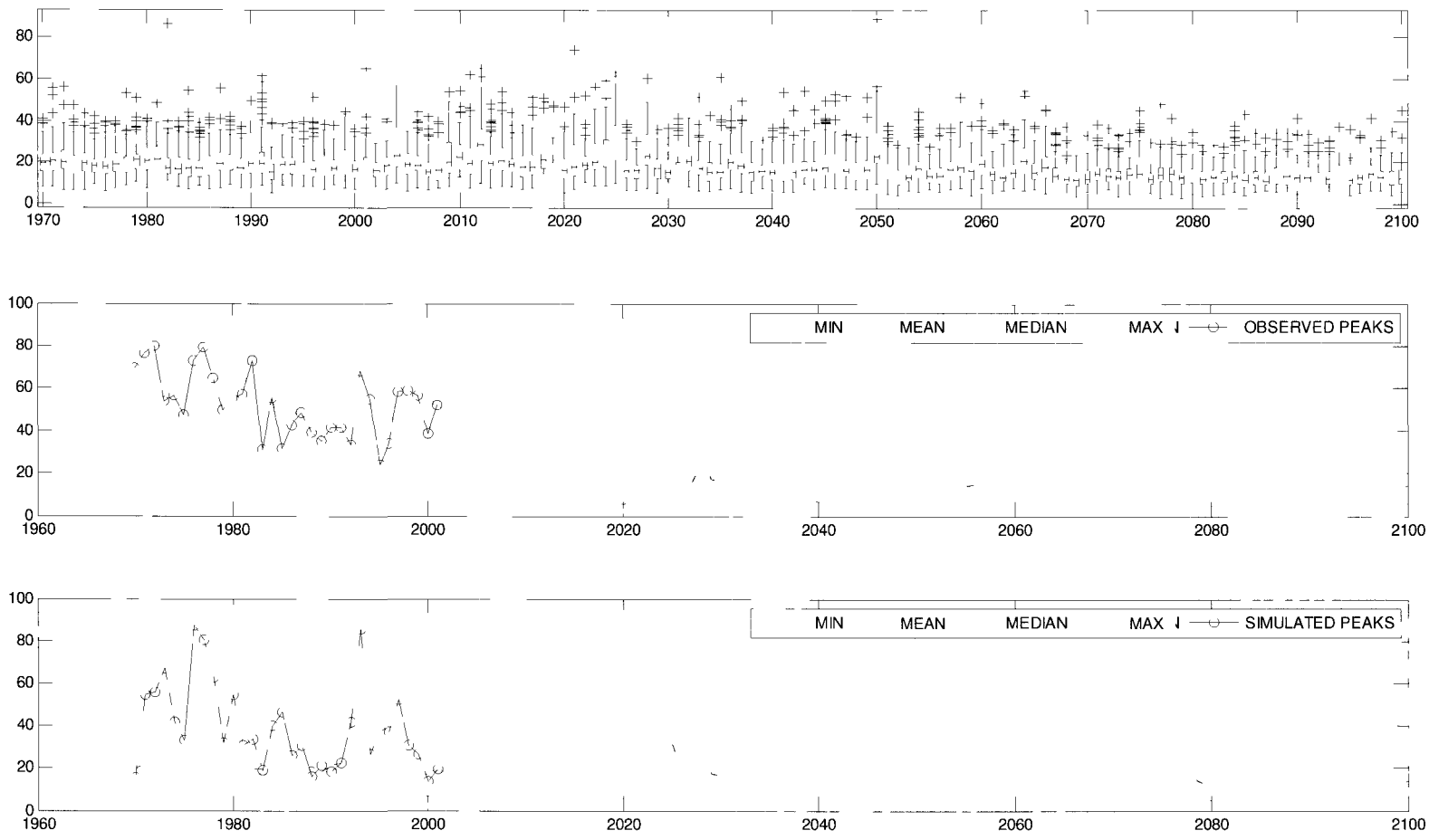

Figure 33: Characteristics of peak flows obtained with ASD downscaled climate data sets, 1970-2001. Upper panel: box plots of simulated peaks; middle panel: minimum, maximum, mean and median peak flow versus observed peak flows; lower panel: minimum, maximum, mean and median peak flow versus peak flows simulated with observed climate.

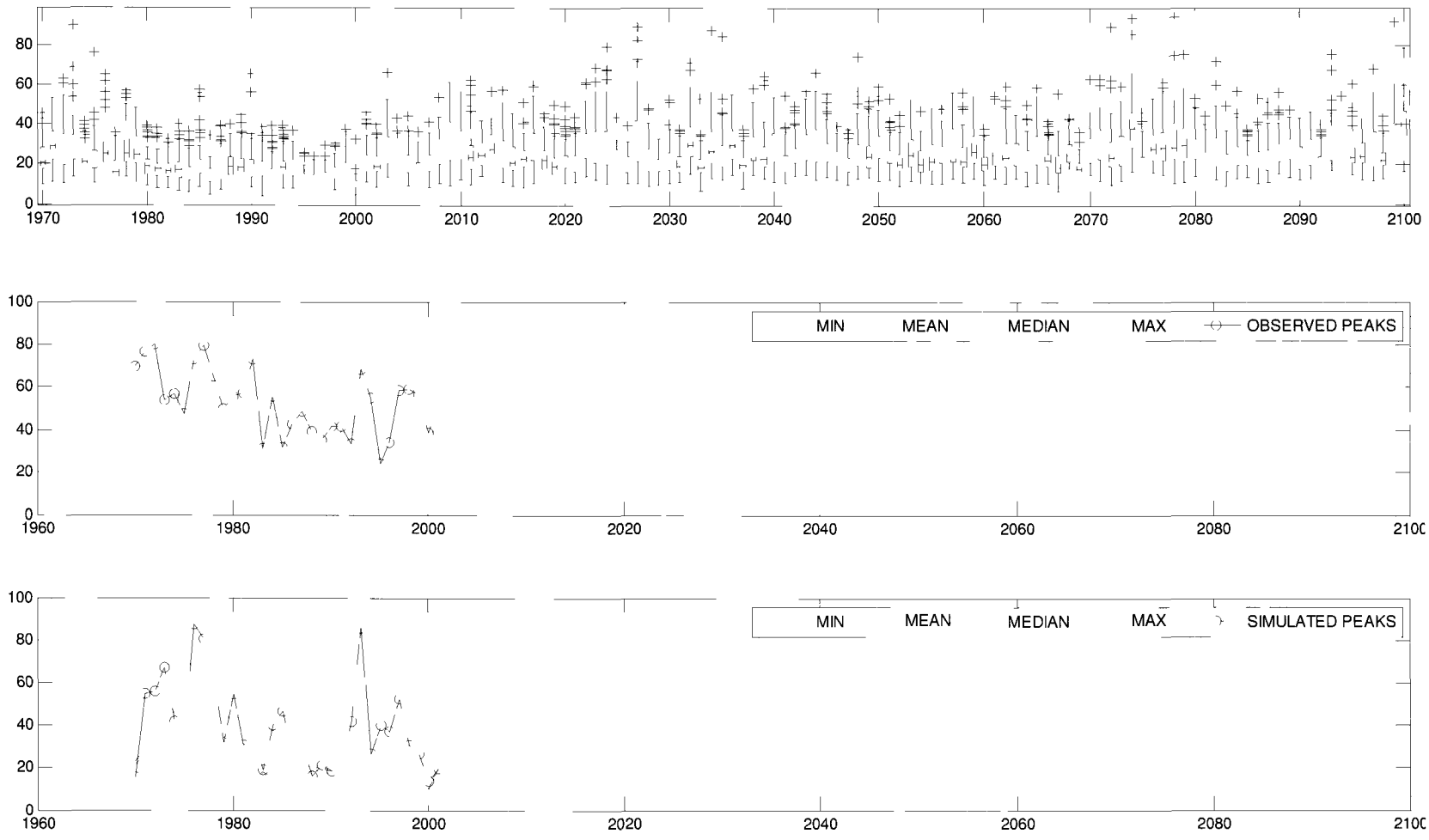

Figure 34: Characteristics of peak flows obtained with revised ASD downscaled climate data sets, 1970-2001. Upper panel: box plots of simulated peaks; middle panel: minimum, maximum, mean and median peak flow versus observed peak flows; lower panel: minimum, maximum, mean and median peak flow versus peak flows simulated with observed climate.

5.2 Extreme Flow Results from SWAT Model

The results of the SWAT modeling indicate that as future precipitation increased, mean flow in the creek would also increase. In order to assess the viability of the peak flow data obtained directly from the SWAT model, a stationary distribution was fit to the observed flow data and the simulated flow data over the period of 1970-2003. As shown in Table 11, the various return period flows generated from the results of the SWAT model are either overestimates or underestimates of the actual return period flows. Thus if an extreme value analysis were conducted directly on the maximum flow values obtained from the SWAT model during the future period, the values generated would likely also be an overestimation. It is for this reason that only the mean flow is extracted from the future SWAT model and applied to GEV.

Table 11: Comparison of peak flows as determined by observed flows and peak flows determined from the results of the SWAT analysis from 1970 to 1996

Return period (years)	Flow based on observed peaks (m^3/s)	Flow based on simulated peaks (m^3/s)
1000	93.79	163.45
100	85.67	108.08
50	82.12	93.64
20	76.28	75.85
10	70.72	63.17
2	50.29	33.91

5.3 Determining Future Flood FlowsData

5.3.1 Model Assessment

In this study, 64 models were tested and the likelihood of their results were compared using Bayes factors. The GEV model was used here in two applications, one in which the distribution of peak flows was being defined by SWAT flows driven by observed data, as would be available for past and present time series, and one in which peak flows were being defined by SWAT flows driven by downscaled climate data, as would be the case for a future time series. The optimal GEV model for each application was selected using the same procedure. The results of the top 6 D-day models as well as the more traditional stationary and linearly varying models for each application are presented in Tables 13 and 14. The results in these tables are ranked so that the model, M_k, which was able to produce results that were more likely than the reference model, M_r, was ranked the best, as outlined in Table 3.

From these results we can see that there is strong evidence in both applications that the GEV distributions which allow the parameters to vary based on mean flow are superior to both stationary models and models in which the parameters vary as a function of time. For the distribution of peak flows based on observed climate, the optimal model is the one in which the scale parameters varies as a function of the 9-day maximum mean flow and the location parameter is constant. For the distribution of peak flows based on downscaled climate, the optimal model is the one in which the scale parameters varies as a function of the 14-day maximum mean flow and the location parameter is constant. The difference in the duration of the optimal time scale window used in these applications is due to the reduction in variability comes with the use of GCM output data versus observed climate data.

Table 12: Bayes factor comparison for parameters calibrated using observed flow

M_k \ M_r		1	2	3	4	5	6	7	8	9	10	Minimum Bayes Factor	Overall Rank
1	$\mu = f(9D)$ $\alpha = \theta$	1.00	1.29	1.36	1.46	1.51	2.08	204.77	800.17	4.52	14.70	1.29	1
2	$\mu = f(7D)$ $\alpha = \theta$	0.77	1.00	1.05	1.13	1.17	1.61	158.34	618.71	3.50	11.36	0.77	2
3	$\mu = f(7D)$ $\alpha = f(7D)$	0.74	0.95	1.00	1.08	1.12	1.54	151.10	590.43	3.34	10.84	0.74	3
4	$\mu = f(8D)$ $\alpha = \theta$	0.68	0.88	0.93	1.00	1.03	1.42	139.93	546.80	3.09	10.04	0.68	4
5	$\mu = f(3D)$ $\alpha = \theta$	0.66	0.85	0.89	0.97	1.00	1.38	135.21	528.34	2.99	9.70	0.66	5
6	$\mu = f(11D)$ $\alpha = \theta$	0.48	0.62	0.65	0.70	0.73	1.00	98.26	383.95	2.17	7.05	0.48	6
7	Stationary model	0.00	0.01	0.01	0.01	0.01	0.01	1.00	3.91	0.02	0.07	0.00	51
8	$\mu = \theta$ $\alpha = f(t)$	0.00	0.00	0.00	0.00	0.00	0.00	0.26	1.00	0.01	0.02	0.00	64
9	$\mu = f(t)$ $\alpha = \theta$	0.22	0.29	0.30	0.32	0.33	0.46	45.28	176.92	1.00	3.25	0.22	18
10	$\mu = f(t)$ $\alpha = f(t)$	0.07	0.09	0.09	0.10	0.10	0.14	13.93	54.45	0.31	1.00	0.07	33

Table 13: Bayes factor comparison for parameters calibrated using simulated flow

	M_k \ M_r	1	2	3	4	5	6	7	8	9	10	Minimum Bayes Factor	Overall Rank
1	$\mu = f(14D)$ $\alpha = \theta$	1.00	1.43	1.61	1.71	1.77	1.94	124.16	121.76	207.90	4.07	1.43	1
2	$\mu = f(18D)$ $\alpha = \theta$	0.70	1.00	1.13	1.19	1.23	1.36	86.58	84.91	144.97	2.83	0.70	2
3	$\mu = f(19D)$ $\alpha = \theta$	0.62	0.89	1.00	1.06	1.09	1.21	76.96	75.47	128.85	2.52	0.62	3
4	$\mu = f(5D)$ $\alpha = \theta$	0.59	0.84	0.95	1.00	1.04	1.14	72.80	71.39	121.90	2.38	0.59	4
5	$\mu = f(14D)$ $\alpha = f(14D)$	0.57	0.81	0.91	0.97	1.00	1.10	70.31	68.94	117.72	2.30	0.57	5
6	$\mu = f(17D)$ $\alpha = \theta$	0.51	0.74	0.83	0.88	0.91	1.00	63.84	62.60	106.89	2.09	0.51	6
7	Stationary model	0.01	0.01	0.01	0.01	0.01	0.02	1.00	0.98	1.67	0.03	0.01	60
8	$\mu = \theta$ $\alpha = f(t)$	0.01	0.01	0.01	0.01	0.01	0.02	1.02	1.00	1.71	0.03	0.01	58
9	$\mu = f(t)$ $\alpha = \theta$	0.00	0.01	0.01	0.01	0.01	0.01	0.60	0.59	1.00	0.02	0.00	62
10	$\mu = f(t)$ $\alpha = f(t)$	0.25	0.35	0.40	0.42	0.43	0.48	30.54	29.95	51.14	1.00	0.25	17

In this study the results of GEV distribution vary according to the design life of the structure and the year of construction. A comparison of the 2 and 10 year return period flows for a structure with a 20 year design life constructed between 1970 and 1982 has been presented in Figure 35. Here the empirical Weibul plotting position has been included to illustrate the true distribution based on observed data as well as the results of three GEV models; at stationary model using observed peak flows, a stationary model using peak flow directly from the ASD driven SWAT hydrograph, and a non-stationary model using peak flows based on ASD driven SWAT simulated mean flow. We can see the proposed non-stationary model does a better job than the stationary analysis in tracking the trends the observed distribution. The stationary observed distribution is one in which the parameters were calibrated based on the observed data taken from 1970-2004 and hence the T-year return period flow remains constant in time. This figure also shows how the use of simulated peak data obtained directly from the SWAT model again leads to an underestimation of extreme events.

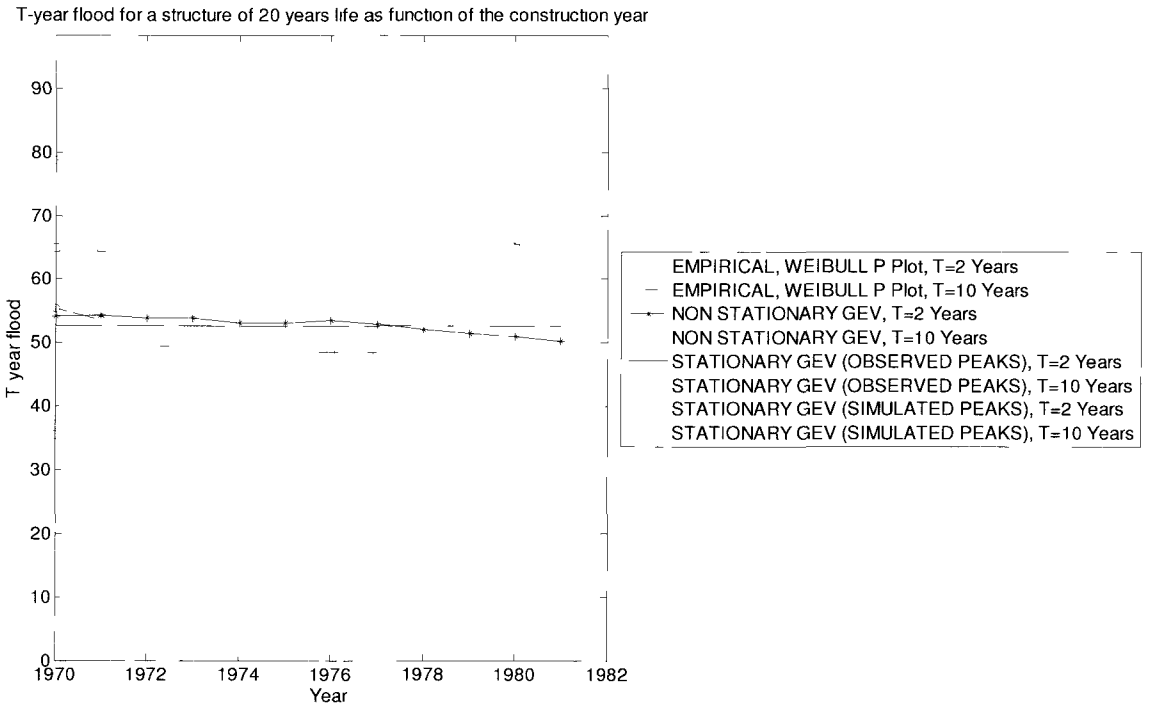

Figure 35: 2-year and 10-year floods on a 20 year sliding window using the non-stationary GEV distribution, the stationary distribution and Weibull plotting position

An example of the results from future GEV distribution as applied to an engineering work constructed with a 50 year design life has been provided in Figure 36. It should be noted that the sharp jumps in flood flows that can be observed at higher return periods are the result of the gradual exaggeration of small shifts in the future climate window.

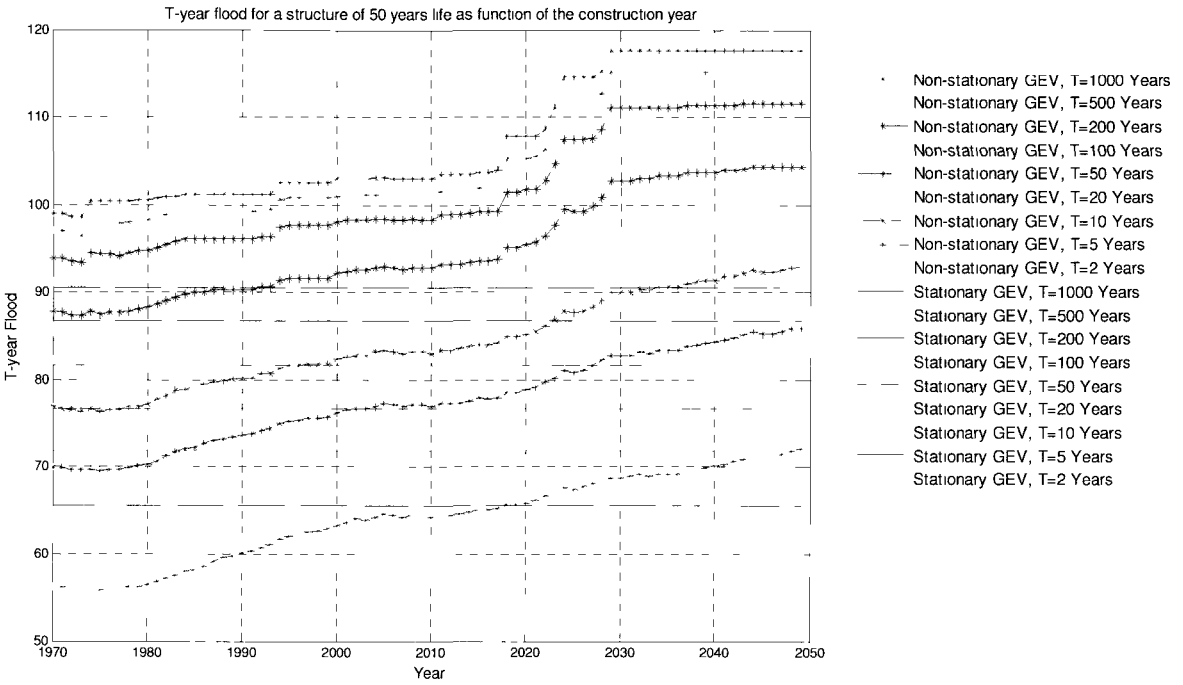

Figure 36: 50-Year design life GEV

From this figure we can see that using the stationary analysis can vastly underestimate the design flows associated with various return periods in the future. A comparison of these flows, as presented in Table 14, illustrates that difference between these two models is approximately 25% for a 100-year event.

Table 14: Comparison of the results of stationary and non stationary GEV assuming project with a 50 year design life being constructed in 2050

Return period (years)	Stationary Model (m^3/s)	Non-stationary Model (m^3/s)	Difference (%)
2	52	72	43%
10	71	92.5	31%
20	78	99	30%
50	82	104	27%
100	85	108.5	28%
1000	91	118	30%

The year of construction can also play a large role in the degree to which an engineering work will be impacted by climate change. In Table 15, the design flows for the same structure constructed in 2000 and 2050 are compared. From this analysis we can see that between these two frames the average return period flow can be expected to increase from 12% to 15%.

Table 15: Comparison of the results of the non-stationary GEV distribution

Return Period (years)	Built in 2000 (m^3/s)	Built in 2050 (m^3/s)	Difference (%)
2	63	72	14%
5	76	86	13%
10	83	93	12%
20	87	99	14%
50	92	104	13 %
100	96	108	13%
200	98	112	14%
500	101	116	15%

5.4 Evaluating the Impacts of Future Flood FlowsData

The calibrated HEC-RAS model obtained from the RVCA was used to generate water surface elevations from the future flow data obtained from the non-stationary GEV analysis. Table 16 provides a comparison between the predicted flood flows at the Kemptville Creek gauge station as determined by the RVCA's flood frequency analysis and the results of the stationary GEV flood frequency distribution from the present study based on a structure constructed in 2050 with a 50 year design life. From this table we can see that the flows generated from the two methods are within a comparable margin.

Table 16: Comparison between results of RVCA stationary flood frequency distribution and the results of our stationary GEV

Return Period (years)	RVCA (m^3/s)	Our Model (m^3/s)	Difference (%)
2	49.7	52	4.63%
5	65.2	66	1.23%
10	73.9	71	3.92%
20	81.3	78	4.06%
50	89.7	82	8.58%
100	95.1	85	10.62%
200	100	87	13.00%
500	106	89	16.04%

Based on the Provincial Policy Statement under the Planning Act, the regulatory flood for regions within the RVCA's jurisdiction is the 1:100 year flood event. For this reason it was decided that the future 1:100 year flood event would be analysed with the HEC-RAS software package based on the distribution produced in Figure 36. These extreme flow values were extrapolated to other points throughout the watershed using the method of area prorating. The results of these calculations for various return periods have been presented in Table 17.

Table 17: Result of extreme flow extrapolation

Subcatchment		Return Period, Flow (m^3/s)							
ID	Area	500	200	100	50	20	10	5	2
K1	330.96	98.05	94.67	91.29	87.91	83.68	78.61	72.70	60.86
K2	377.94	108.46	104.72	100.98	97.24	92.57	86.96	80.41	67.32
K3	401.34	113.53	109.61	105.70	101.79	96.89	91.02	84.17	70.47
K4	412.87	116.00	112.00	108.00	104.00	99.00	93.00	86.00	72.00
K5-	416.94	116.87	112.84	108.81	104.78	99.74	93.70	86.64	72.54
K5	443.72	122.53	118.30	114.08	109.85	104.57	98.24	90.84	76.05
K6	454.42	124.77	120.47	116.16	111.86	106.48	100.03	92.50	77.44

Once applied to the Hec-RAS model, the resulting upstream water surface profiles at various locations along the Creek were generated. For this study the author has selected 3 sample cross sections and compared the results to those obtained in the study conducted by the RVCA. These cross sections have been presented in Figures 37 to 42. In general one can see that the water surface depth during a 100-year flow event at these cross sections will increase by approximately 6 – 12 cm in the future. The remainder of the cross sections generated by HEC-RAS are presented in Appendix C.

As seen in Figure 37 and Figure 38 however, even this small change in elevation can lead to flooding issues. At this cross section the increase in the 100-year water level could lead to the Creek topping its banks and lead to the development of a second flow channel to the right of the bridge. While the anticipated flow depth in this channel is minor (approximately 4 cm), introducing flow to this new area could lead to increased erosion, which could ultimately undermine the bridge. The increase in the energy grade line elevation could result in dangerous flow conditions immediately upstream of the bridge as flow levels could be within 2 cm of the bottom of the bridge deck.

Figure 39 and Figure 40 illustrate the increase in water level depth expected at the Oxford Mills Dam. Here the increase in both the water level depth and energy grade line is greater than in the previous cross section. The greater increase here is likely due to downstream conditions as the width of the creek decreases significantly in that area.

Figure 41 and Figure 42 illustrate a cross section taken from an area located south of Hutchins Corners. One can see that in both RVCA study and the present study the elevation of the 100-year water is higher than the right abutment of the bridge located at this cross section. In this area one can notice that increases in the 100-year flow event will likely merely serve to exasperate existing issues with local infrastructure.

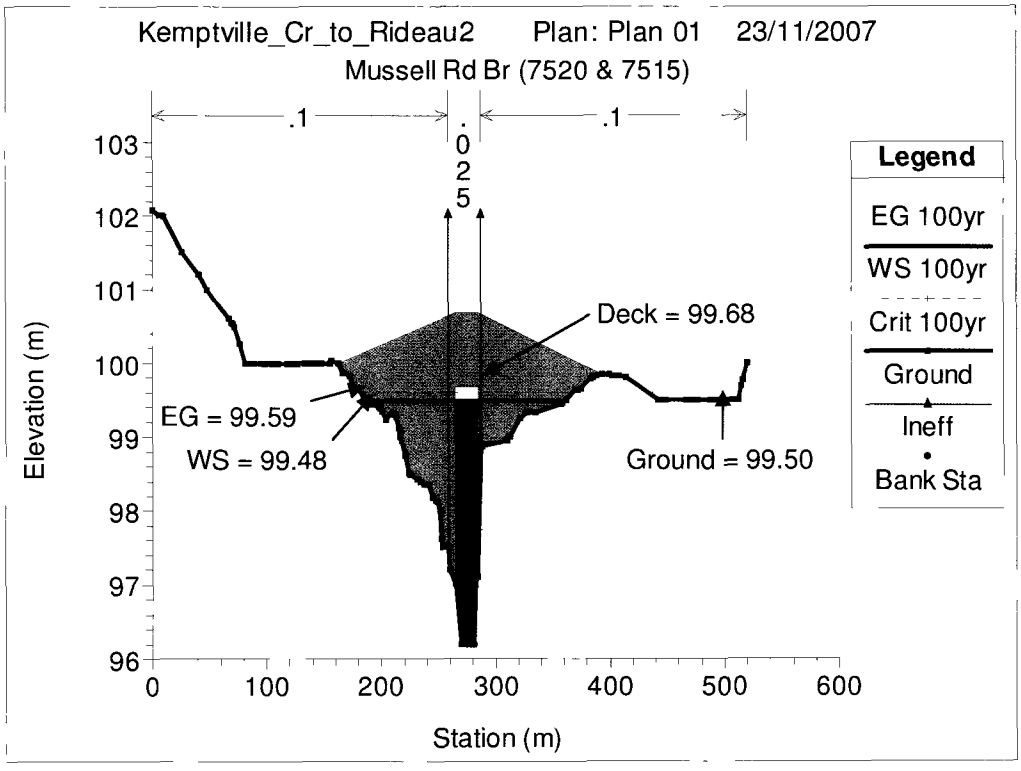

Figure 37: Hec-RAS cross-section at Mussell Rd Bridge under RVCA analysis

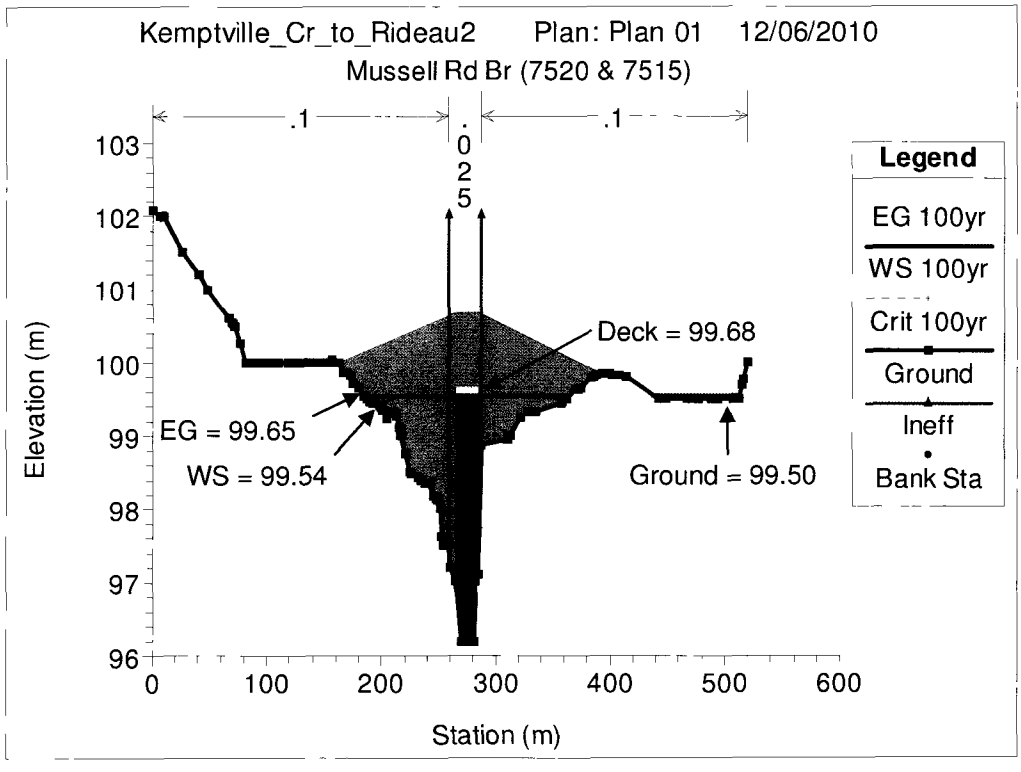

Figure 38: Hec-RAS cross-section at Mussell Rd Bridge under future analysis

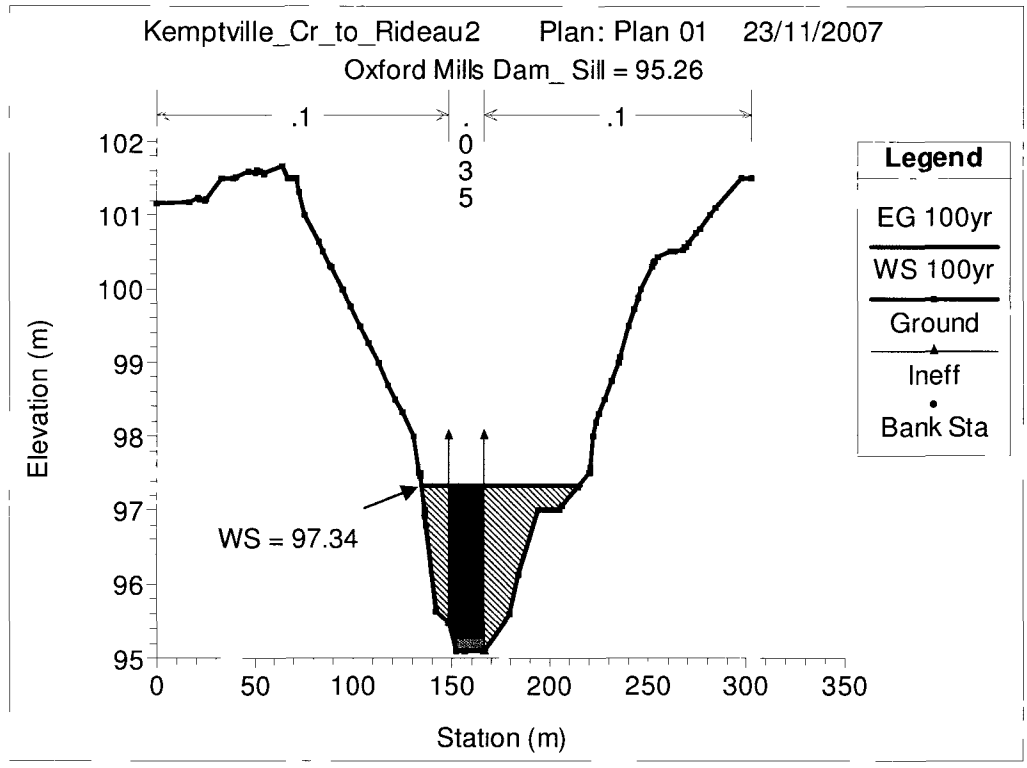

Figure 39: Hec-RAS cross-section at Oxford Mills Dam under RVCA analysis

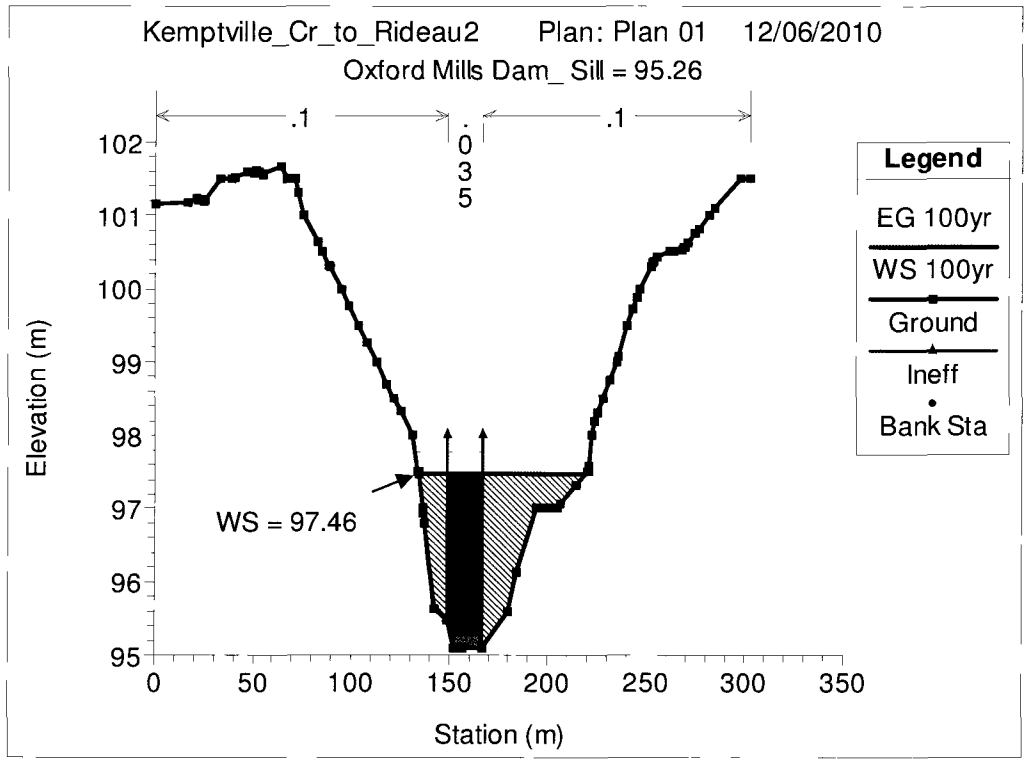

Figure 40: Hec-RAS cross-section at Oxford Mills Dam under future analysis

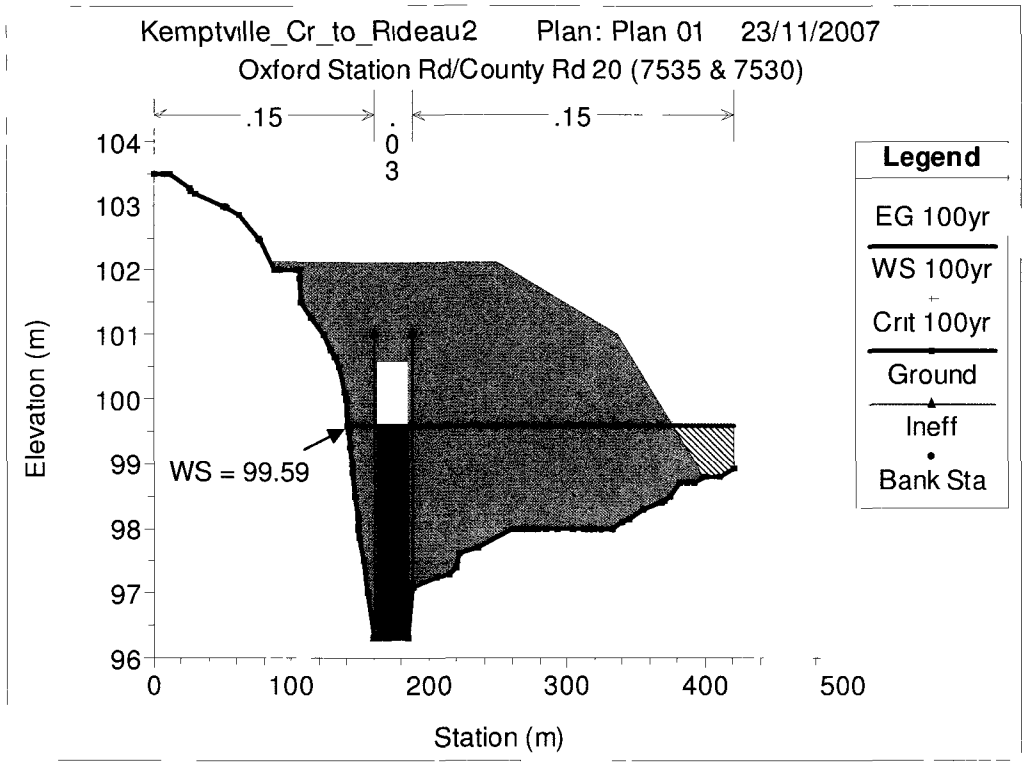

Figure 41: Hec-RAS cross-section at Oxford Station Road Bridge under RVCA analysis

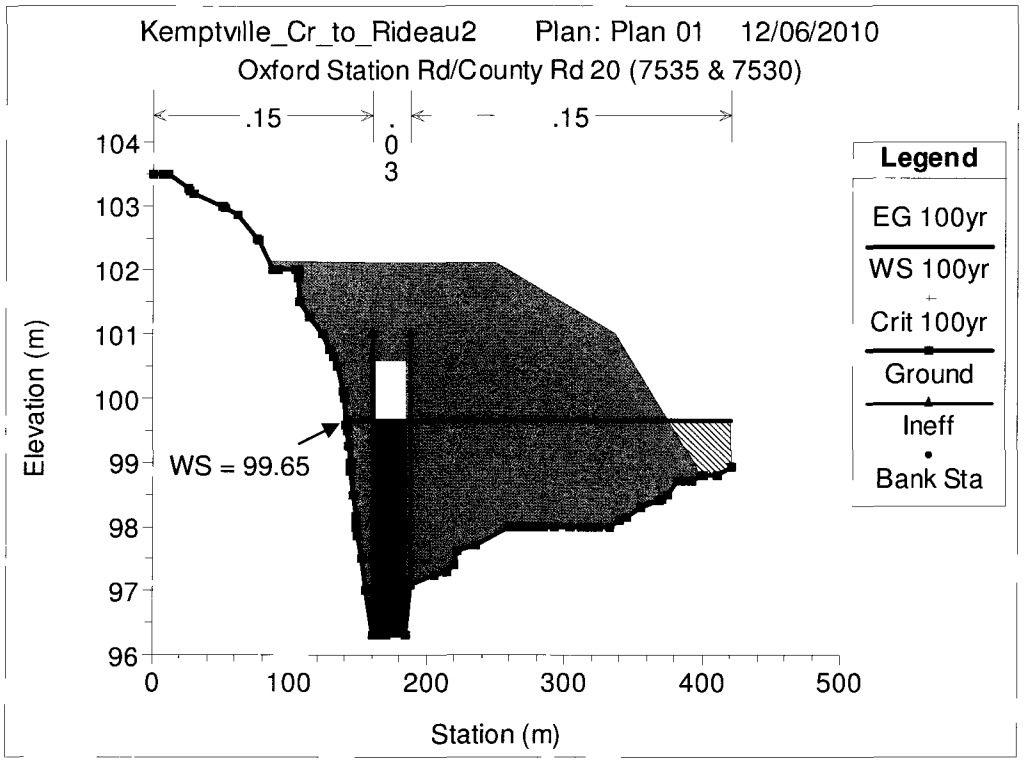

Figure 42: Hec-RAS cross-section at Oxford Station Road Bridge under future analysis

6 DISCUSSION

The possible impacts of climate change continue to be a hotly contested issue among many groups of scientists, engineers and decision-making bodies. While many in the science and engineering field feel that the impacts will be significant, there remains disagreement as to how best quantify the extent of these impacts. There remain many aspects of the climate modeling process that introduce unnecessary error or assumptions that only serve to decrease the overall confidence in the final result. In this study the author attempts to reduce some of that error by following an approach which allows the distribution of future extreme events to be tied to the results of GCM. Through this approach one removes the uncertainty that can be introduced when artificial assumptions as to the future trend of climate change are applied to extreme value analysis. Here the trend used to analyse future extreme value distributions will be dictated by the results of physically based GCM under a chosen emission scenario. As GCM model data are readily available and widely used it is felt that its inclusion will likely increase the reliability and applicability of the analysis.

6.1 Climate Change Modeling

The methodology proposed in this study involves the application of downscaled GCM output to a non-stationary extreme value distribution. It is felt that through this application the non-stationary trend of the distribution will be better defined and thus more likely to produce a more realistic result. This study was carried out in six main stages; a SWAT model was calibrated and validated using observed data, GCM outputs were downscaled to a local scale and applied to the SWAT model, the optimal D-day flow was extracted from the present and future simulated flow series, a probability distribution was calibrated based on present simulated flow and applied to the future flow series, and finally future extreme flow values were routed through a hydraulic model.

Although other studies have examined the impacts of climate change using one or more of the elements covered in this thesis, none could be found which utilized them all. The author believes that using the approach proposed in this study maximizes the strengths of these elements while

minimizing the possible error that is inevitably introduced when using one or more of these elements by themselves. A discussion of each of the elements utilized by this study is presented below.

6.1.1 Downscaling of Climate Data

For this study the ASD downscaling tool was used for the downscaling of CGCM3.1 climate modeling data resulting from the application of the A2 SRES climate change scenario. Downscaling of climate data are required because generally GCMs are operated on grids with a very coarse resolution and as such they can't be applied directly to the study area. Statistical downscaling models such as ASD establish a relationship between past local climate and past GCM outputs and extend this relationship into the future to generate future local climate series from future GCM output. It was found that the preliminary results obtained from the ASD tool were unsuitable for application in this study and therefore modifications of the equations used by the tool were undertaken. These modifications improved the responsiveness of the ASD model to local trends such as the number of rain days and produced what was thought to be a more reasonable result. The improved variability in mean flow observed in the revised model results was the main driver for deciding to go forward with the revised ASD model, as future mean flow prediction is ultimately the most important output from the rainfall-runoff modeling.

ASD itself is a fairly new downscaling tool that was developed in Quebec and is based heavily on the SDSM downscaling approach developed by R.L. Wilby. ASD sought to simplify the SDSM model and make it increase its ease of use for people with limited experience in the downscaling of climate data. It accomplished this by automating the statistical downscaling process; instead of requiring user input along the downscaling process, such as determining which downscaling parameters should be selected based on correlation to observed data, the ASD model does all of these steps internally. It works almost like a black box where the inputs are given to the program along with a few modeling preferences and it then outputs the desired number of downscaled climate scenarios. The problem with this approach, however, is that with reduced user interaction, it becomes more difficult for a user to get a feel for the quality of the downscaled data. The degree of correlation between the selected parameters and the observed data are not directly apparent in the ASD model and can lead the user to extract the output

without gauging its validity. As this field is expanding and more catchment scale studies are being undertaken by local government and private agencies, it is important that these models clearly highlight the degree of confidence one should have in the results. It also highlights the user's responsibility to analyze and scrutinize the model output to ensure that the investigation being undertaken is as reliable as the current modeling allows. It is felt that the adjustments made to the ASD tool in this study improve the overall reliability of the model and as such should be considered for inclusion in subsequent versions of the software package.

6.1.2 Rainfall-Runoff Modeling

The hydrologic rainfall-runoff model SWAT was used to analyse the rainfall runoff patterns of the selected catchment and transform the downscaled climate data into flow data. Rainfall-runoff models are traditionally not able to accurately reproduce peak flow events but generally have much better reliably in the capturing trends in mean flow. This is mainly due to the fact that these models are usually calibrated using mean flow data and the equations and variables selected for calibration generally aren't able to accurately capture peak flow trends. The approach taken in this study avoids this issue by using the results of the SWAT model in conjunction with a GEV distribution which is better suited for peak flow predictions.

The model was generated using inputs obtained from the WaterBase organization website and was calibrated/validated using 27 years of mean monthly flow data obtained from the Kemptville Creek hydraulic monitoring station. The model was found to provide better results when operated on a monthly time scale as opposed to a daily time scale, which is not uncommon for physically based models such as SWAT as they generally perform better in reproducing long term trends over short term variability. The R^2 value for the monthly calibration period was 0.84 and 0.77 for the validation period. In other words the model was able to account for 84% and 77% of the variability in the observed data during the calibration and validation periods, respectively. It was felt that these values indicated that the model was suitable for application to this study. While the relative error of approximately 36% observed during calibrated and validated was not as encouraging, it was felt that these values were inflated and did not truly represent the quality of the model as low flows are known to have higher errors.

The calibrated SWAT model was then run under the application of 100 synthetic climate data sets for the future period of 2011 to 2100. From this modeling 100 simulated hydrographs were produces, each with an equal likelihood of occurrence. The mean of all these scenarios was then taken and this flow series was then applied to the calibrated GEV model to generate future peak flow data series. As the main goal of the SWAT modeling was to establish a reasonable mean flow prediction for the future, it was felt that taking the mean of 100 possible hydrographs would be the most effective way to establish the future mean flow trend.

With the increasing availability of higher quality inputs for use in these GIS based rainfall-runoff models, hopefully it will allow more regions to develop models capable of capturing the hydrologic process taking place within their watersheds. These models can be key in assessing what impacts different climatic changes may have on individual watersheds. While it is likely not feasible for all watersheds to be modeled for every scenario, a sporadic sampling of regional watershed models could be useful in assessing which areas are more susceptible than others to changes in precipitation and temperature. Areas requiring more attention can be identified and examined in greater depth.

6.1.3 Non-stationary Probability Distribution

In an attempt to select the distribution model that would best be able to reproduce future flood frequency distributions under a changing climate, 64 GEV models were compared for this study. These models included the traditional stationary approach, where all three parameters of the GEV distribution remained constant with time, a linear trend approach, where either/both the scale and/or the location parameters would vary linearly with time and the remaining parameter(s) would be constant, and the proposed approach, where either/both the scale and/or the location parameters would vary linearly with the annual D-day mean flow and the remaining shape parameter would remain constant. The models which examined the parameters as a function of flow each had a different time scale over which the D-day flow was taken, ranging from 1 day to 20 days. It was found that the model with the greatest likelihood of reproducing observed maximums from observed flow was the model where the location parameter varied linearly with the maximum annual 9-day mean flow and both the scale and shape parameters would be constant. The model with the greatest likelihood of reproducing

observed maximums from simulated flow was the model where the location parameter varied linearly with the maximum annual 14-day mean flow and both the scale and shape parameters would be constant. The observed flows required a longer D-day averaging period due to the fact that when using downscaled data the peak events are not reproduced as well and such have a better correlation with the average flow over a longer time window. Through this mechanism of parameter variation, GCM outputs are able to be incorporated into the trend of the distribution.

The maximum mean annual D-day flow was taken from the results of the SWAT model run under downscaled climate data and used to define the location parameter of the extreme value distribution associated with that year. Allowing the GEV distribution to predict peak flows based on mean flows values eliminates the need to apply an external trend to the distribution which in general reduces the amount of assumptions a modeller must make in such an analysis. In assessing the validity of our approach, the results of the GEV distribution calibrated using SWAT flow generated under observed climate data was compared to the Weibul plotting position. From this it was observed that the proposed GEV model was better than the traditional stationary approach in reproducing observed trends as reproduced by the Weibul distribution.

In this thesis the calculation of the future GEV distribution was set up so that the design life of the structure would be taken into account in as far as the resulting return period flood flows would represent associated risk over the entire design life of the structure. This concept could be especially useful in the field of consulting engineering where presently small scale engineering works such as stormwater management ponds, culverts, and other overland conveyance systems are generally being designed using flows generated from precipitation values obtained from a single stationary IDF curve that was derived in the 1990's from data ranging back to the 1970's and earlier. Regardless of the design life of these works or the year they are constructed, presently most designs are all being based on the past conditions, not the future. With municipalities like Peterborough, Ontario, facing two 100-year or greater storm events within a 2 year period between 2002 and 2004, perhaps the validity of these stationary distributions should be assessed both under present conditions and in the future. The consequences of under designing such small scale engineering works can be great because these works are the foundation of the overland flow routing system. Unlike large scale hydraulic structures, small scale works are implemented in great quantity across every established community. Once these

mechanisms are exceeded, issues of flooding, property damage, and damage to the mechanisms themselves arise which can prove to be both very detrimental and very costly. The same applies to the delineation of flood plains. Structures are presently being constructed just beyond the border of the 100-year flow level as if the 100-year water level elevation is as stationary as the building. While this may hold true in the near future, the risk of that structure failing varies over its lifespan if it subjected to a changing climate and the actual occurrence interval at which it may fail with also vary.

While the application of future flood frequency distributions generating based on design life would be of good use in the basic examples given above, its application to large scale engineering works such as bridges and dams is significantly more critical. In these works the implications of failure are much more dramatic and beyond being merely costly, failure of these structures can result in the complete destruction of entire communities and the loss of human lives.

While this thesis attempts to analyse the impacts climate change on peak flow events, it should be noted that the impact of climate change on mean flow levels can be just as important. Many constructed wetlands and other stormwater management faculties are designed based on an assumed ability of the attributing catchment to generate enough runoff to maintain the permanent storage volume of the facility. This water level is designed to ensure that proper settling and pollutant removal can be achieved by the facility so that the effluent can meet the required standards for quality. Wetlands also rely on their permanent pools to support aquatic life and plant growth. Under a changing climate mean flows may decrease in certain areas, including the Southern Ontario region, which may lead to lower permanent pool volumes and in turn could lead to lower water quality in the area and lower ecological diversity. Lower lake levels can have very costly effects on navigation and hydropower production. Not only can the hydroelectric power generating potential be decreased due to the lower head levels, but the efficiency of turbine may also be impacted as the system many no longer be operating within the designed peak efficiency conditions. Overall this could lead to decreased revenue and increased demand upon other sources of energy.

6.1.4 *Hydraulic Routing of Flood Flows*

This study utilized an existing HEC-GeoRAS model of the study area produced by the RVCA to conduct the hydraulic modeling of the projected future flood flow values. The model was initially run by the RVCA based on the results of a single site stationary flood frequency analysis, conducted at the same site used for this study, the Kemptville Creek hydraulic monitoring station. The present study followed an approach similar to that taken by the RVCA where the method of area prorating was used to distribute the peak flood flows from the single site throughout the watershed.

The fact is that as more local municipalities or conservation authorities develop better models of their regional watershed and hydraulic systems, the better they will ultimately be able to assess any impacts that a change in peak flows will bring and allow for better mitigation approaches to be developed and tested. In fact many of the previously constructed models already developed for this area could be used in an approach similar to the one outlined in this study to assess local impacts of different climate change scenarios.

6.2 **Regional Impacts**

One of the underlying aspects of climate change impact assessments is need for regional based studies. Different regions will see different changes in climate over the coming decades and regions will react to these changes in different ways. It is important to examine the impacts on a local scale to assess what possible risks could be encountered and what local mitigation is required, if any.

In this study the impact of climate change on the Kemptville Creek watershed was assessed. A detailed analysis was conducted for the area using a sample design scenario assessing the 100-year design flow for a structure with a 50-year design life, such as a culvert under a major roadway or a small outbuilding. The results of this study suggest that the 100-year design flow under the A2 SRES scenario for such a structure would result in a flow increase from 95.1 m^3/s to 108.5 m^3/s, an increase of 10%, over the present RVCA modeling results if the structure was constructed in the year 2050.

6.2.1 *Impact on Regulatory Flood Levels in the Kemptville Creek*

While the Kemptville Creek watershed is sparsely populated, a few small towns and villages are located along the banks of the Kemptville Creek. From the results of the Hec-GeoRAS analysis, the 100-year floodplain maps for three small developments within the Kemptville Creek watershed were produced based on the sample design scenario mentioned above. The floodplain maps of the Kemptville, Oxford Mills, and a development south of Hutchins Corners have been provided in Figures 43 to 45. Included in these maps is the approximate level of inundation at structures located within the floodplain that can be expected to occur based on this study's findings. These inundation depths were based on the difference between the DEM elevation and the uninterpolated water level elevation values and therefore many not necessarily correspond exactly to the interpolated extents of the Creek displayed in the mapping. Discrepancies between the actual banks of the Creek and the plotted 100-year stream flow extents are mainly the result of interpolation errors. These errors are usually corrected through the application smoothing techniques but this process was not applied here due to the preliminary nature of this study.

The floodplain map of the Kemptville region (Figure 43) illustrates that approximately 9 structures will be impacted by flood waters during the 100-year storm event. These structures, ranging low significance rear yard buildings such as shed to commercial and residential properties, could face inundation levels of 0.3 m to over 2 m.

The floodplain map of Oxford Mills (Figure 44) illustrates that approximately 8 structures will be impacted by flood waters. Again these structures include mostly outbuildings along a few residential properties and inundation levels are mainly in the 0.4 m to 1.4 meter range. The Oxford Mills Dam is located on this map just southeast of the main bridge though town.

The floodplain map of the area just south of Hutchins Corners (Figure 45) illustrates that only a few structures will be impacted by flood waters that and level of inundation expected at these structures is below 0.3 m. This map does illustrate, however, that the extents of the Creek at the north bridge go well beyond the banks of the river. The water level profile can be seen in Figure 42.

In general these impacts were not found to have placed much additional stress on the existing system. It should be noted, however, that due to the degree of uncertainly introduced by various inputs and process throughout application of this analysis, this type of study should be used as more of a rough gage as to the overall region impacts of climate change and less as an exact determination as to how climate change may impact a specific reach of the river.

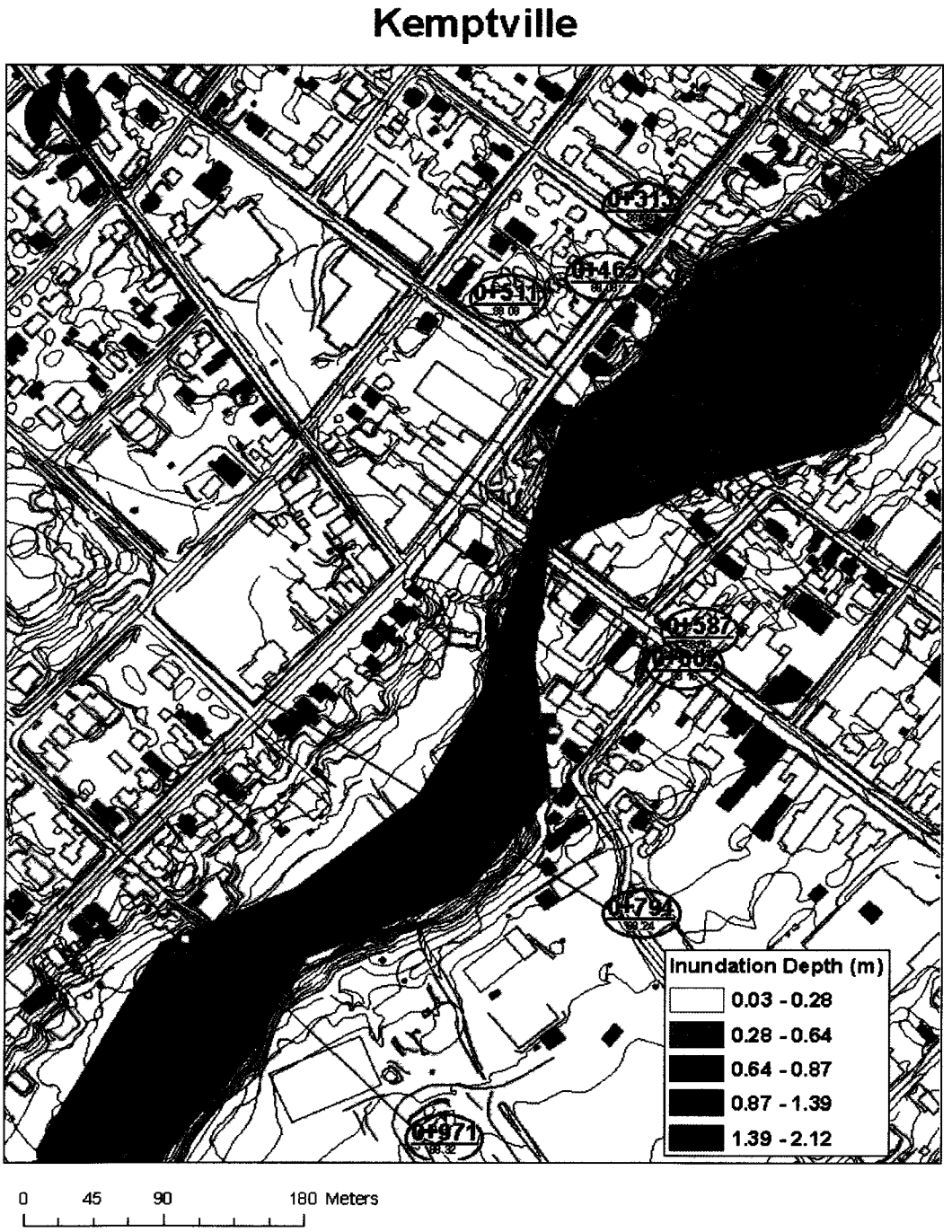

Figure 43: 100-Year Floodplain map for Kemptville based on a structure with a 50 year design life constructed in 2050

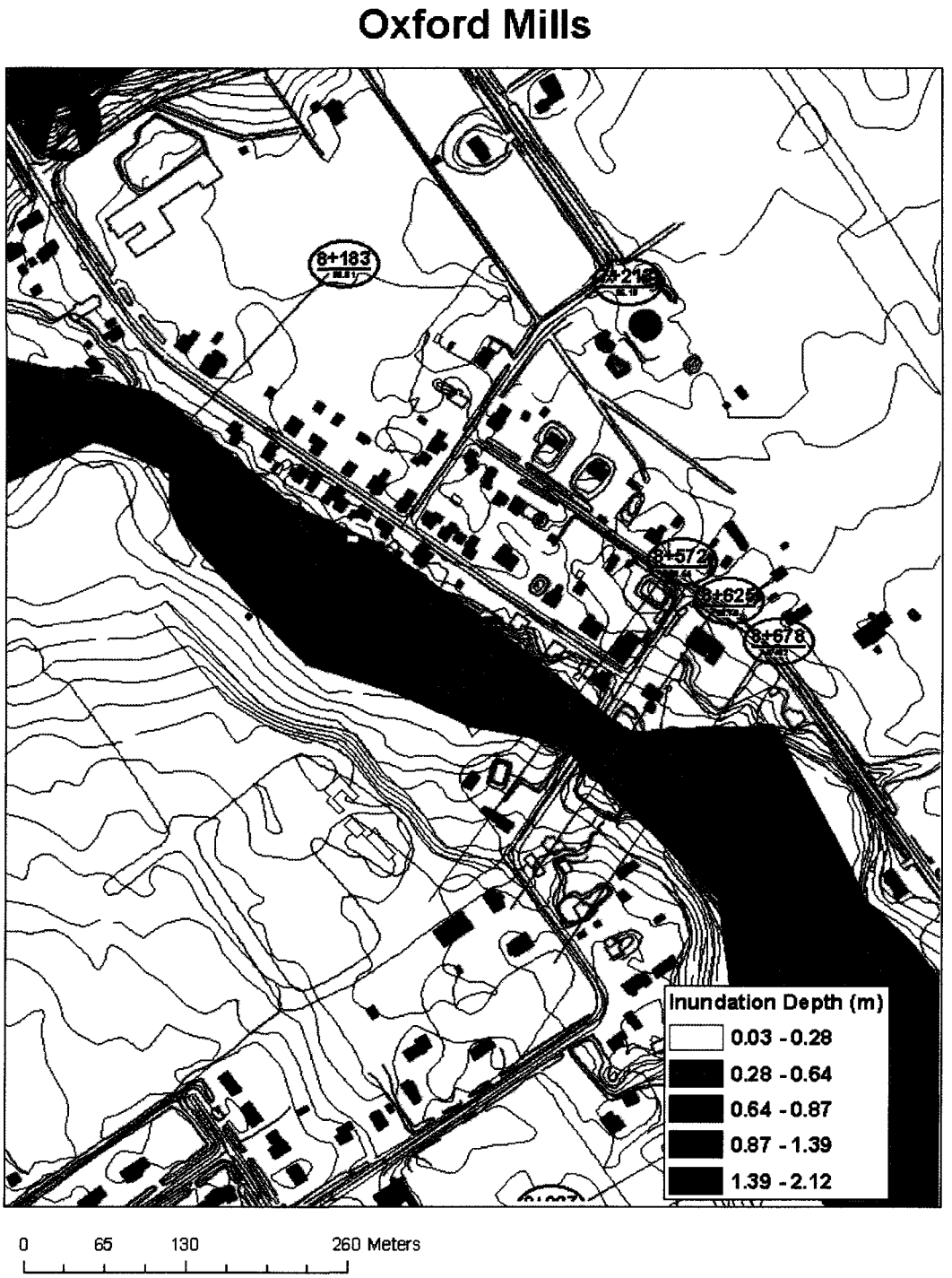

Figure 44: 100-Year Floodplain map for Oxford Mills based on a structure with a 50 year design life constructed in 2050

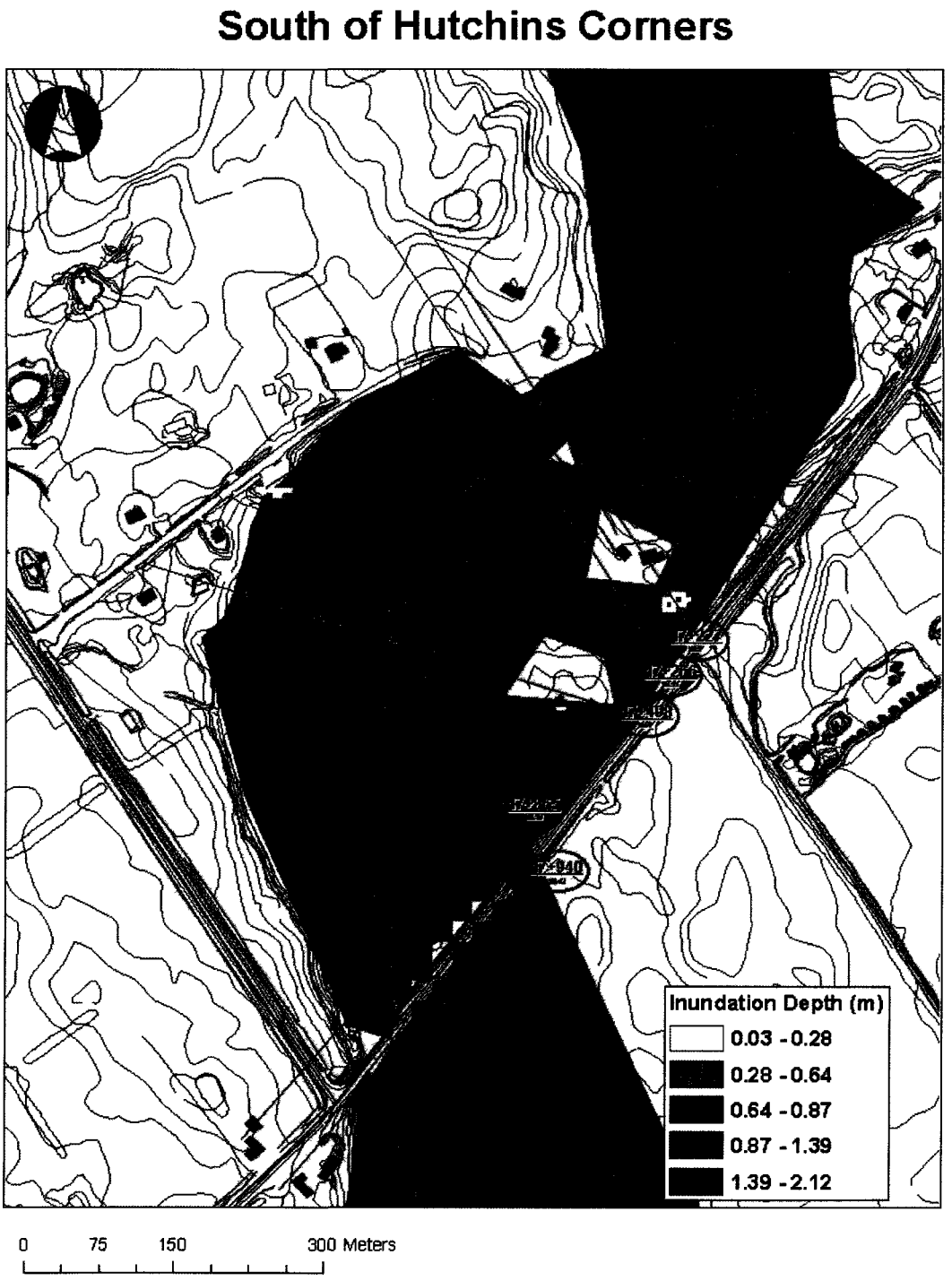

Figure 45: 100-Year Floodplain map for Hutchins Corners based on a structure with a 50 year design life constructed in 2050

7 CONCLUSIONS

In this thesis a novel approach for modeling the impacts of climate change at the catchment scale was proposed and applied to a watershed located near Ottawa, Canada. The proposed approach takes advantage of two techniques for the assessment of the impact of climate change on extreme events; non-stationary probability distributions and downscaled GCM data. Individually these techniques have their own drawbacks and limitations, but when combined these two techniques complement one another and ultimately produce a method which is more reliable and realistic.

The interchange between these two techniques takes place in the definition of the parameters of the non-stationary probability distribution. A change in climate almost inherently implies a change in the frequency and/or magnitude of extreme flow events. It imposes conditions which leave traditional stationary probability distributions out of sync with reality. The implication being that under a changing climate, the risk associated with a defined extreme event such as the 100-year flood changes with it. The challenge then comes in deciding how best to incorporate the non-stationary trend of climate change into probability distributions. Many have approached this by making an assumption as to how the climate will vary with time. Linear trends, step-change trends, and other artificial trends have all been evaluated. These approaches, however, raise the issue as to whether imposing what could likely be an unrealistic relationship is the optimal way to account for the non-stationary trend. In this thesis, the author addressed this by examining a model where the non-stationary trend of climate change is incorporated through the use of CGMs outputs. Here the future distribution of extreme events was linked to future trends in mean flow as determined by the results of downscaled GCM data.

In this study GCM data were downscaled to catchment scale through the application of the statistical downscaling tool ASD. Through the course of this study it was realized that alterations could be made to the ASD model that would improve its methods and ultimately produce a more realistic result. These changes, as presented in the paper by Sediou et al. (2010), improved upon the programs ability to reproduce observed trends and produce a more usable end result.

The downscaled climate data was then applied to the rainfall-runoff model SWAT to generate future mean flow data.

The GEV probability distribution was selected to evaluate the future probability distribution of extreme flows. Sixty-four separate models were evaluated, including stationary and time varying models, and it was found that based on a Bayes factor comparison the distribution which produced the most likely results when calibrated using observed climate was one in which the location parameter was constant and the scale parameter varied linearly with the maximum 9-day mean annual flow. When the distribution was calibrated using downscaled climate the optimal model was one in which the location parameter was constant and the scale parameter varied linearly with the maximum 14-day mean annual flow.

This methodology was then applied to the Kemptville Creek watershed and the possible impacts of a future change in climate were assessed. The results of the modeling indicate that while flow depths and the extent of floodplain will likely increase in the future, the extent of the increased impact will likely be minor. The results also showed that most existing infrastructure will be able to withstand the higher peak flow events without added risk.

8 FUTURE WORK

There remains a great deal of work to be done in the field of climate change impact assessments. Alterations to statistical downscaling techniques such as ASD are required to improve the reliability of the results. Beyond that the actual validity of applying a stationary downscaling relationship established based on past data to the future needs to be examined. Wilby (2002b) looked at this by trying to incorporate non-stationary trends through the parameters of a GEV distribution to improve the results of statistical downscaling method. The study concluded that more research was required in determining how to incorporate low frequency forcing patterns, such as observed hydrologic patterns, into statistical downscaling models. The hope being that the model parameters can be conditioned to remove some of the over dispersion that can arise in downscaling monthly precipitation.

Future work can also be done in looking at additional non-stationary GEV models which examine optimizing parameters through non-linear variations with mean flow such as powers. Also studies can examine the impacts of SRES scenarios on local mean flows and generate a range of possible impacts for the region.

Lastly, the development of streamline models which incorporate all of the elements in this study could be produced to simplify the process for municipalities. These models could then be used to monitor risks at the watershed and assess the impacts of various design conditions and scenarios quickly and efficiently.

9 REFERENCES

Ahmed, Ferdous, and Adam McGreath. "Kemptville Creek Flood Risk Mapping - Estimation of Flows." *Techical Memo Rideau Valley Conservation Authority.* 2007. http://209.5.125.108/IM/Documents/FPM/RV2/Hydrology_Report/Kemptville_designQ.pdf.

Ahmend, Ferdous Nazrul Howlander, Amanda Soutar, and Ewan Hardy. "Kemptville Creek Flood Risk Mapping - Hydrolic Modeling and Map Production." *Techical Memo Rideau Valley Conservation Authority.* 2009. http://209.5.125.108/IM/Documents/FPM/RV2/Hydraulics_Report/Kemptville_Mapping_Final_Report.pdf.

Barredo, J. I. "Normalized flood losses in Europe." *Hazards Earth Syst. Sci* (http://www.nat-hazards-earth-syst-sci.net/9/97/2009/.) 9 (2009): 97-104.

Benito, Gerardo, Andrés Diez-Herrero, and Maria Fernándes de Villalta. "Magnitude and Frequency of Flooding in the Tagus Basin (Central Spain) over the Last Millennium." *Climatic Change* 58, no. 1-2 (2003): 171-192.

Chang, H., J. Franczyk, E-S. Im, W-T. Kwon, D-H. Bae, and L-W. Jung. *Vulnerability of Korean water resources to climate change and population growth.* Vol. 56 No 4, in *Water Science and Technology*, 57-62. IWA Publishing, 2007.

Crisci, A., B. Grozzini, F. Meneguzzo, S. Pagliara, and G. Maracchi. "Extreme rainfall in a changing climate: regional analysis and hydrological implications in Tuscany." *Hydrological Processes* 16 (2002): 1261-1274.

Douglas, E.M., Vogel, R.M., Kroll, C.N. "Trends in floods and low flows in the United States: impact of spatial correlation." *Journal of hydrology*, 2000: 90-105.

El Adlouni, S., T. B. Ouarda, X. Zhang, R. Roy, and B. Bobèe. "Generalized maximum likelyhppd estimators for the nonstationary generalized extreme value model." *Water Resour. Res. 43*, 2007.

Feng, Song, Saralees Nadarajah, and Qi Hu. "Modeling Annual Extreme Precipitation in China Using the Generalized Extreme Value Distribution." *Journal of the Meteorological Society of Japan*, 2007: Vol. 85, No. 5 pp.599-613.

Ferro, V, and P. Porto. " Regional analysis of rainfall-depth-duration equation for south Italy." *J. Hydrologic Engineering*, 1999: 326-336.

Fowler, H.J. and C.G. Kilsby. "A regional frequency analysis of United Kingdom extreme rainfall from 1961-2000." *Int. J. Climatol*, 2003: 1313-1334.

Franczyk, Jon, and Heejun Chang. "The effects of climate change and urbanization on the runoff of the Rock Creek basin in the Portland metropolitan area, Oregon, USA." *Hydrological processes* 23, no. 6 (2009): 805-815.

Gachon, P., et al. "Groupe de travail II : Variabilité, extrêmes et changements climatiques au Sahel : de l'observation à la modélisation." 2007.

Gassman, P. W., M. Reyes, C. H. Green, and J. G. Arnold. "The Soil and Water Assessment Tool: Historical development, applications and future directions." *Trans ASABE* 50(4) (2007): 1212-1250.

GCRIO. *U.S. Climate Action Report.* 2002. http://www.gcrio.org/CAR2002/ (accessed August 2010).

Gee, D. Michael, and Gary W. Brunner. "Dam Break Flood Routing using HEC-RAS and NWS-FLDWAV." *Proceedings of the 2005 World Water and Environmental Resoures Congress.* ASCE, 2005.

Githui, Faith, Wilson Gitau, Francis Mutua, and Willy Bauwens. "Climate change impacts on SWAT simulated streamflow in western Kenya." *International Journal of Climatology* 29, no. 12 (2009): 1823-1834.

Graham, L. P., B. Andréasson, and B. Carlsson. "Assessing climate change impacts on hydrology from an ensemble of regional climate models, model scales and linking methods—A case study on the Lule River Basin." *Clim. Change* 81 (2007): 293-307.

Harvey, Michael D., and Robert A. Mussetter. "Difficulties of Identifying Design Discharges in Steep, Coarse-Grained Channels in the Arid Southwestern US." *Proceedings of the 2005 World Water and Environmental Resoures Congress.* ASCE.

Haylock, M. R., G. C. Cawley, C. Harpham, R. L. Wilby, and C. Goodess. "Downscaling heavy precipitaiton over the UK: A comparison of dynamic and statistical methods and their future scenarios." *Int. J. Climatol.* 26 (2006): 1397-1415.

Hessami, M., P. Gachon, T. Ouarda, and A. St-Hilaire. "Automated regression-based statistical downscaling tool." *Environ Model Software* 23(6) (2008): 813-834.

Hessami, Masoud, Philippe Gachon, Taha B. M. J. Ouarda, and André St-Hilaire. "ASD Users Guide Version 1." 2007. http://loki.ouranos.ca/DAI/doc/technique/ASD%20User's%20Guide %20Version%201-1.pdf.

IJC. "Advice to Governments on their Review of the Great Lakes Water Quality Agreement." *International Joint Commission (IJC).* 2006. http://www.ijc.org/rel/pdf/advicefinalwc.pdf.

IPCC. "Contribution of Working Groups I, II and III to the Fourth Assessment Report of the Intergovernmental Panel on Climate Change." Edited by R. K. Pachauri and A. Reisinger. *Climate Change 2007: Synthesis Report.* IPCC, 2007a.

IPCC. *Special Report on Emissions Scenarios. A report by the Intergovernmental Panel on Climate Change.* Cambridge UK: Cambridge University Press, 2000.

IPCC: Bates, B C., Z. W. Kundzewicz, S. Wu, and J. P. Palutikof. "Technical Pater of the Intergovernmental Panel on Climate Change." *Climate Change and Water.* IPCC Secretariat Geneva, 2008.

IPCC: Kundzewicz, Z. W., et al. "Freshwater resources and their management. Climate Change 2007: Impacts, Adaptation and Vulnerability. Contribution of Working Group II to the Fourth Assessment Report of the Intergovernmental Panel on Climate Change." Edited by C. E. Parry, O. F. Canziani, J. P. Palutikof, P. J. van der Lindin and C. E. Hanson. IPCC, 2007b. 173-210.

Jha, Manoj, Jeffery G. Arnold, Phillip W. Grassman, Filippo Giorgi, and Roy R. Gu. "Climate Change Sensitivity Assessment on Upper Mississippi River Basin Streamflows Using SWAT." *Journal of the American Water Resources Association* 42, no. 4 (2006): 997-1015.

Kalnay, E., et al. "The NCEPéNCAR 40-year reamalysis project." *Bulletin of the American Meteoroligical Soceity* 77 (1996): 437-471.

Kanamitsu, M., et al. "NCEP/DOE AMIP-II (R-2)." *Bull. Amer. Meteor. Soc.* 83 (2002): 1631-1643.

Kang, Boosik, Seung-Jong Lee, Dong-Hyun Kang, and Young-Oh Kim. "A flood risk projection for Yongdam dam against future climate change." *Journal of Hydro-environment Research* 1, no. 2 (December 2007).

Kistler, R. "The NCEP–NCAR 50-Year Reanalysis: Monthly means CD-ROM and documentation." *Bull. Amer. Meteor. Soc.*, no. 82 (2001): 247-267.

Kling, George W., Katharine Hayhoe, Lucinda B. Johnson, John J. Magnuson, Stephen Polasky, Scott K. Robinson, et al. *Confronting Climate Change in the Great Lakes Region: Impacts on Our Communities and Ecosystems.* The Union of Concerned Scientists: Cambridge, MA, and The Ecological Society of America: Washington, D.C., 2003.

Kundzewicz, Z. W., et al. "Summer floods in Central Eourpe: climate change trackÉ." *Nat Hazards* 36 (2005): 165-189.

Leadbetter, M. R., Lindgren, G. and Rootz´en, H. "Extremes and Related Properties of Random Sequences and Processes." *Springer*, 1983.

Leclerc, Martin, and Taha B.M.J. Ouarda. "Non-stationary regional flood frequency analysis at ungauged sites." *Journal of Hydrology* 343, no. 3-4 (2007): 254-265.

Legates, D. R., McCabe Jr., G. J. "Evaluating the use of "goodness-of-fit" Measures in hydrologic and hydroclimatic model validation." *Water Resour. Res.* 35(1) (1999): 233-241.

Mareuil, A., R. Laconte, F. Brissette, and M. Minville. "Impacts of climate change on the frequency and severity of floods in the Châteauguay River basin, Canada." *Canadian Journal of Civil Engineering* 34(9) (2007): 1048-1060.

Marshall, E., and T. Randhir. "Effect of climate change on watershed system: a regional analysis." *Clim. Change* 89 (2008): 236-280.

Martins, E. S., and J. R. Stedinger. "Generlized maximum likelihood pareto-poisson estimators for partial duration series." *Water Resour. Res.* 37(10) (2001): 2551-2557.

Merz, B., J. Hall, M. Disse, and A. Schumann. "Fluvial flood risk management in a changing world." 2010. http://www.nat-hazards-earth-syst-sci.net/10/509/2010/nhess-10-509-2010.pdf.

Mesinger, and Fedor. "North American Regional Reanalysis." *Bull. Amer. Meteor. Soc.* 87 (2006): 343-360.

Min, Seung-Ki, Daniel Simonis, and Andreas Hense. "Probabilistic climate change predictions applying Bayesian model averaging." *Phil. Trans. R. Soc.* 356 (2007): 2103-2116.

Neitsch, S. L., A. G. Arnold, J. R. Kiiniry, J. R. Srinivasan, and J. R. Willaims. *Soil and Water Assessment Tool Input/Output File Documentation: Version 2005.* Soil and Water Research Laboratory, Agricultural Research Service.

Newton, M., and A. Raftery. "Approximate Bayasian inference by the weighted liklihood bootstrap." *Journal of the Royal Stastical Society* Ser B 56 (1994): 1-48.

NRCAN: Lemmen, D.S.,Warren, F.J., Lacroix, J., and Bush, E., editors. *From Impacts to Adaptation: Canada in a Changing Climate.* NRCAN, 2007.

Ouranos. "Adapting to Climate Change." Montreal, Canada, 2004. 91.

Perreault, L., B. Bobée, and E. Parent. "Bayesian change-point analysis in hydrometeorological time series. Part 1. The normal model revisited." *J. Hydrol.* 235 (2000): 221-241.

Renard B. Lang M, Bois P. "Stistical analysis of extreme events in a non-stationary context via a Bayesian framework: case study with paek-over threshold data." *Stoch. Environ. Res. Risk Assess.* 21(2) (2006): 97-122.

RVCA. "Kemptville Creek Watershed Plan Update." March 2007. http://209.5.125.108/IM/Documents/watershed_planning/KemptvilleCr/KCWP_UPDATE_2007.pdf.

Sankarasubramanian, A., and U. Lall. "Flood quantiles in a changing climate: Seasonal forecasts and causal relations." *Water Resour. Res.* 39(5) (2003): 1134.

Sediou, Ousmane, Andrea Ramsay, Ioan Nistor " Climate change impacts extreme floods II: Improving flood future peaks simulation non-stationary frequency" submitted to Tenth Symposium on Stochastic Hydraulics Fifth International Conference on Water Resources and Environment Research, 2010

Sarif, Mohammed, Donald Rurn, and Azhar hussain. "Climate Change Impacts on Extreme Flow Measures in Satluj River Basin in India." *ASCE Conf. Proc.* 2010.

Schmidli, J., et al. "Statistical and dynamic downscaling of precipitation: an evaluation and comparison of scenarios for the European Alps." *Journal fo Geophysical Research* 112 (2007).

Sik, Byung, Hung Soo Kim, Byung Ha Seoh, and Nam Won Kim. "Impact of climate change on water resources in Yongdam Dam Basin, Korea." *Proceedings of the 2005 World Water and Environmental Resoures Congress.* ASCE, 2005. 272.

Somura, H., J. Arnold, D. Hoffman, I. Takeda, Y. Mori, and M. DiLuzio. "), Impact of climate change on the Hii River basin and salinity in Lake Shinji: a case study using the SWAT model and a regression curve." *Hrdrological Processes* 23 (2009): 1887-1900.

Thodsen, H. "The influence of climate change on stream flow in Danish rivers." *Journal of Hydrology* 333 (2005): 226-238.

Vescovi, Luc, Pierre Baril, Claude Desjarlais, André Musy, and René Roy. *Water and climate change in Québec.* The United Nations World Water Assessment Pregramme Scientific Paper UNESCO, 2009.

Wang, X. L., F. W. Zwiers, and V. Swail. "North Atlantic Ocean wave climate scenarios for the 21st century." *J. Clim.* 17 (2004): 2368-2383.

WateBase. United Nations University. 2010. http://www.waterbase.org (accessed April 2010).

Wilby, R. L,, S. P. Charles, E. Zorita, B. Timbal, P. Whetton, and L. O. Mearns. *Guidelines for the use of climate scenarios developed from statistical downscaling methods.* DDC of IPCC, 2004.

Wilby, R. L., and T. M. L. Wigley. "Downscaling general circulation model output: a review of methods and limitations." *Progress in Physical Geography* 21 (1997): 530-548.

Wilby, R. L., C. W. Dawson, and E. M. Barrow. "SDSM - a decision support tool for the assessment of regional climate change impacts." *Environmental Modelling and Software* 17 (2002): 147-159.

Wilby, R. L., D. Conway, and P. D. Jones. "Prospects for downscaling seasonal precipitation variability using conditioned weather generator parameters." *Hydrological Processes 16,* 2002b: 1215–1234.

Wuebbles, D.J., and K. Hayhoe. "Climate Change: A Real Issue with Real Concerns for the Midwest." *Proceedings of the International Conference on Climate Change and Environmental Policy.* Illinois, 2003.

Zhang, X., R. Srinivasan, and F. Hao. "Predicting hydologic response to climate change in the Luohe River basin using the SWAT model." *Trans ASABE* 50(3) (2007): 901-910.

APPENDICES

A- Rainfall/Flow Data

Table 18: NCEP Data

	NCEP Data													
	Precipitation (mm)													
Year	Jan	Feb	March	April	May	June	July	Aug	Sept	Oct	Nov	Dec	**Sum**	**Avg**
1948	1 29	2 26	3 06	4 42	4 11	5 93	5 38	2 32	1 72	3 08	3 16	2 87	9 11	3 30
1949	2 97	2 18	1 89	3 39	4 39	4 58	4 62	3 64	3 52	1 02	2 00	1 83	4 85	3 00
1950	3 13	2 08	2 89	2 33	3 29	4 81	5 83	5 21	1 35	1 70	3 58	1 04	6 32	3 10
1951	1 65	2 44	2 49	3 21	2 51	4 54	4 21	3 55	2 70	1 96	3 75	2 60	8 32	2 97
1952	2 43	1 63	2 31	2 44	4 98	5 44	4 58	3 31	2 46	1 13	1 99	3 34	6 46	3 00
1953	2 18	1 61	3 26	2 87	5 49	4 83	6 42	3 47	2 83	1 02	1 42	2 29	4 73	3 14
1954	2 66	3 11	2 58	4 57	3 21	8 35	4 42	5 36	4 70	1 94	2 58	2 50	7 02	3 83
1955	1 13	1 17	4 42	2 46	5 02	7 39	5 30	6 65	1 88	4 39	1 00	1 41	6 80	3 52
1956	1 41	1 67	2 38	2 65	4 72	5 37	4 48	3 58	2 95	0 74	0 99	1 20	2 94	2 68
1957	0 99	0 92	0 57	2 39	3 20	5 88	4 94	1 28	4 65	1 52	1 98	2 75	6 25	2 59
1958	2 33	2 53	0 87	3 58	2 82	3 85	5 48	2 73	3 25	1 93	1 88	0 92	4 74	2 68
1959	2 74	2 09	2 02	1 71	3 34	5 16	3 95	6 11	3 44	3 54	2 96	2 12	8 62	3 27
1960	1 42	3 61	1 06	2 57	3 55	5 30	3 69	1 59	1 36	1 65	1 70	0 80	4 15	2 36
1961	0 72	2 82	2 20	3 48	4 04	4 59	7 75	5 52	2 84	0 88	1 25	2 08	4 22	3 18
1962	2 55	2 28	1 18	3 08	3 98	4 08	4 21	3 90	3 25	2 67	1 73	1 63	6 02	2 88
1963	1 16	1 10	2 69	3 04	3 70	4 84	5 08	6 78	1 83	0 37	3 65	0 57	4 58	2 90
1964	1 84	0 45	2 43	1 66	3 16	2 51	7 04	2 00	0 46	0 71	1 72	1 98	4 42	2 16
1965	1 90	3 29	0 84	2 42	3 37	3 35	2 21	4 53	1 71	3 39	3 60	1 83	8 82	2 70
1966	1 80	1 25	3 15	1 74	1 91	4 20	4 23	4 04	2 58	1 14	2 08	2 30	5 52	2 54
1967	2 33	1 67	0 80	3 47	3 03	4 94	5 55	4 43	2 41	3 15	2 72	2 28	8 15	3 06
1968	1 38	0 95	2 92	3 04	3 53	5 05	3 79	2 78	2 22	2 18	2 87	3 17	8 22	2 82
1969	2 06	1 12	1 91	3 88	6 55	4 16	3 88	2 86	1 78	1 97	2 90	2 13	7 00	2 93
1970	1 10	2 27	1 85	3 64	2 35	3 78	7 11	5 71	3 23	1 62	1 77	3 13	6 52	3 13
1971	1 73	4 64	2 63	3 17	2 97	3 73	3 26	2 92	2 67	1 33	1 85	3 13	6 32	2 84
1972	1 73	3 06	3 06	2 36	3 18	7 71	6 63	5 64	2 65	3 42	3 92	4 82	12 16	4 02
1973	2 10	2 02	3 96	4 28	5 32	6 98	2 97	4 38	3 21	2 12	3 16	5 64	10 92	3 85
1974	2 50	1 84	3 46	3 92	6 46	5 22	6 05	3 56	2 22	1 23	4 42	3 12	8 77	3 67
1975	2 33	3 15	3 50	4 38	4 01	4 05	4 68	2 62	4 06	2 12	2 31	3 19	7 62	3 37
1976	3 55	4 65	4 20	2 71	6 33	7 20	5 69	3 45	2 55	4 01	1 93	1 64	7 58	3 99
1977	1 96	2 03	3 60	2 84	2 60	5 84	4 18	5 08	4 75	3 50	3 18	3 74	10 42	3 61
1978	4 35	0 48	2 73	2 76	3 18	5 32	4 21	4 01	2 05	2 49	1 76	3 07	7 31	3 03
1979	4 09	1 49	2 52	3 37	4 41	5 12	4 64	3 89	3 10	3 52	2 19	2 36	8 07	3 39
1980	1 19	1 18	2 89	3 55	3 16	5 51	5 99	4 56	3 63	3 31	2 77	1 97	8 05	3 31
1981	0 67	5 55	2 11	3 22	4 22	5 61	4 91	4 46	2 89	2 74	2 18	1 10	6 02	3 31

	NCEP Data													
	Precipitation (mm)													
Year	Jan	Feb	March	April	May	June	July	Aug	Sept	Oct	Nov	Dec	**Sum**	**Avg**
1982	2 52	2 02	3 03	2 89	2 70	4 15	2 79	3 48	2 05	1 21	2 87	1 96	6 05	2 64
1983	1 65	2 31	2 37	4 56	5 91	3 20	4 83	4 09	1 96	2 31	4 30	4 02	10 63	3 46
1984	1 03	2 42	1 67	3 22	5 26	3 48	2 91	4 91	0 55	0 94	2 42	2 94	6 30	2 65
1985	2 09	2 89	3 20	3 40	3 80	4 56	4 36	2 59	3 05	1 71	3 18	1 40	6 29	3 02
1986	2 43	1 53	3 78	2 53	5 41	4 20	6 77	6 46	3 41	1 66	2 18	2 64	6 49	3 58
1987	1 70	0 89	2 58	2 78	2 92	6 39	6 02	3 15	3 02	2 04	3 47	1 83	7 34	3 07
1988	1 26	2 37	1 89	3 44	3 50	2 60	5 70	6 36	2 02	3 17	3 31	1 29	7 77	3 08
1989	1 94	1 54	2 77	1 98	5 68	7 15	4 93	4 66	3 07	2 51	3 71	1 12	7 34	3 42
1990	2 18	2 95	2 05	3 55	3 79	6 54	4 30	4 41	2 46	3 37	1 88	4 17	9 41	3 47
1991	1 92	1 55	4 02	4 07	3 21	3 04	3 31	5 65	2 13	2 16	1 76	2 49	6 41	2 94
1992	1 96	2 20	2 59	2 47	3 82	3 38	5 30	4 18	2 57	1 78	2 57	1 20	5 55	2 84
1993	2 72	1 62	1 38	2 79	2 82	4 49	5 30	6 43	3 44	1 90	2 86	2 08	6 84	3 15
1994	2 27	1 76	1 78	3 31	5 30	5 75	6 14	4 13	1 90	0 42	3 03	1 47	4 92	3 10
1995	2 07	1 42	1 27	2 34	3 15	2 40	8 03	3 35	1 97	5 28	3 12	1 86	10 26	3 02
1996	3 33	2 45	1 02	4 06	2 30	4 20	6 77	4 37	3 35	2 26	2 87	2 78	7 91	3 31
1997	2 58	2 80	3 11	2 69	4 83	4 14	5 41	4 90	3 61	1 78	3 00	1 53	6 31	3 37
1998	4 47	1 53	3 84	1 49	4 07	8 24	5 23	4 19	2 91	1 54	1 84	1 93	5 32	3 44
1999	3 89	1 26	3 51	1 18	2 49	5 13	6 37	2 34	4 91	1 44	2 62	2 08	6 13	3 10
2000	2 61	2 39	2 51	4 31	4 16	3 72	5 39	4 94	2 50	1 44	2 28	3 28	6 99	3 29
2001	1 42	2 83	2 05	1 27	2 89	3 28	4 50	4 22	3 23	2 44	2 22	1 87	6 53	2 69
2002	2 70	2 43	3 57	3 27	4 74	5 60	3 70	3 13	2 80	3 97	3 63	2 10	9 69	3 47
2003	1 28	2 55	2 47	1 33	4 01	3 09	6 71	6 22	3 40	4 73	4 23	3 65	12 62	3 64
2004	1 07	1 25	3 49	2 55	3 75	3 02	7 97	5 30	3 15	1 41	2 74	4 31	8 45	3 33
2005	2 15	2 03	0 89	4 10	1 97	6 32	5 25	4 82	3 87	3 18	3 17	2 92	9 27	3 39
2006	3 25	2 41	1 49	2 38	3 52	5 30	6 85	4 97	3 77	5 07	1 64	2 82	9 53	3 62
2007	2 84	1 04	2 33	4 23	1 94	5 04	6 61	3 84	2 00	3 03	3 27	4 00	10 31	3 35
Average	2 16	2 31	2 66	3 24	3 99	4 87	5 10	4 39	2 74	2 38	2 78	2 60	7 75	3 27

Table 19: Observed Climate Data

	Observed Data	
	Average Precipitation (mm)	Average Flow (m^3/s)
1970	2.62	4.70
1971	1.94	5.15
1972	3.31	5.94
1973	2.99	5.92
1974	2.50	5.67
1975	2.41	4.62
1976	2.85	6.02
1977	3.11	4.96
1978	2.29	5.07
1979	2.75	4.82
1980	2.51	4.99
1981	2.92	6.38
1982	2.75	5.22
1983	2.93	5.52
1984	2.66	4.36
1985	2.24	3.44
1986	2.93	6.84
1987	2.53	4.26
1988	2.17	3.56
1989	2.50	3.88
1990	2.51	5.60
1991	2.27	4.89
1992	2.48	3.97
1993	3.06	5.82
1994	2.48	4.37
1995	2.74	2.84
1996	2.66	6.88
1997	2.75	5.00
1998	2.93	5.17
1999	2.62	4.17
2000	2.28	6.16
2001	2.94	3.14
2002	2.52	3.94
2003	2.17	4.28
2004	2.49	5.80

B- SWAT Calibration/Validation Output

Model Calibration –Calibration Input

```
1
    SWAT  Sept '05 VERSION2005                                                    0/ 0/   0      0: 0: 0

    General Input/Output section (file.cio): ArcSWAT 2.3.4
    03/04/2010 12:00:00 AMARCGIS-SWAT interface AV

         Number of years in run:   17
         Area of watershed:      416.430 km2
         Random number generator cycles: 0, use default numbers

         Initial random number seed: wet/dry day prob        748932582
         Initial random number seed: radiation              1948832765
         Initial random number seed: precipitation           857034417
         Initial random number seed: 0.5 hr rainfall          67377721
         Initial random number seed: wind speed              366304404
         Initial random number seed: irrigation             1094585182
         Initial random number seed: relative humidity      1767585417
         Initial random number seed: max temperature         608439319
         Initial random number seed: min temperature         592757081

         Precipitation data used in run:
          Multiple gages read for watershed
             Daily rainfall data used

         Temperature data used in run:
```

Multiple gages read for watershed

PET method used: Penman-Monteith

Rainfall/Runoff/Routing Option:

Daily rainfall data

Runoff estimated with curve number method

Daily stream routing

Variable Storage routing method

Channel dimensions remain constant

Subbasin algae/CBOD loadings modeled

In-stream nutrient transformations modeled using QUAL2E equations

Subbasin Input Summary:

Sub	Latitude	Elev(m)	#HRUs	Ponds	Elevbnds	Wetlnd
1	44.93	99.00	1			
2	44.91	109.00	1			
3	44.86	106.00	1			
4	44.87	109.00	1			
5	44.86	108.00	1			
6	44.83	109.00	1			
7	44.77	116.00	1			

HRU Input Summary Table 1:

Sub	HRU	Area(ha)	Slope	SlpLgth(m)	Ovrlnd_N	CondII_CN	TimeConc(hr)	ESCO	EPCO
1	1	11907.00	0.004	121.95	0.100	77.00	4.931	0.95	1.00
2	2	5607.00	0.004	121.95	0.100	83.00	3.765	0.95	1.00

3	3	3969.00	0.004	121.95	0.100	66.00	3.073	0.95	1.00
4	4	3654.00	0.005	121.95	0.100	83.00	2.379	0.95	1.00
5	5	1134.00	0.004	121.95	0.100	66.00	2.321	0.95	1.00
6	6	5529.00	0.003	121.95	0.100	66.00	3.291	0.95	1.00
7	7	10143.00	0.004	121.95	0.100	66.00	5.439	0.95	1.00

HRU CN Input Summary Table:

Sub	HRU	Area(ha)	LULC	Soil	CN1	CN2	CN3	Wilting Point (mm H2O)	Field Capacity (mm H2O)	Saturation (mm H2O)
1	1	11907.00	FODB	Be18-2a-	59.3	77.0	89.9		88.1	180.0
561.0										
2	2	5607.00	FODB	Be1-2a-4	67.0	83.0	93.1		129.6	180.0
368.5										
3	3	3969.00	FODB	Po10-1b-	46.8	66.0	83.0		57.8	90.0
470.5										
4	4	3654.00	FODB	Be1-2a-4	67.0	83.0	93.1		129.6	180.0
368.5										
5	5	1134.00	FODB	Po10-1b-	46.8	66.0	83.0		57.8	90.0
470.5										
6	6	5529.00	FODB	Po10-1b-	46.8	66.0	83.0		57.8	90.0
470.5										
7	7	10143.00	FODB	Po10-1b-	46.8	66.0	83.0		57.8	90.0
470.5										

HRU Input Summary Table 2:

Sub	HRU	Area(ha)	SoilName	Hydgrp	MaxRtDpth(mm)	Albedo	USLE_K	USLE_P	USLE_LS	ProfileAWC(mm)	IniSoilH2O(mm)
1	1	11907.00	Be18-2a-4658	C	1000.00	0.10	0.10	1.00	0.10	180.000	0.683
2	2	5607.00	Be1-2a-4648	D	1000.00	0.10	0.29	1.00	0.10	180.000	0.000
3	3	3969.00	Po10-1b-4951	B	720.00	0.15	0.25	1.00	0.10	90.000	0.000
4	4	3654.00	Be1-2a-4648	D	1000.00	0.10	0.29	1.00	0.11	180.000	0.000

5	5	1134.00	Po10-1b-4951	B	720.00	0.15	0.25	1.00	0.10	90.000	0.000
6	6	5529.00	Po10-1b-4951	B	720.00	0.15	0.25	1.00	0.09	90.000	0.000
7	7	10143.00	Po10-1b-4951	B	720.00	0.15	0.25	1.00	0.10	90.000	0.000

HRU Input Summary Table 3:

Sub	HRU	Area(ha)	Urban	Irrig	DrainTiles	Pothole	Pstcide	Biomix
1	1	11907.00						0.20
2	2	5607.00						0.20
3	3	3969.00						0.20
4	4	3654.00						0.20
5	5	1134.00						0.20
6	6	5529.00						0.20
7	7	10143.00						0.20

HRU Input Summary Table 4 (Groundwater):

Sub	HRU	Area(ha)	GWdelay(days),	GWalpha(days)	GWQmin(mm)	GWrevap	Revapmin(mm)	Deepfr	NO3(ppm)	SolP(ppm)
1	1	11907.00	31.000	0.048	0.000	0.020	1.000	0.050	0.000	0.000
2	2	5607.00	31.000	0.048	0.000	0.020	1.000	0.050	0.000	0.000
3	3	3969.00	31.000	0.048	0.000	0.020	1.000	0.050	0.000	0.000
4	4	3654.00	31.000	0.048	0.000	0.020	1.000	0.050	0.000	0.000
5	5	1134.00	31.000	0.048	0.000	0.020	1.000	0.050	0.000	0.000
6	6	5529.00	31.000	0.048	0.000	0.020	1.000	0.050	0.000	0.000
7	7	10143.00	31.000	0.048	0.000	0.020	1.000	0.050	0.000	0.000

Tributary/Main Channel Characteristics

	Tributary					Main				
Sub	Length(km)	Slope	Width(m)	Cond(mm/hr)	N	Length(km)	Slope	Width(m)	Depth(m)	Cond(mm/hr)	N

1	19.58	0.001	16.23	0.5000	0.014	18.98	0.001	34.40	1.16	0.0000	0.014
2	12.09	0.001	10.33	0.5000	0.014	9.61	0.001	10.33	0.52	0.0000	0.014
3	8.32	0.001	8.39	0.5000	0.014	3.80	0.001	8.39	0.45	0.0000	0.014
4	6.99	0.002	7.99	0.5000	0.014	2.95	0.000	7.99	0.44	0.0000	0.014
5	5.30	0.002	3.96	0.5000	0.014	4.95	0.001	22.26	0.87	0.0000	0.014
6	11.24	0.002	9.90	0.5000	0.014	7.32	0.000	9.90	0.51	0.0000	0.014
7	21.87	0.001	14.74	0.5000	0.014	16.75	0.001	14.74	0.66	0.0000	0.014

Model Calibration – Auto Calibration Results

```
================================================
          Parameter list of changepar.dat
 ================================================


        INITIAL PARAMETER VALUES AND PARAMETER BOUNDS
        =============================================

  PARAMETER      INITIAL VALUE      LOWER BOUND      UPPER BOUND
  ---------      -------------      -----------      -----------
   1    0.00000    1.00000     1    1 2001  Alpha_Bf
   2    0.00000   10.00000     7    1 2001     Canmx
   3    0.00000  150.00000    54    1 2001     Ch_K2
   4  -25.00000   25.00000    10    3 2001       Cn2
   5    0.00000    1.00000    27    1 2001      Esco
   6  -10.00000   10.00000     2    2 2001  Gw_Delay
   7   -0.03600    0.03600     3    2 2001  Gw_Revap
   8 -100.00000  100.00000     5    2 2001   Revapmn
   9    0.00000   10.00000    33    1    0    Surlag
  10    0.00000    1.00000    38    1    0      Tlmp
 Objective functions are (objmet.dat):
OBJECTIVE FUNCTION  1 =
SSQ   for flow             (m^3/s) at location  1
 Response functions are (responsmet.dat):
OUTPUT   1 =
```

for flow (m^3/s) at location 1

sce control parameters

SCE CONTROL PARAMETER	MAX TRIALS ALLOWED	REQUIRED IMPROVEMENT PERCENT	NO. LOOPS	RANDOM SEED
_____	20000	1.0	5	1667

SCE ALGORITHM CONTROL PARAMETERS

NUMBER OF COMPLEXES	POINTS PER COMPLEX	POINTS IN INI. POPUL.	POINTS PER SUB-COMPLX	EVOL. STEPS PER COMPLEX
10	21	210	11	21

INITIAL PARAMETER VALUES AND PARAMETER BOUNDS

PARAMETER	INITIAL VALUE	LOWER BOUND	UPPER BOUND
OF # obs| average |variance			
1 6208	0.527E+01	0.923E+02	

```
 ==================================================
 ENTER THE SHUFFLED COMPLEX EVOLUTION GLOBAL SEARCH
 ==================================================
Initial Nash-Sutcliff efficiency of OF            1 =  -1.39978342946653

RESULTS FOR LOOP   0
----------------------
best result corresponds to simulation         125

LOOP TRIALS COMPLXS  PAR RNG
   0   210      10 0.992
Lowest Nash-Sutcliff efficiency of OF           1 =  0.525537522727478


*** UNCERTAINTY ANALYSIS RESULT ***

Results using X1 squared statistics
*****statistics of the entire space*****
minimum global objective function   3103.94335937500
total number of runs =          210
minimum objective functions
     0.27174E+06
maximum objective function values
     0.18428E+07

minimum output values
```

```
     0.11727E+02
maximum output values
     0.60374E+02

*****statistics of selected space  *****
97.5% probability uncertainty analysis
 Total number of observations =         6208
 Number of free parameters =           10
 Limit on global objective function =    3114.20119596977
 number of selections           1

minimum parameter values
     0.78973E+00 0.21481E+01 0.12761E+03 0.72628E+01 0.30934E+00 0.91129E+00-0.19395E-01-0.62906E+02 0.72102E+00 0.39124E+00
maximum parameter values
     0.78973E+00 0.21481E+01 0.12761E+03 0.72628E+01 0.30934E+00 0.91129E+00-0.19395E-01-0.62906E+02 0.72102E+00 0.39124E+00
percentage of range
         0.00000     0.00000     0.00000     0.00000     0.00000     0.00000     0.00000     0.00000     0.00000     0.00000

mimimum objective function values
     0.27174E+06
maximum objective function values
     0.27174E+06

minimum output values
     0.40593E+02
maximum output values
     0.40593E+02
```

```
percentage of range
         0.00000
best result corresponds to simulation         125

LOOP TRIALS COMPLXS  PAR RNG
   1   516      10 0.990
Lowest Nash-Sutcliff efficiency of OF           1 =  0.525546198905441


*** UNCERTAINTY ANALYSIS RESULT ***

Results using X1 squared statistics
*****statistics of the entire space*****
minimum global objective function   3104.00000000000
total number of runs =          516
minimum objective functions
     0.27174E+06
maximum objective function values
     0.18428E+07

minimum output values
     0.66205E+01
maximum output values
     0.10000E+03

*****statistics of selected space  *****
97.5% probability uncertainty analysis
```

```
 Total number of observations =         6208
 Number of free parameters =           10
 Limit on global objective function =    3114.25802377933
 number of selections           2

minimum parameter values
     0.23502E+00 0.21481E+01 0.12491E+03 0.14214E+01 0.00000E+00-0.43894E+01-0.19395E-01-0.62906E+02 0.72102E+00 0.39124E+00
maximum parameter values
     0.78973E+00 0.94932E+01 0.12761E+03 0.72628E+01 0.30934E+00 0.91129E+00 0.21001E-01 0.10000E+03 0.10129E+01 0.47725E+00
percentage of range
        55.47100    73.45100     1.80000    11.68280    30.93400    26.50345    56.10556    81.45300     2.91880     8.60100

mimimum objective function values
     0.27174E+06
maximum objective function values
     0.27253E+06

minimum output values
     0.35438E+02
maximum output values
     0.40593E+02
percentage of range
         5.52048
best result corresponds to simulation         896

LOOP TRIALS COMPLXS  PAR RNG
   2   898      10 0.946
```

```
Lowest Nash-Sutcliff efficiency of OF           1 =  0.558099424994420


*** UNCERTAINTY ANALYSIS RESULT ***

Results using Xi squared statistics
*****statistics of the entire space*****
minimum global objective function   3104.05664062500
total number of runs =          898
minimum objective functions
     0.25310E+06
maximum objective function values
     0.19123E+07

minimum output values
     0.66205E+01
maximum output values
     0.10000E+03

*****statistics of selected space  *****
97.5% probability uncertainty analysis
 Total number of observations =         6208
 Number of free parameters =           10
 Limit on global objective function =    3114.31485158889
 number of selections           1

minimum parameter values
```

```
     0.51208E+00 0.48753E+01 0.13425E+03 0.39839E+00 0.00000E+00 0.79616E+00-0.22818E-01-0.24358E+02 0.85590E+00 0.36080E+00
maximum parameter values
     0.51208E+00 0.48753E+01 0.13425E+03 0.39839E+00 0.00000E+00 0.79616E+00-0.22818E-01-0.24358E+02 0.85590E+00 0.36080E+00
percentage of range
         0.00000     0.00000     0.00000     0.00000     0.00000     0.00000     0.00000     0.00000     0.00000     0.00000

minimum objective function values
     0.25310E+06
maximum objective function values
     0.25310E+06

minimum output values
     0.40093E+02
maximum output values
     0.40093E+02
percentage of range
         0.00000
best result corresponds to simulation         934

LOOP TRIALS COMPLXS  PAR RNG
   3  1311      10 0.786
Lowest Nash-Sutcliff efficiency of OF           1 =  0.565060325456621


*** UNCERTAINTY ANALYSIS RESULT ***

Results using X1 squared statistics
```

```
*****statistics of the entire space*****
minimum global objective function   3104.01782226562
total number of runs =         1311
minimum objective functions
     0.24911E+06
maximum objective function values
     0.24178E+07

minimum output values
     0.66205E+01
maximum output values
     0.10000E+03

*****statistics of selected space  *****
97.5% probability uncertainty analysis
 Total number of observations =         6208
 Number of free parameters =           10
 Limit on global objective function =    3114.27590494354
 number of selections           2

minimum parameter values
     0.67811E+00 0.40594E+01 0.10707E+03-0.76641E+01 0.54045E-01 0.89996E+01 0.10240E-01-0.66829E+02 0.57384E+00 0.44613E+00
maximum parameter values
     0.74259E+00 0.50356E+01 0.11903E+03-0.47089E+01 0.13038E+00 0.10000E+02 0.16549E-01-0.37742E+02 0.60809E+00 0.50213E+00
percentage of range
         6.44800     9.76200     7.97333     5.91040     7.63350     5.00200     8.76250    14.54350     0.34250     5.60000
```

```
mimimum objective function values
     0.24911E+06
maximum objective function values
     0.24983E+06

minimum output values
     0.37130E+02
maximum output values
     0.37162E+02
percentage of range
         0.03427
best result corresponds to simulation         934

LOOP TRIALS COMPLXS  PAR RNG
   4  1656      10 0.815
Lowest Nash-Sutcliff efficiency of OF           1 =  0.565057825897308


*** UNCERTAINTY ANALYSIS RESULT ***

Results using X1 squared statistics
*****statistics of the entire space*****
minimum global objective function   3104.00000000000
total number of runs =         1656
minimum objective functions
     0.24911E+06
maximum objective function values
```

```
     0.24178E+07

minimum output values
     0.66205E+01
maximum output values
     0.10000E+03

*****statistics of selected space  *****
97.5% probability uncertainty analysis
 Total number of observations =         6208
 Number of free parameters =           10
 Limit on global objective function =    3114.25802377933
 number of selections           5

minimum parameter values
     0.37317E+00 0.40594E+01 0.10707E+03-0.76641E+01 0.63242E-02 0.13084E+01 0.10240E-01-0.66829E+02 0.51367E+00 0.33417E+00
maximum parameter values
     0.74259E+00 0.69973E+01 0.11903E+03 0.79643E+01 0.29753E+00 0.10000E+02 0.30685E-01-0.25874E+02 0.95848E+00 0.50213E+00
percentage of range
        36.94200    29.37900     7.97333    31.25680    29.12058    43.45800    28.39583    20.47750     4.44810    16.79600

mimimum objective function values
     0.24911E+06
maximum objective function values
     0.25154E+06

minimum output values
```

```
     0.37130E+02
maximum output values
     0.40045E+02
percentage of range
         3.12167
best result corresponds to simulation        1685

LOOP TRIALS COMPLXS  PAR RNG
   5  1977      10 0.754
Lowest Nash-Sutcliff efficiency of OF           1 =  0.575640295236906


*** UNCERTAINTY ANALYSIS RESULT ***

Results using X1 squared statistics
*****statistics of the entire space*****
minimum global objective function   3104.01318359375
total number of runs =         1977
minimum objective functions
     0.24305E+06
maximum objective function values
     0.24178E+07

minimum output values
     0.66205E+01
maximum output values
     0.10000E+03
```

```
*****statistics of selected space  *****
97.5% probability uncertainty analysis
 Total number of observations =         6208
 Number of free parameters =           10
 Limit on global objective function =    3114.27125094190
 number of selections          10

minimum parameter values
     0.33685E+00 0.43900E+01 0.10849E+03 0.56674E+00 0.00000E+00 0.13369E+01 0.10410E-01-0.10000E+03 0.54082E+00 0.35018E+00
maximum parameter values
     0.85993E+00 0.74917E+01 0.15000E+03 0.59520E+01 0.25458E+00 0.10000E+02 0.36000E-01-0.66407E+01 0.93849E+00 0.48039E+00
percentage of range
        52.30800    31.01700    27.67333    10.77052    25.45800    43.31550    35.54167    46.67965     3.97670    13.02100

mimimum objective function values
     0.24305E+06
maximum objective function values
     0.24615E+06

minimum output values
     0.38144E+02
maximum output values
     0.40867E+02
percentage of range
         2.91606
best result corresponds to simulation        2279
```

```
LOOP TRIALS COMPLXS  PAR RNG
   6  2282      10 0.642
Lowest Nash-Sutcliff efficiency of OF           1 =  0.583140899236123


*** UNCERTAINTY ANALYSIS RESULT ***

Results using Xi squared statistics
*****statistics of the entire space*****
minimum global objective function   3103.96044921875
total number of runs =         2282
minimum objective functions
     0.23875E+06
maximum objective function values
     0.24178E+07

minimum output values
     0.66205E+01
maximum output values
     0.10000E+03

*****statistics of selected space  *****
97.5% probability uncertainty analysis
 Total number of observations =         6208
 Number of free parameters =           10
 Limit on global objective function =    3114.21834229162
```

```
 number of selections           6

minimum parameter values
     0.41587E+00 0.56439E+01 0.12737E+03-0.30492E+01 0.00000E+00 0.96846E+01 0.32125E-01-0.10000E+03 0.52555E+00 0.34563E+00
maximum parameter values
     0.89405E+00 0.88177E+01 0.15000E+03 0.68433E+01 0.17640E+00 0.10000E+02 0.36000E-01-0.61568E+02 0.92638E+00 0.44173E+00
percentage of range
        47.81800    31.73800    15.08667    19.78500    17.64000     1.57700     5.38194    19.21600     4.00830     9.61000

mimimum objective function values
     0.23875E+06
maximum objective function values
     0.24098E+06

minimum output values
     0.38402E+02
maximum output values
     0.40689E+02
percentage of range
         2.44915
best result corresponds to simulation        2469

LOOP TRIALS COMPLXS  PAR RNG
   7  2606      10 0.681
Lowest Nash-Sutcliff efficiency of OF           1 =  0.585509884246291
```

```
*** UNCERTAINTY ANALYSIS RESULT ***

Results using Xi squared statistics
*****statistics of the entire space*****
minimum global objective function   3104.04931640625
total number of runs =         2606
minimum objective functions
     0.23740E+06
maximum objective function values
     0.24178E+07

minimum output values
     0.66205E+01
maximum output values
     0.10000E+03

*****statistics of selected space  *****
97.5% probability uncertainty analysis
 Total number of observations =         6208
 Number of free parameters =           10
 Limit on global objective function =    3114.30750316524
 number of selections          44

minimum parameter values
     0.41587E+00 0.47319E+01 0.11077E+03-0.34373E+01 0.00000E+00 0.72859E+01 0.26974E-01-0.10000E+03 0.55353E+00 0.28013E+00
maximum parameter values
     0.94793E+00 0.10000E+02 0.15000E+03 0.10425E+02 0.28874E+00 0.10000E+02 0.36000E-01-0.79371E+01 0.92638E+00 0.47432E+00
```

```
percentage of range
        53.20600    52.68100    26.15333    27.72460    28.87400    13.57050    12.53611    46.03145     3.72850    19.41900

mimimum objective function values
     0.23740E+06
maximum objective function values
     0.24046E+06

minimum output values
     0.37951E+02
maximum output values
     0.41414E+02
percentage of range
         3.70852
best result corresponds to simulation        2634

LOOP TRIALS COMPLXS  PAR RNG
   8  2934      10 0.355
Lowest Nash-Sutcliff efficiency of OF           1 =  0.587588267087533


*** UNCERTAINTY ANALYSIS RESULT ***

Results using Xi squared statistics
*****statistics of the entire space*****
minimum global objective function   3104.05444335938
total number of runs =         2934
```

```
minimum objective functions
     0.23621E+06
maximum objective function values
     0.24178E+07

minimum output values
     0.66205E+01
maximum output values
     0.10000E+03

*****statistics of selected space  *****
97.5% probability uncertainty analysis
 Total number of observations =         6208
 Number of free parameters =           10
 Limit on global objective function =    3114.31264706179
 number of selections          66

minimum parameter values
     0.43740E+00 0.50607E+01 0.12910E+03-0.35515E+01 0.00000E+00 0.81780E+01 0.28873E-01-0.10000E+03 0.55881E+00 0.28236E+00
maximum parameter values
     0.75830E+00 0.10000E+02 0.15000E+03 0.10425E+02 0.25327E+00 0.10000E+02 0.36000E-01-0.45810E+02 0.87309E+00 0.47521E+00
percentage of range
        32.09000    49.39300    13.93333    27.95300    25.32700     9.11000     9.89861    27.09500     3.14280    19.28500

mimimum objective function values
     0.23621E+06
maximum objective function values
```

```
     0.23936E+06

minimum output values
     0.38354E+02
maximum output values
     0.41414E+02
percentage of range
         3.27695
best result corresponds to simulation        3237

LOOP TRIALS COMPLXS  PAR RNG
   9  3238      10 0.669
Lowest Nash-Sutcliff efficiency of OF           1 =  0.588349632115755


*** UNCERTAINTY ANALYSIS RESULT ***

Results using X1 squared statistics
*****statistics of the entire space*****
minimum global objective function   3104.00292968750
total number of runs =         3238
minimum objective functions
     0.23577E+06
maximum objective function values
     0.24178E+07

minimum output values
```

```
     0.66205E+01
maximum output values
     0.10000E+03

*****statistics of selected space  *****
97.5% probability uncertainty analysis
 Total number of observations =         6208
 Number of free parameters =           10
 Limit on global objective function =    3114.26096314879
 number of selections         178

minimum parameter values
     0.43740E+00 0.56009E+01 0.12910E+03-0.46449E+01 0.00000E+00 0.82641E+01 0.28873E-01-0.10000E+03 0.51389E+00 0.28236E+00
maximum parameter values
     0.86376E+00 0.10000E+02 0.15000E+03 0.96215E+01 0.25327E+00 0.10000E+02 0.36000E-01-0.45810E+02 0.87080E+00 0.48788E+00
percentage of range
        42.63600    43.99100    13.93333    28.53280    25.32700     8.67950     9.89861    27.09500     3.56910    20.55200

mimimum objective function values
     0.23577E+06
maximum objective function values
     0.23890E+06

minimum output values
     0.38354E+02
maximum output values
     0.40802E+02
```

```
percentage of range
         2.62156
best result corresponds to simulation        3345

LOOP TRIALS COMPLXS  PAR RNG
  10  3565      10 0.781
Lowest Nash-Sutcliff efficiency of OF           1 =  0.589662513234077


*** UNCERTAINTY ANALYSIS RESULT ***

Results using X1 squared statistics
*****statistics of the entire space*****
minimum global objective function   3104.02856445312
total number of runs =         3565
minimum objective functions
     0.23502E+06
maximum objective function values
     0.24178E+07

minimum output values
     0.66205E+01
maximum output values
     0.10000E+03

*****statistics of selected space  *****
97.5% probability uncertainty analysis
```

```
 Total number of observations =         6208
 Number of free parameters =           10
 Limit on global objective function =    3114.28668263156
 number of selections         306

minimum parameter values
     0.43952E+00 0.61424E+01 0.13595E+03-0.36367E+01 0.00000E+00 0.86329E+01 0.31302E-01-0.10000E+03 0.50902E+00 0.33058E+00
maximum parameter values
     0.86376E+00 0.10000E+02 0.15000E+03 0.70171E+01 0.25327E+00 0.10000E+02 0.36000E-01-0.30942E+02 0.87281E+00 0.48788E+00
percentage of range
        42.42400    38.57600     9.36667    21.30760    25.32700     6.83550     6.52500    34.52900     3.63790    15.73000

mimimum objective function values
     0.23502E+06
maximum objective function values
     0.23815E+06

minimum output values
     0.38354E+02
maximum output values
     0.40802E+02
percentage of range
         2.62156
best result corresponds to simulation       3752

LOOP TRIALS COMPLXS  PAR RNG
  11  3928      10 0.684
```

```
Lowest Nash-Sutcliff efficiency of OF           1 =  0.590093761212252


*** UNCERTAINTY ANALYSIS RESULT ***

Results using Xi squared statistics
*****statistics of the entire space*****
minimum global objective function   3103.98876953125
total number of runs =         3928
minimum objective functions
     0.23477E+06
maximum objective function values
     0.24178E+07

minimum output values
     0.66205E+01
maximum output values
     0.10000E+03

*****statistics of selected space  *****
97.5% probability uncertainty analysis
 Total number of observations =         6208
 Number of free parameters =           10
 Limit on global objective function =    3114.24675619640
 number of selections         527

minimum parameter values
```

```
     0.42181E+00 0.61424E+01 0.13595E+03-0.36367E+01 0.00000E+00 0.86329E+01 0.31302E-01-0.10000E+03 0.50902E+00 0.33058E+00
maximum parameter values
     0.80004E+00 0.10000E+02 0.15000E+03 0.70171E+01 0.23345E+00 0.10000E+02 0.36000E-01-0.30942E+02 0.87156E+00 0.48788E+00
percentage of range
        37.82300    38.57600     9.36667    21.30760    23.34500     6.83550     6.52500    34.52900     3.62540    15.73000

mimimum objective function values
     0.23477E+06
maximum objective function values
     0.23789E+06

minimum output values
     0.38354E+02
maximum output values
     0.40802E+02
percentage of range
         2.62156
best result corresponds to simulation        3752

LOOP TRIALS COMPLXS  PAR RNG
  12  4300      10 0.785
Lowest Nash-Sutcliff efficiency of OF           1 =  0.590095242205897


*** UNCERTAINTY ANALYSIS RESULT ***

Results using X1 squared statistics
```

```
*****statistics of the entire space*****
minimum global objective function   3104.00000000000
total number of runs =         4300
minimum objective functions
     0.23477E+06
maximum objective function values
     0.24178E+07

minimum output values
     0.66205E+01
maximum output values
     0.10000E+03

*****statistics of selected space  *****
97.5% probability uncertainty analysis
 Total number of observations =         6208
 Number of free parameters =           10
 Limit on global objective function =    3114.25802377933
 number of selections         845

minimum parameter values
     0.42181E+00 0.61424E+01 0.13595E+03-0.36367E+01 0.00000E+00 0.86329E+01 0.31302E-01-0.10000E+03 0.50902E+00 0.33058E+00
maximum parameter values
     0.80004E+00 0.10000E+02 0.15000E+03 0.70171E+01 0.23345E+00 0.10000E+02 0.36000E-01-0.29948E+02 0.87156E+00 0.48788E+00
percentage of range
        37.82300    38.57600     9.36667    21.30760    23.34500     6.83550     6.52500    35.02600     3.62540    15.73000
```

```
mimimum objective function values
     0.23477E+06
maximum objective function values
     0.23790E+06

minimum output values
     0.38322E+02
maximum output values
     0.40802E+02
percentage of range
         2.65583
best result corresponds to simulation        4469

LOOP TRIALS COMPLXS  PAR RNG
  13  4653      10 0.481
Lowest Nash-Sutcliff efficiency of OF           1 =  0.590286261155981


*** UNCERTAINTY ANALYSIS RESULT ***

Results using Xi squared statistics
*****statistics of the entire space*****
minimum global objective function   3103.99218750000
total number of runs =         4653
minimum objective functions
     0.23466E+06
maximum objective function values
```

```
     0.24178E+07

minimum output values
     0.66205E+01
maximum output values
     0.10000E+03

*****statistics of selected space  *****
97.5% probability uncertainty analysis
 Total number of observations =         6208
 Number of free parameters =           10
 Limit on global objective function =    3114.25018546077
 number of selections        1121

minimum parameter values
     0.42181E+00 0.61424E+01 0.13595E+03-0.36367E+01 0.00000E+00 0.86329E+01 0.31302E-01-0.10000E+03 0.50902E+00 0.33058E+00
maximum parameter values
     0.80004E+00 0.10000E+02 0.15000E+03 0.70171E+01 0.23345E+00 0.10000E+02 0.36000E-01-0.54814E+01 0.86260E+00 0.48788E+00
percentage of range
        37.82300    38.57600     9.36667    21.30760    23.34500     6.83550     6.52500    47.25930     3.53580    15.73000

mimimum objective function values
     0.23466E+06
maximum objective function values
     0.23778E+06

minimum output values
```

```
     0.38322E+02
maximum output values
     0.40802E+02
percentage of range
         2.65583


*** OPTIMIZATION TERMINATED BECAUSE THE CRITERION VALUE HAS NOT CHANGED
     1.00 PERCENT IN  5 SHUFFLING LOOPS ***

*** AUTOCALIBRATION SUCCESSFULLY ENDED ***



*** UNCERTAINTY ANALYSIS RESULT ***

Results using X1 squared statistics
*****statistics of the entire space*****
minimum global objective function   3104.00000000000
total number of runs =         4653
minimum objective functions
     0.23466E+06
maximum objective function values
     0.24178E+07

minimum output values
     0.66205E+01
```

```
maximum output values
     0.10000E+03

*****statistics of selected space  *****
97.5% probability uncertainty analysis
 Total number of observations =         6208
 Number of free parameters =           10
 Limit on global objective function =    3114.25802377933
 number of selections        1123

minimum parameter values
     0.42181E+00 0.61424E+01 0.13595E+03-0.36367E+01 0.00000E+00 0.86329E+01 0.31302E-01-0.10000E+03 0.50902E+00 0.33058E+00
maximum parameter values
     0.80004E+00 0.10000E+02 0.15000E+03 0.70171E+01 0.23345E+00 0.10000E+02 0.36000E-01-0.54814E+01 0.86260E+00 0.48788E+00
percentage of range
        37.82300    38.57600     9.36667    21.30760    23.34500     6.83550     6.52500    47.25930     3.53580    15.73000

mimimum objective function values
     0.23466E+06
maximum objective function values
     0.23779E+06

minimum output values
     0.38322E+02
maximum output values
     0.40802E+02
percentage of range
```

2.65583

Model Validation –Validation Inputs

```
1
     SWAT  Sept '05 VERSION2005                                                    0/ 0/   0       0: 0: 0

     General Input/Output section (file.cio): ArcSWAT 2.3.4
     12/04/2010 12:00:00 AMARCGIS-SWAT interface AV

          Number of years in run:   10
          Area of watershed:      416.430 km2
          Random number generator cycles: 0, use default numbers

          Initial random number seed: wet/dry day prob        748932582
          Initial random number seed: radiation              1948832765
          Initial random number seed: precipitation           857034417
          Initial random number seed: 0.5 hr rainfall          67377721
          Initial random number seed: wind speed              366304404
          Initial random number seed: irrigation             1094585182
          Initial random number seed: relative humidity      1767585417
          Initial random number seed: max temperature         608439319
          Initial random number seed: min temperature         592757081

          Precipitation data used in run:
           Multiple gages read for watershed
              Daily rainfall data used

          Temperature data used in run:
```

Multiple gages read for watershed

PET method used: Penman-Monteith

Rainfall/Runoff/Routing Option:

Daily rainfall data

Runoff estimated with curve number method

Daily stream routing

Variable Storage routing method

Channel dimensions remain constant

Subbasin algae/CBOD loadings modeled

In-stream nutrient transformations modeled using QUAL2E equations

Subbasin Input Summary:

Sub	Latitude	Elev(m)	#HRUs	Ponds	Elevbnds	Wetlnd
1	44.93	99.00	1			
2	44.91	109.00	1			
3	44.86	106.00	1			
4	44.87	109.00	1			
5	44.86	108.00	1			
6	44.83	109.00	1			
7	44.77	116.00	1			

HRU Input Summary Table 1:

Sub	HRU	Area(ha)	Slope	SlpLgth(m)	Ovrlnd_N	CondII_CN	TimeConc(hr)	ESCO	EPCO
1	1	11907.00	0.004	121.95	0.100	77.00	4.931	0.95	1.00
2	2	5607.00	0.004	121.95	0.100	83.00	3.765	0.95	1.00

3	3	3969.00	0.004	121.95	0.100	66.00	3.073	0.95	1.00
4	4	3654.00	0.005	121.95	0.100	83.00	2.379	0.95	1.00
5	5	1134.00	0.004	121.95	0.100	66.00	2.321	0.95	1.00
6	6	5529.00	0.003	121.95	0.100	66.00	3.291	0.95	1.00
7	7	10143.00	0.004	121.95	0.100	66.00	5.439	0.95	1.00

HRU CN Input Summary Table:

Sub	HRU	Area(ha)	LULC	Soil	CN1	CN2	CN3	Wilting Point (mm H2O)	Field Capacity (mm H2O)	Saturation (mm H2O)
1	1	11907.00	FODB	Be18-2a-	59.3	77.0	89.9	88.1	180.0	561.0
2	2	5607.00	FODB	Be1-2a-4	67.0	83.0	93.1	129.6	180.0	368.5
3	3	3969.00	FODB	Po10-1b-	46.8	66.0	83.0	57.8	90.0	470.5
4	4	3654.00	FODB	Be1-2a-4	67.0	83.0	93.1	129.6	180.0	368.5
5	5	1134.00	FODB	Po10-1b-	46.8	66.0	83.0	57.8	90.0	470.5
6	6	5529.00	FODB	Po10-1b-	46.8	66.0	83.0	57.8	90.0	470.5
7	7	10143.00	FODB	Po10-1b-	46.8	66.0	83.0	57.8	90.0	470.5

HRU Input Summary Table 2:

Sub	HRU	Area(ha)	SoilName	Hydgrp	MaxRtDpth(mm)	Albedo	USLE_K	USLE_P	USLE_LS	ProfileAWC(mm)	IniSoilH2O(mm)
1	1	11907.00	Be18-2a-4658	C	1000.00	0.10	0.10	1.00	0.10	180.000	0.683
2	2	5607.00	Be1-2a-4648	D	1000.00	0.10	0.29	1.00	0.10	180.000	0.000
3	3	3969.00	Po10-1b-4951	B	720.00	0.15	0.25	1.00	0.10	90.000	0.000
4	4	3654.00	Be1-2a-4648	D	1000.00	0.10	0.29	1.00	0.11	180.000	0.000

5	5	1134.00	Po10-1b-4951	B	720.00	0.15	0.25	1.00	0.10	90.000	0.000
6	6	5529.00	Po10-1b-4951	B	720.00	0.15	0.25	1.00	0.09	90.000	0.000
7	7	10143.00	Po10-1b-4951	B	720.00	0.15	0.25	1.00	0.10	90.000	0.000

HRU Input Summary Table 3:

Sub	HRU	Area(ha)	Urban	Irrig	DrainTiles	Pothole	Pstcide	Biomix
1	1	11907.00						0.20
2	2	5607.00						0.20
3	3	3969.00						0.20
4	4	3654.00						0.20
5	5	1134.00						0.20
6	6	5529.00						0.20
7	7	10143.00						0.20

HRU Input Summary Table 4 (Groundwater):

Sub	HRU	Area(ha)	GWdelay(days),	GWalpha(days)	GWQmin(mm)	GWrevap	Revapmin(mm)	Deepfr	NO3(ppm)	SolP(ppm)
1	1	11907.00	31.000	0.048	0.000	0.020	1.000	0.050	0.000	0.000
2	2	5607.00	31.000	0.048	0.000	0.020	1.000	0.050	0.000	0.000
3	3	3969.00	31.000	0.048	0.000	0.020	1.000	0.050	0.000	0.000
4	4	3654.00	31.000	0.048	0.000	0.020	1.000	0.050	0.000	0.000
5	5	1134.00	31.000	0.048	0.000	0.020	1.000	0.050	0.000	0.000
6	6	5529.00	31.000	0.048	0.000	0.020	1.000	0.050	0.000	0.000
7	7	10143.00	31.000	0.048	0.000	0.020	1.000	0.050	0.000	0.000

Tributary/Main Channel Characteristics

	Tributary					Main				
Sub	Length(km)	Slope	Width(m)	Cond(mm/hr)	N	Length(km)	Slope	Width(m)	Depth(m)	Cond(mm/hr)	N

1	19.58	0.001	16.23	0.5000	0.014	18.98	0.001	34.40	1.16	0.0000	0.014
2	12.09	0.001	10.33	0.5000	0.014	9.61	0.001	10.33	0.52	0.0000	0.014
3	8.32	0.001	8.39	0.5000	0.014	3.80	0.001	8.39	0.45	0.0000	0.014
4	6.99	0.002	7.99	0.5000	0.014	2.95	0.000	7.99	0.44	0.0000	0.014
5	5.30	0.002	3.96	0.5000	0.014	4.95	0.001	22.26	0.87	0.0000	0.014
6	11.24	0.002	9.90	0.5000	0.014	7.32	0.000	9.90	0.51	0.0000	0.014
7	21.87	0.001	14.74	0.5000	0.014	16.75	0.001	14.74	0.66	0.0000	0.014

C- HEC-RAS Cross Sections

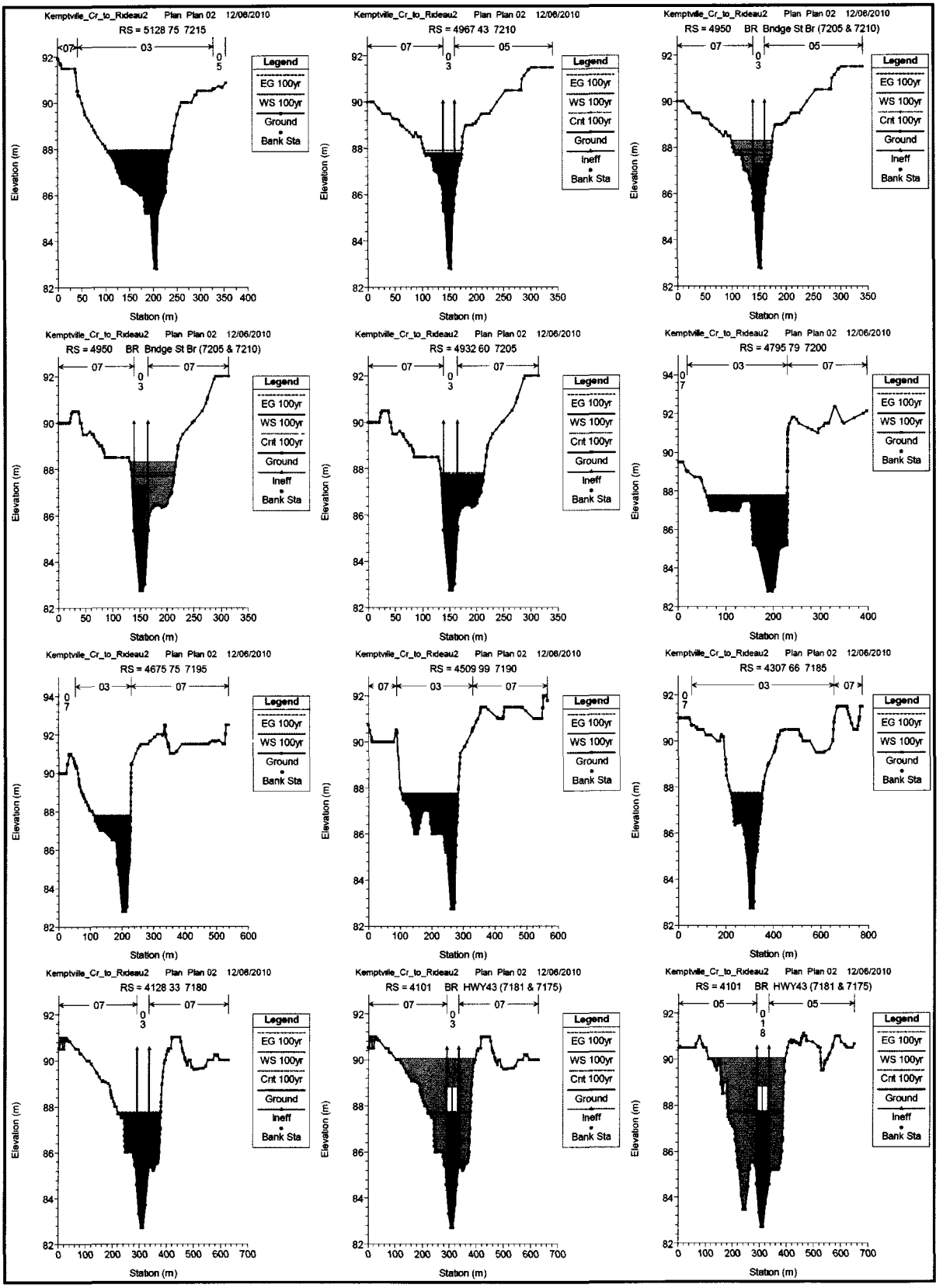
Kemptville_Cr_to_Rideau2 Plan: Plan 02 12/06/2010
RS = 5128.75 7215
RS = 4967.43 7210
RS = 4950 BR: Bridge St Br (7205 & 7210)
RS = 4950 BR: Bridge St Br (7205 & 7210)
RS = 4932.60 7205
RS = 4795.79 7200
RS = 4675.75 7195
RS = 4509.99 7190
RS = 4307.66 7185
RS = 4128.33 7180
RS = 4101 BR: HWY43 (7181 & 7175)
RS = 4101 BR: HWY43 (7181 & 7175)
Legend
EG 100yr
WS 100yr
Crit 100yr
Ground
Ineff
Bank Sta
Elevation (m)
Station (m)

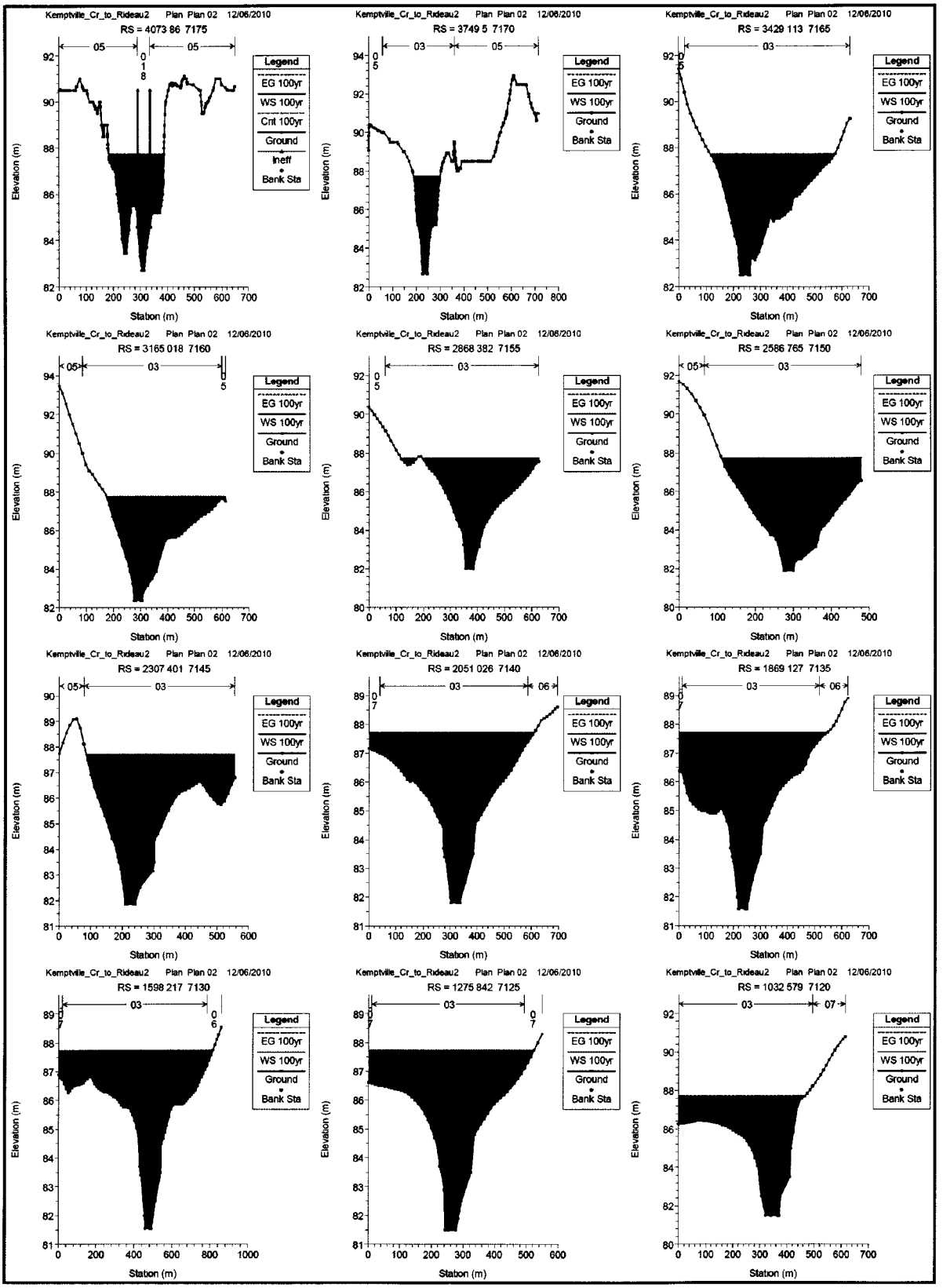
Kemptville_Cr_to_Rideau2 Plan Plan 02 12/06/2010
RS = 4073.86 7175
RS = 3749.5 7170
RS = 3429.113 7165
RS = 3165.018 7160
RS = 2868.382 7155
RS = 2586.765 7150
RS = 2307.401 7145
RS = 2051.026 7140
RS = 1869.127 7135
RS = 1598.217 7130
RS = 1275.842 7125
RS = 1032.579 7120
Legend
EG 100yr
WS 100yr
Crit 100yr
Ground
Ineff
Bank Sta
Elevation (m)
Station (m)

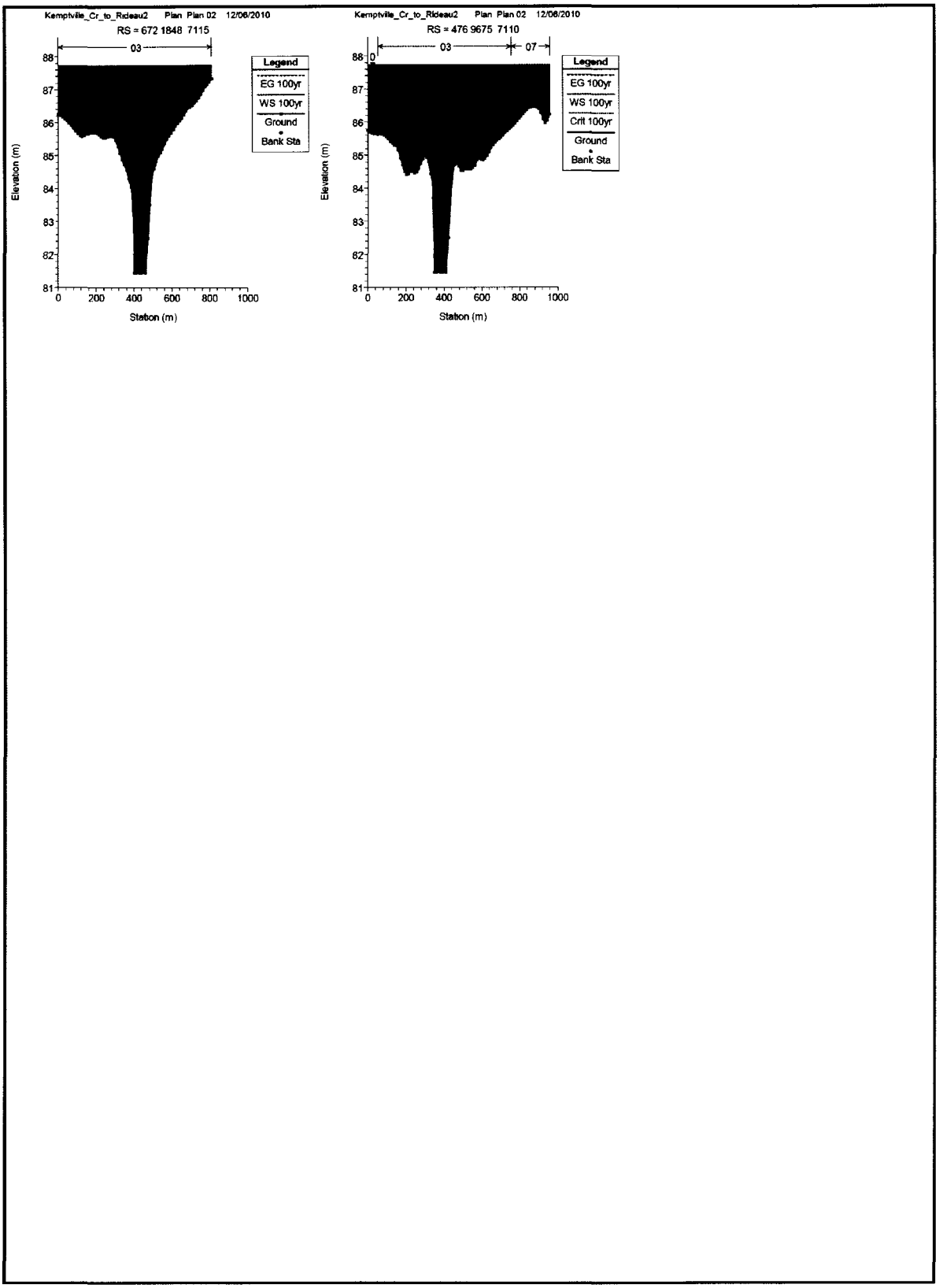
Kemptville_Cr_to_Rideau2 Plan: Plan 02 12/06/2010
RS = 672 1848 7115
03
Legend
EG 100yr
WS 100yr
Ground
Bank Sta
Elevation (m)
Station (m)
Kemptville_Cr_to_Rideau2 Plan: Plan 02 12/06/2010
RS = 476 9675 7110
03
07
Legend
EG 100yr
WS 100yr
Crit 100yr
Ground
Bank Sta
Elevation (m)
Station (m)

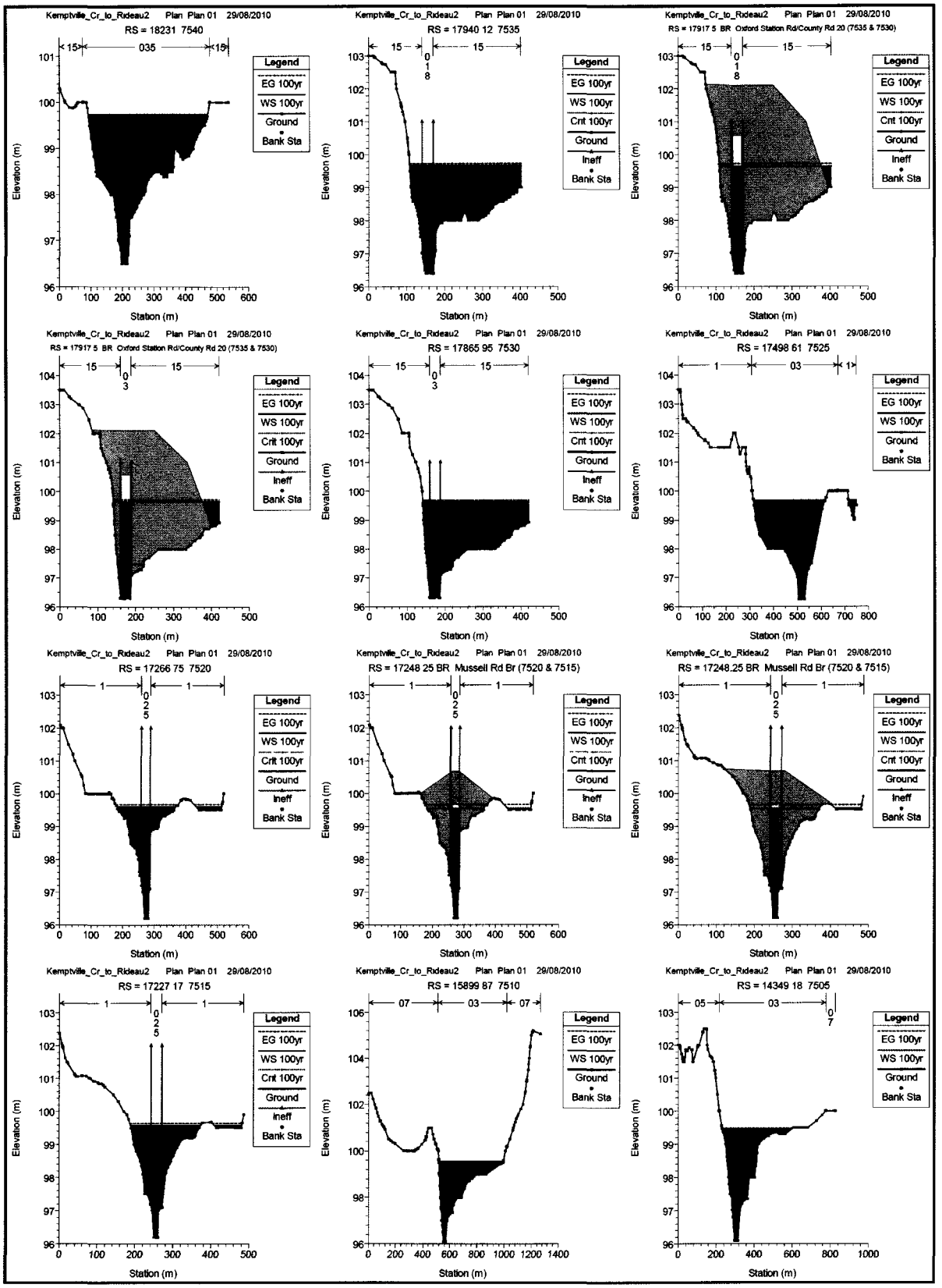
Kemptville_Cr_to_Rideau2 Plan Plan 01 29/08/2010
RS = 18231 7540
RS = 17940 12 7535
RS = 17917 5 BR Oxford Station Rd/County Rd 20 (7535 & 7530)
RS = 17865 95 7530
RS = 17498 61 7525
RS = 17266 75 7520
RS = 17248 25 BR Mussell Rd Br (7520 & 7515)
RS = 17227 17 7515
RS = 15899 87 7510
RS = 14349 18 7505
Legend
EG 100yr
WS 100yr
Crit 100yr
Ground
Ineff
Bank Sta
Elevation (m)
Station (m)

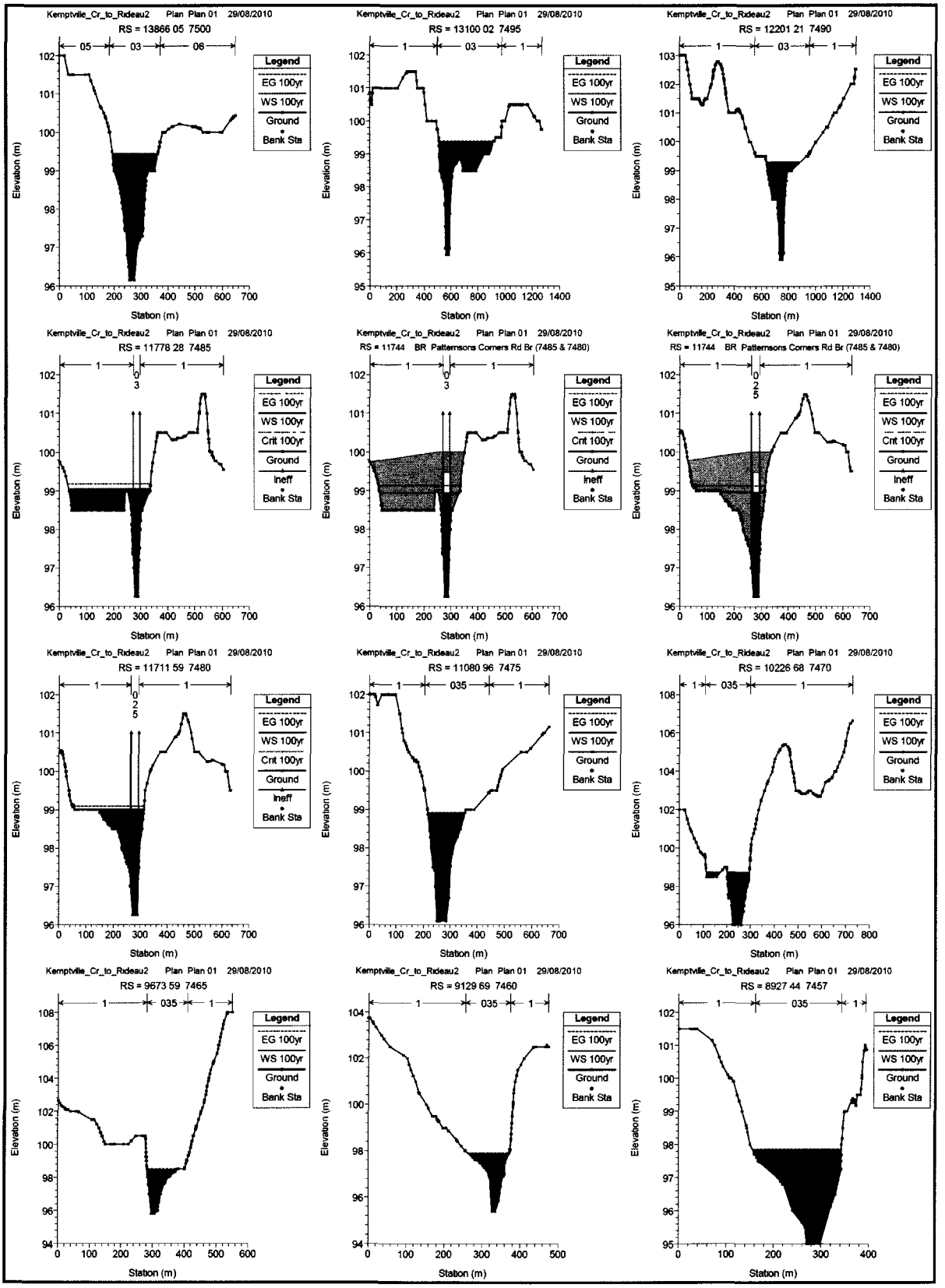
Kemptville_Cr_to_Rideau2 Plan: Plan 01 29/08/2010
RS = 13866.05 7500
RS = 13100.02 7495
RS = 12201.21 7490
RS = 11778.28 7485
RS = 11744 BR Pattemsons Corners Rd Br (7485 & 7480)
RS = 11711.59 7480
RS = 11080.96 7475
RS = 10226.68 7470
RS = 9673.59 7465
RS = 9129.69 7460
RS = 8927.44 7457
Legend
EG 100yr
WS 100yr
Crit 100yr
Ground
Ineff
Bank Sta
Elevation (m)
Station (m)

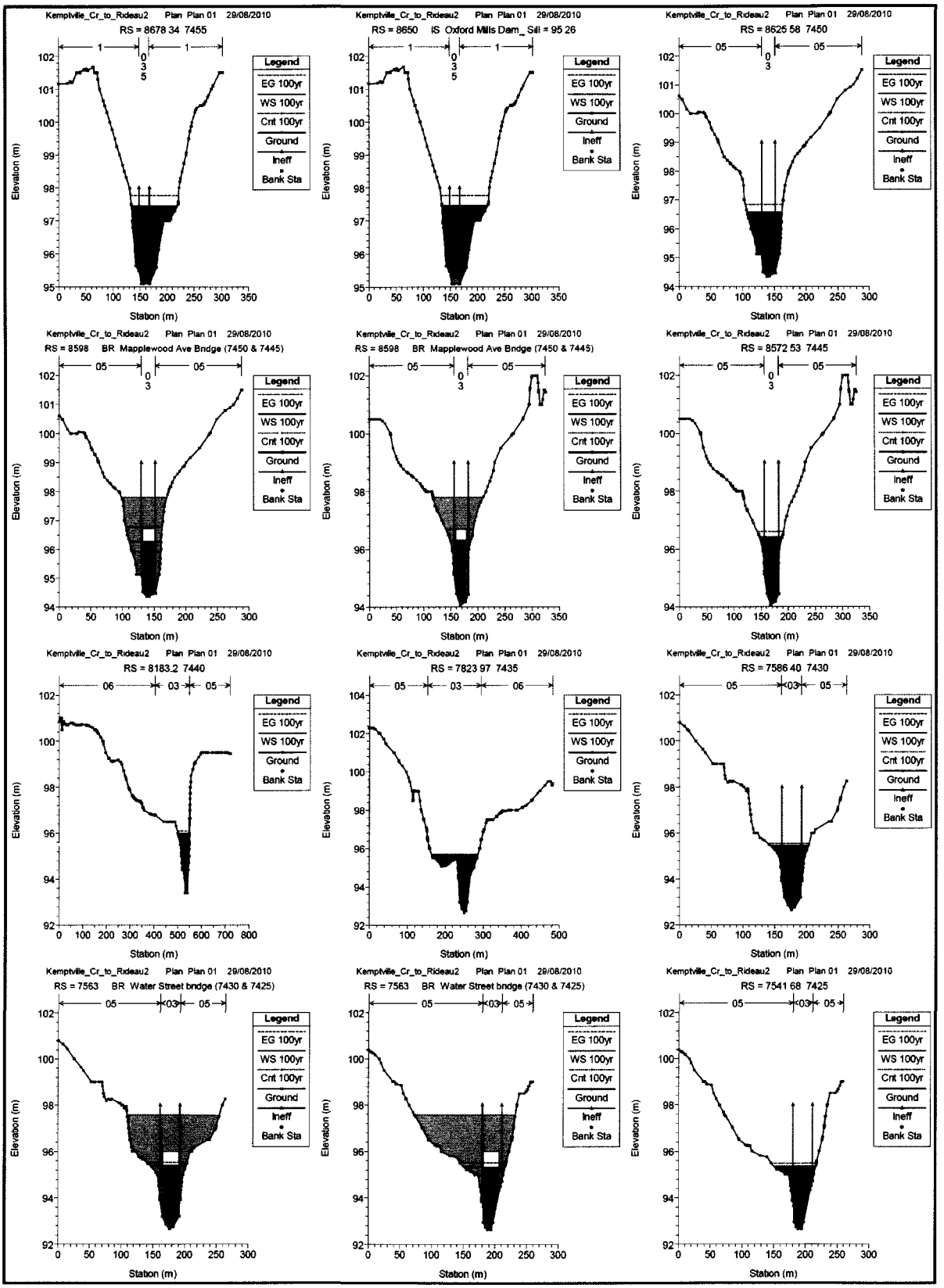
Kemptville_Cr_to_Rideau2 Plan Plan 01 29/08/2010
RS = 8678.34 7455
RS = 8650 iS Oxford Mills Dam_ Sill = 95.26
RS = 8625.58 7450
RS = 8598 BR Mapplewood Ave Bridge (7450 & 7445)
RS = 8572.53 7445
RS = 8183.2 7440
RS = 7823.97 7435
RS = 7586.40 7430
RS = 7563 BR Water Street bridge (7430 & 7425)
RS = 7541.68 7425
Legend
EG 100yr
WS 100yr
Crit 100yr
Ground
Ineff
Bank Sta
Elevation (m)
Station (m)

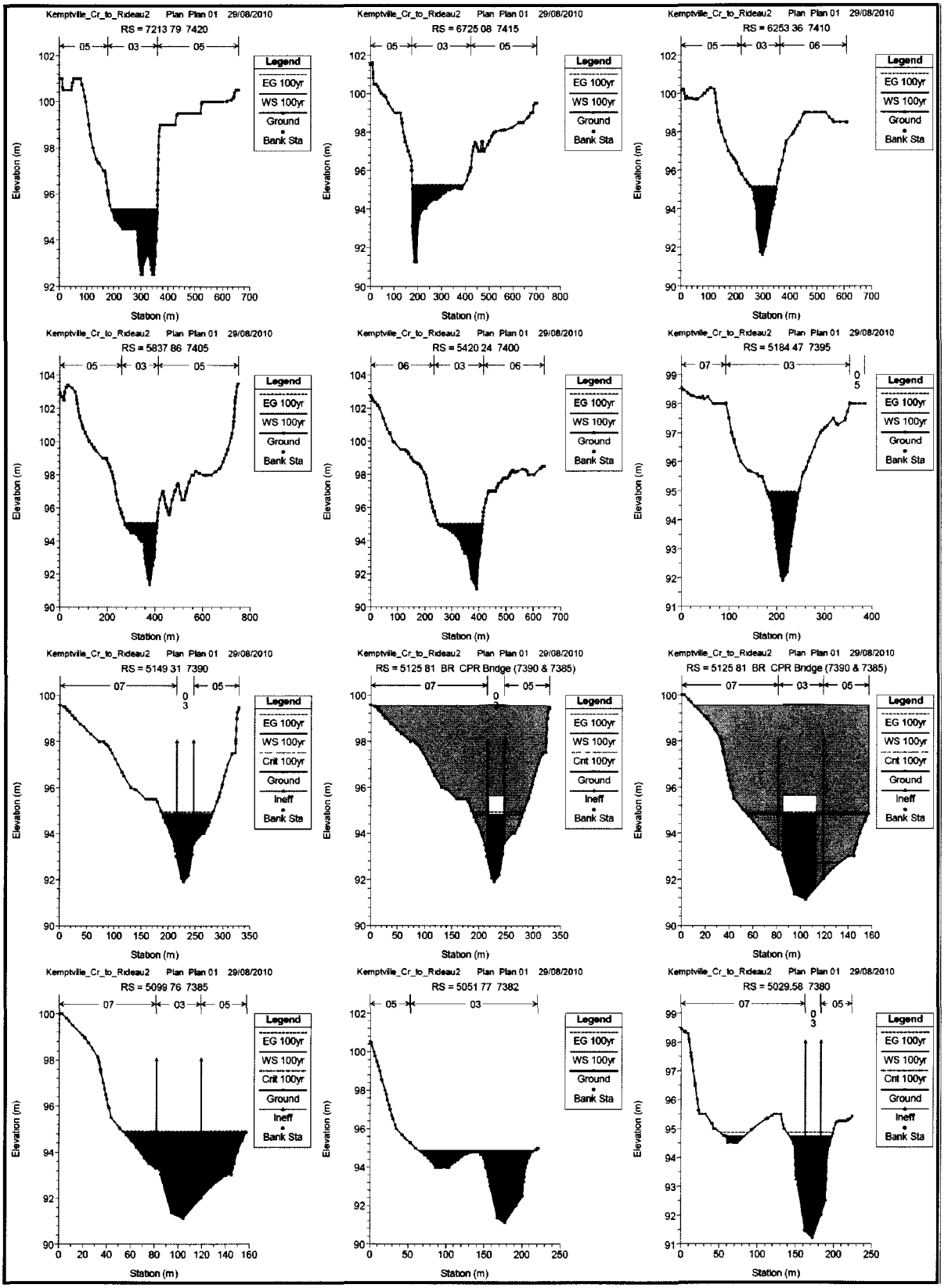
Kemptville_Cr_to_Rideau2 Plan: Plan 01 29/08/2010
RS = 7213.79 7420
RS = 6725.08 7415
RS = 6253.36 7410
RS = 5837.86 7405
RS = 5420.24 7400
RS = 5184.47 7395
RS = 5149.31 7390
RS = 5125.81 BR CPR Bridge (7390 & 7385)
RS = 5099.76 7385
RS = 5051.77 7382
RS = 5029.58 7380
Legend
EG 100yr
WS 100yr
Crit 100yr
Ground
Ineff
Bank Sta
Elevation (m)
Station (m)

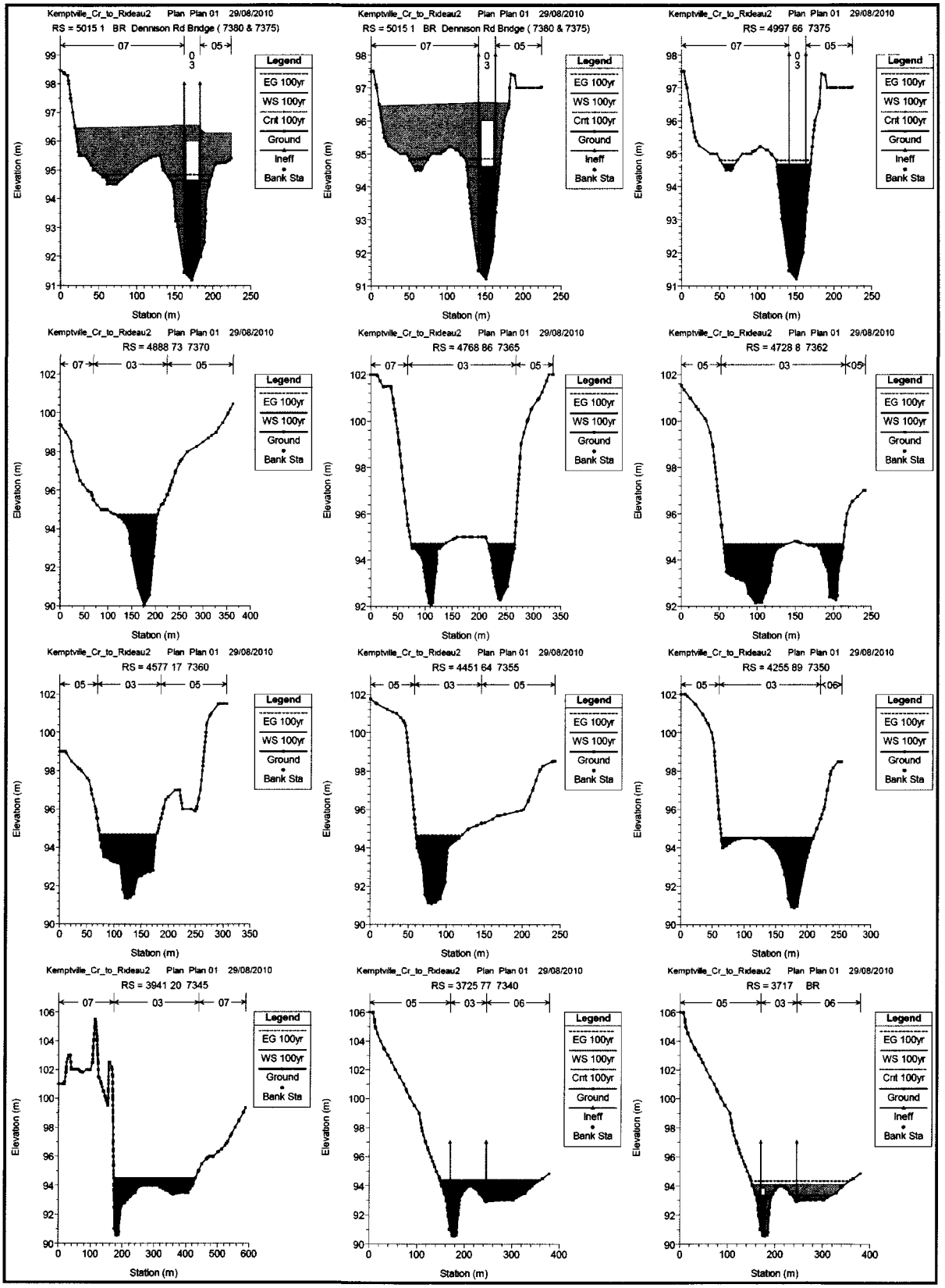
Kemptville_Cr_to_Rideau2 Plan Plan 01 29/08/2010
RS = 5015 1 BR Dennison Rd Bridge (7380 & 7375)
RS = 4997 66 7375
RS = 4888 73 7370
RS = 4768 86 7365
RS = 4728 8 7362
RS = 4577 17 7360
RS = 4451 64 7355
RS = 4255 89 7350
RS = 3941 20 7345
RS = 3725 77 7340
RS = 3717 BR
Legend
EG 100yr
WS 100yr
Crit 100yr
Ground
Ineff
Bank Sta
Elevation (m)
Station (m)

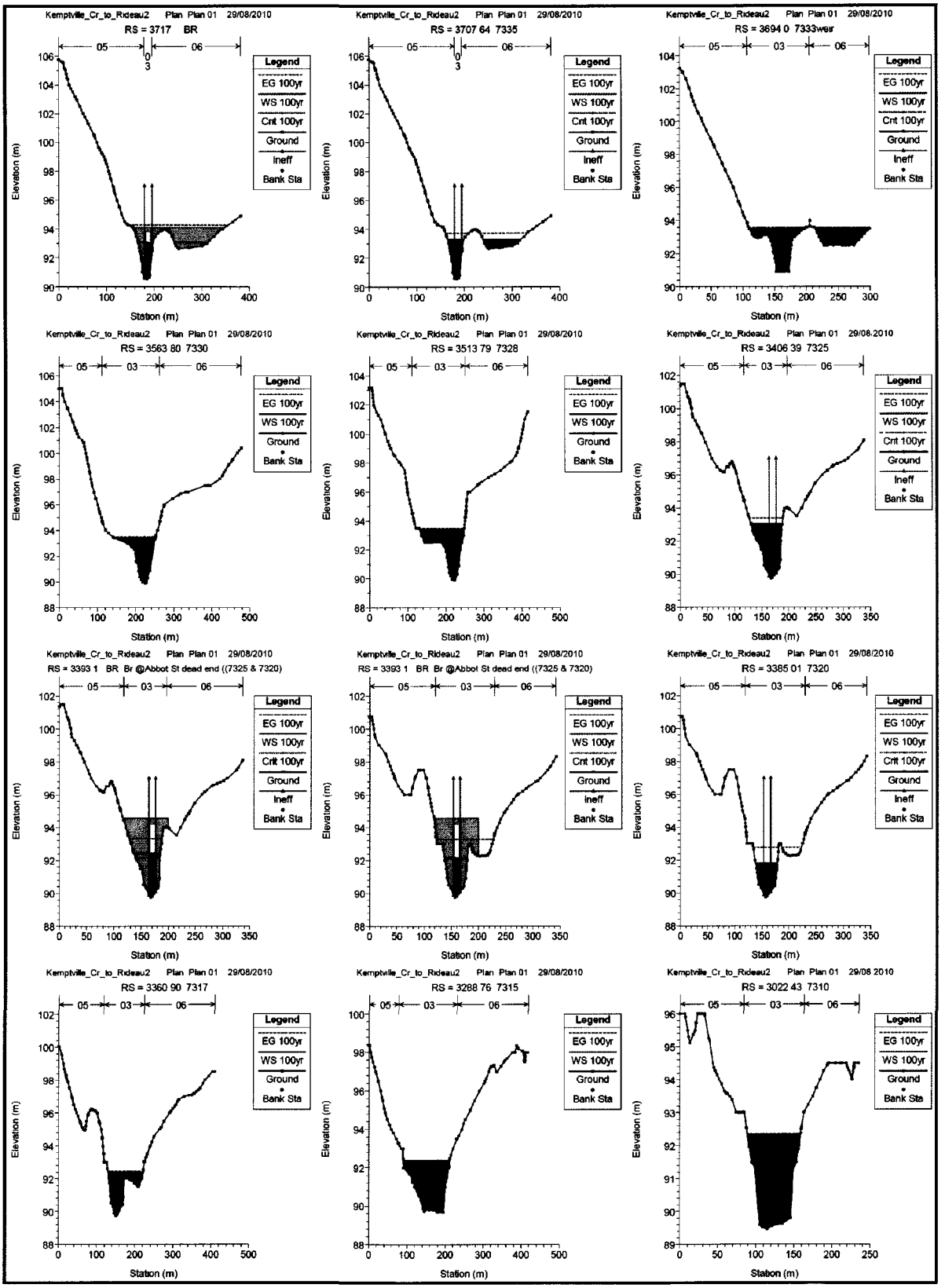
Kemptville_Cr_to_Rideau2 Plan: Plan 01 29/08/2010
RS = 3717 BR
RS = 3707.64 7335
RS = 3694.0 7333weir
RS = 3563.80 7330
RS = 3513.79 7328
RS = 3406.39 7325
RS = 3393.1 BR Br @Abbot St dead end ((7325 & 7320)
RS = 3385.01 7320
RS = 3360.90 7317
RS = 3288.76 7315
RS = 3022.43 7310
Legend
EG 100yr
WS 100yr
Crit 100yr
Ground
Ineff
Bank Sta
Elevation (m)
Station (m)

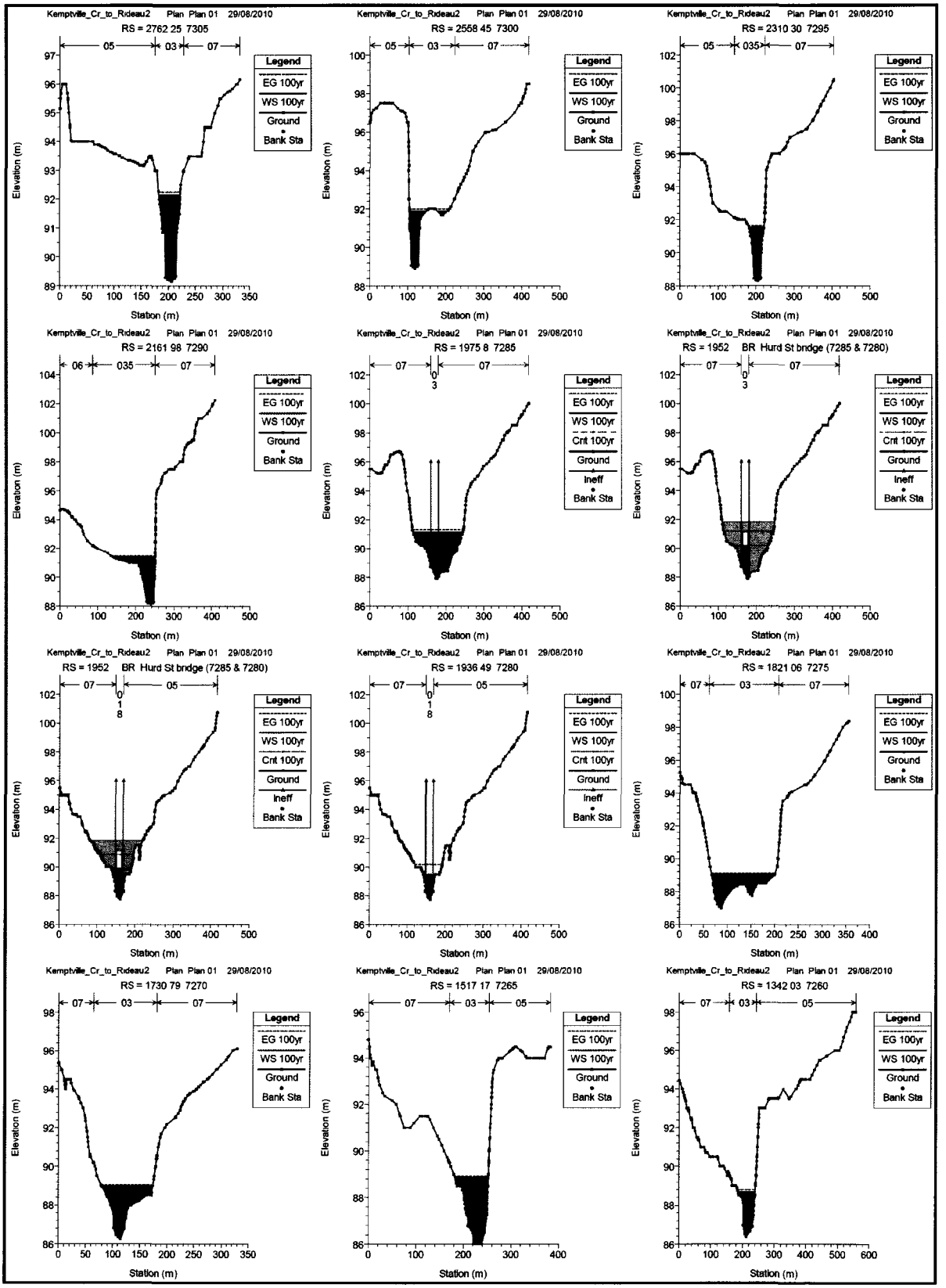
Kemptville_Cr_to_Rideau2 Plan Plan 01 29/08/2010
RS = 2762.25 7305
05 03 07
Legend
EG 100yr
WS 100yr
Ground
Bank Sta
Elevation (m)
Station (m)
Kemptville_Cr_to_Rideau2 Plan Plan 01 29/08/2010
RS = 2558.45 7300
05 03 07
Legend
EG 100yr
WS 100yr
Ground
Bank Sta
Elevation (m)
Station (m)
Kemptville_Cr_to_Rideau2 Plan Plan 01 29/08/2010
RS = 2310.30 7295
05 035 07
Legend
EG 100yr
WS 100yr
Ground
Bank Sta
Elevation (m)
Station (m)
Kemptville_Cr_to_Rideau2 Plan Plan 01 29/08/2010
RS = 2161.98 7290
06 035 07
Legend
EG 100yr
WS 100yr
Ground
Bank Sta
Elevation (m)
Station (m)
Kemptville_Cr_to_Rideau2 Plan Plan 01 29/08/2010
RS = 1975.8 7285
07 07
Legend
EG 100yr
WS 100yr
Crit 100yr
Ground
Ineff
Bank Sta
Elevation (m)
Station (m)
Kemptville_Cr_to_Rideau2 Plan Plan 01 29/08/2010
RS = 1952 BR Hurd St bridge (7285 & 7280)
07 07
Legend
EG 100yr
WS 100yr
Crit 100yr
Ground
Ineff
Bank Sta
Elevation (m)
Station (m)
Kemptville_Cr_to_Rideau2 Plan Plan 01 29/08/2010
RS = 1952 BR Hurd St bridge (7285 & 7280)
07 05
Legend
EG 100yr
WS 100yr
Crit 100yr
Ground
Ineff
Bank Sta
Elevation (m)
Station (m)
Kemptville_Cr_to_Rideau2 Plan Plan 01 29/08/2010
RS = 1936.49 7280
07 05
Legend
EG 100yr
WS 100yr
Crit 100yr
Ground
Ineff
Bank Sta
Elevation (m)
Station (m)
Kemptville_Cr_to_Rideau2 Plan Plan 01 29/08/2010
RS = 1821.06 7275
07 03 07
Legend
EG 100yr
WS 100yr
Ground
Bank Sta
Elevation (m)
Station (m)
Kemptville_Cr_to_Rideau2 Plan Plan 01 29/08/2010
RS = 1730.79 7270
07 03 07
Legend
EG 100yr
WS 100yr
Ground
Bank Sta
Elevation (m)
Station (m)
Kemptville_Cr_to_Rideau2 Plan Plan 01 29/08/2010
RS = 1517.17 7265
07 03 05
Legend
EG 100yr
WS 100yr
Ground
Bank Sta
Elevation (m)
Station (m)
Kemptville_Cr_to_Rideau2 Plan Plan 01 29/08/2010
RS = 1342.03 7260
07 03 05
Legend
EG 100yr
WS 100yr
Ground
Bank Sta
Elevation (m)
Station (m)

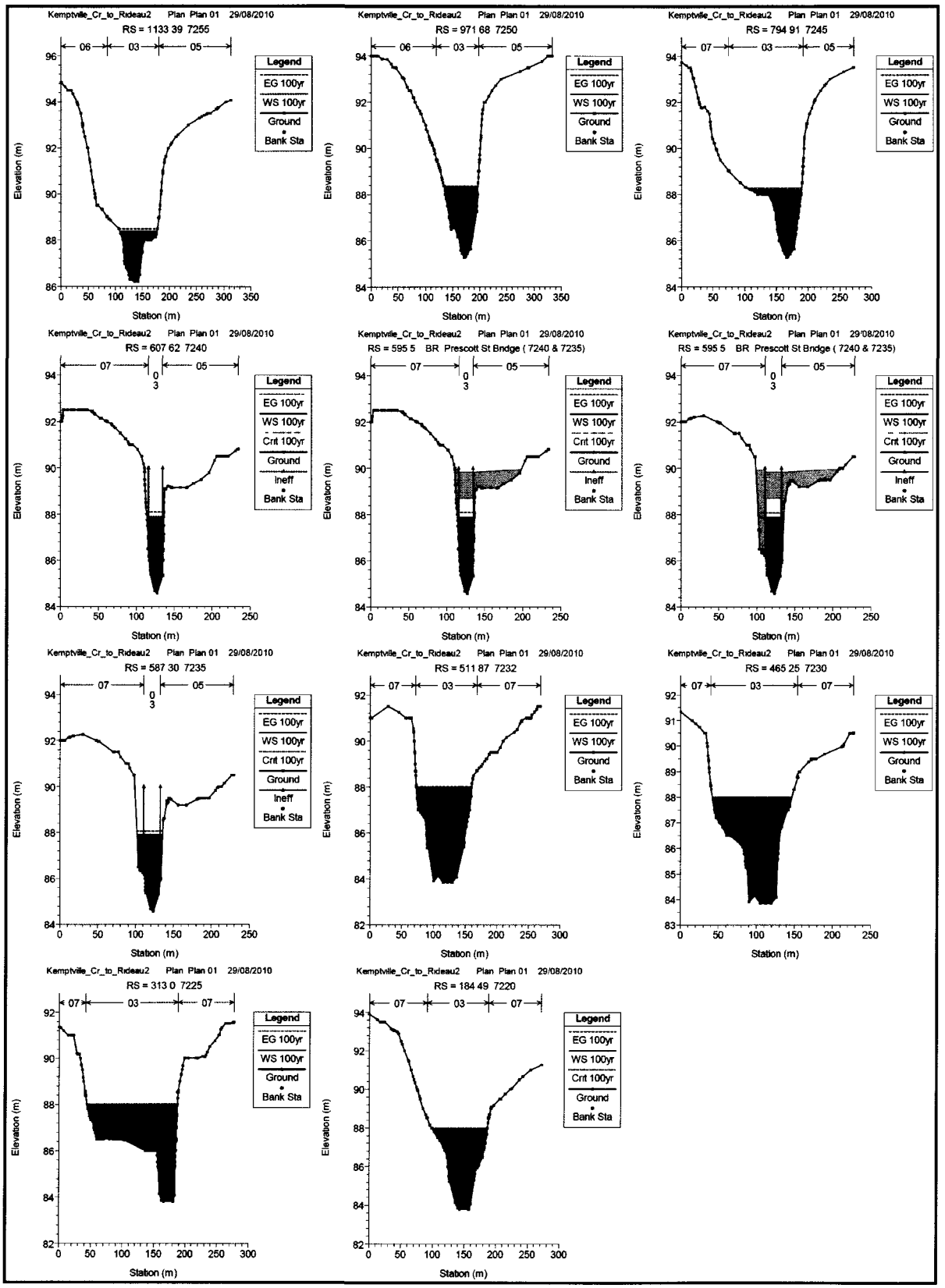
Kemptville_Cr_to_Rideau2 Plan Plan 01 29/08/2010
RS = 1133 39 7255
RS = 971 68 7250
RS = 794 91 7245
RS = 607 62 7240
RS = 595 5 BR Prescott St Bridge (7240 & 7235)
RS = 587 30 7235
RS = 511 87 7232
RS = 465 25 7230
RS = 313 0 7225
RS = 184 49 7220
Legend
EG 100yr
WS 100yr
Crit 100yr
Ground
Ineff
Bank Sta
Elevation (m)
Station (m)

D- Generalized Pareto Distributions

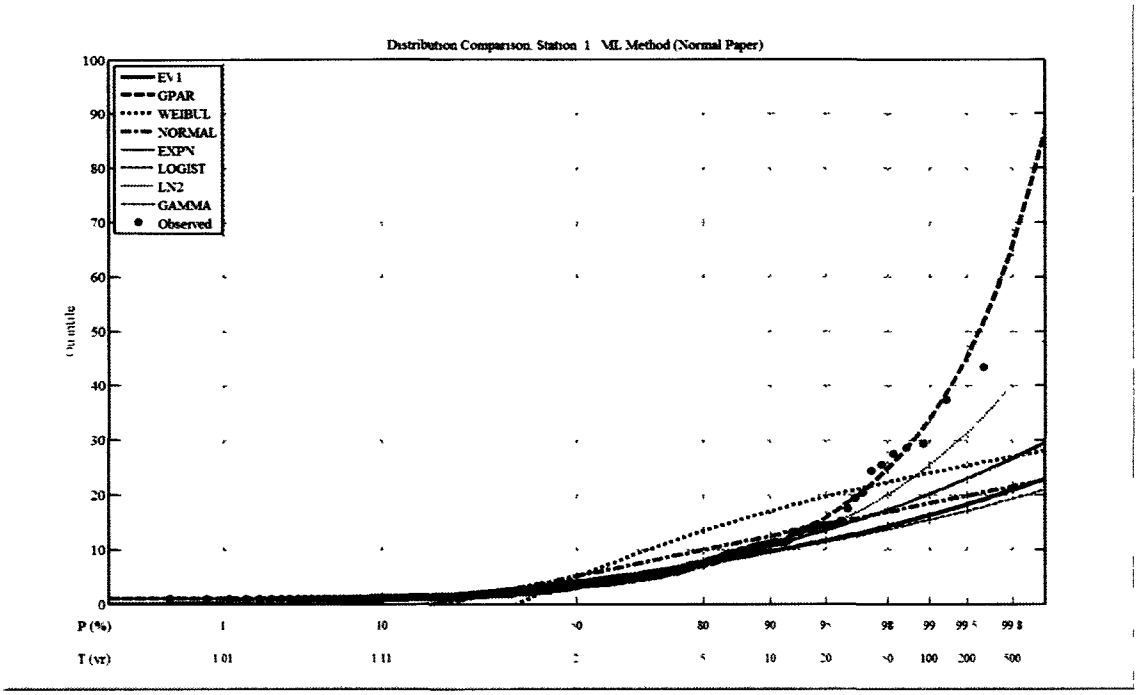

Figure 46: Distribution for Month of January

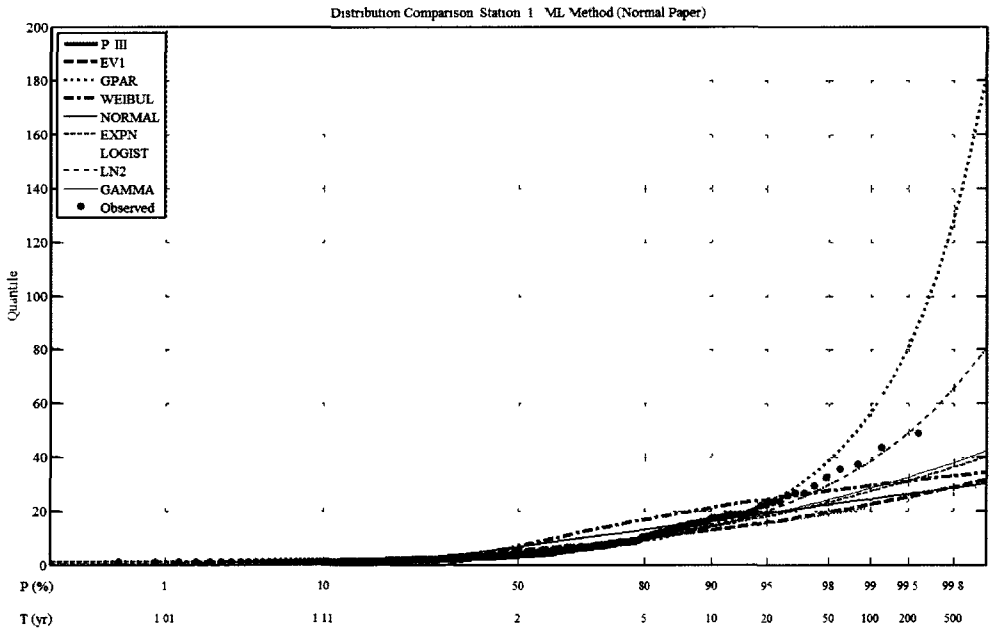

Figure 47: Distribution for Month of February

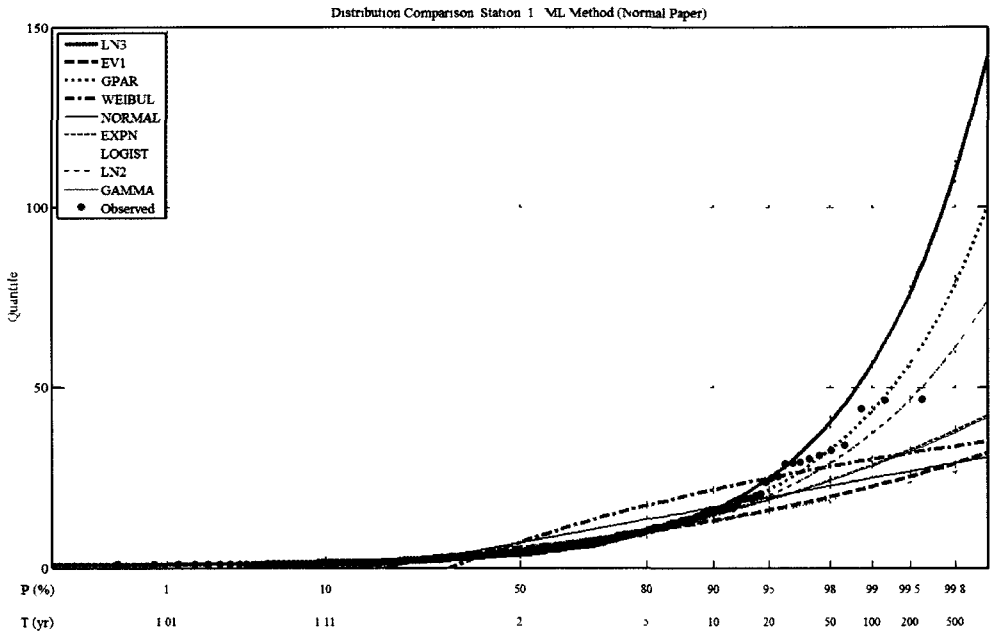

Figure 48: Distribution for Month of March

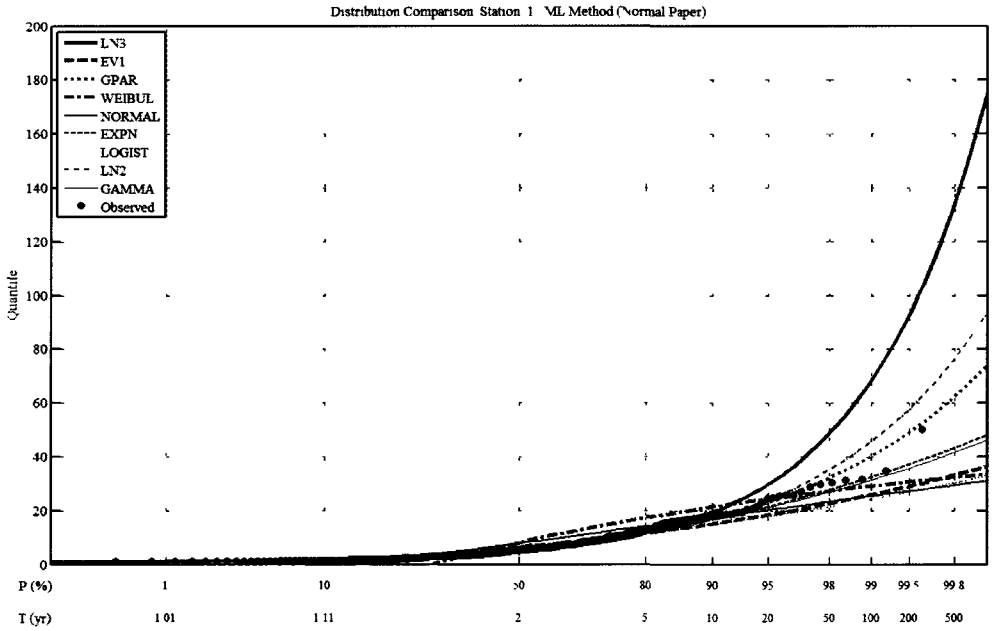

Figure 49: Distribution for Month of April

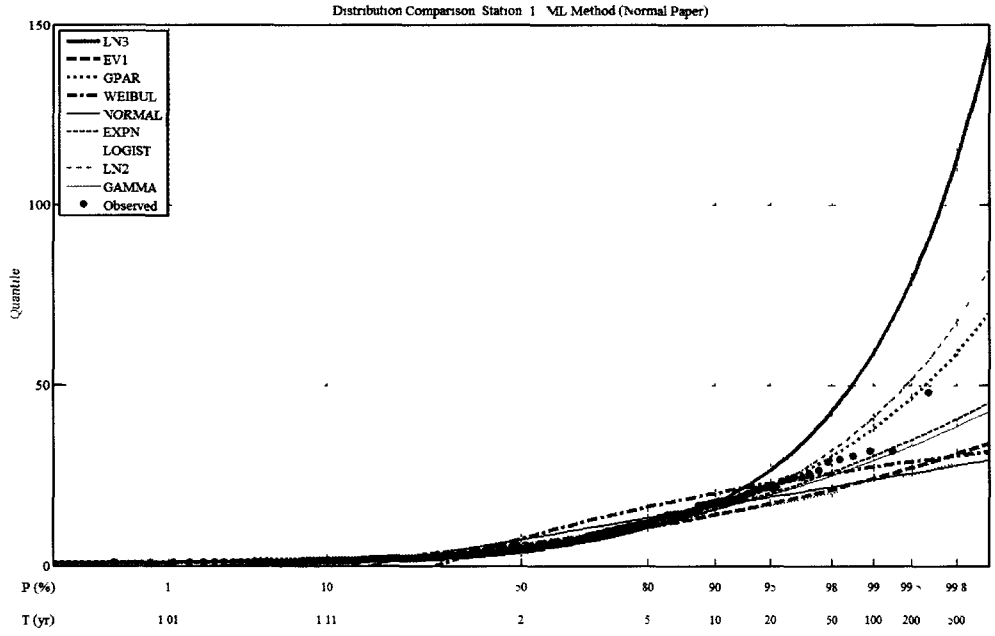

Figure 50: Distribution for Month of May

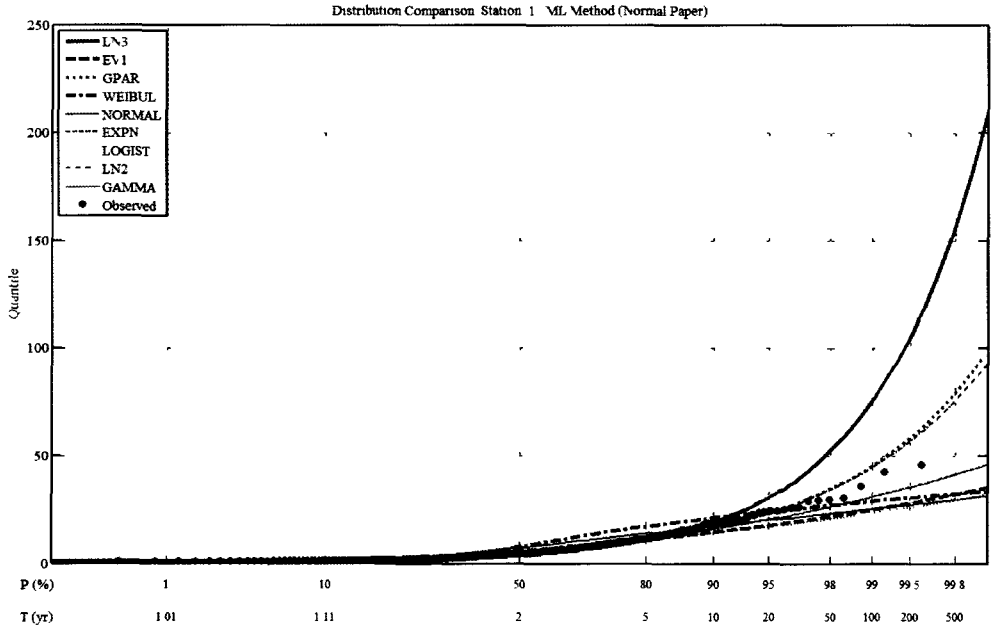

Figure 51: Distribution for Month of June

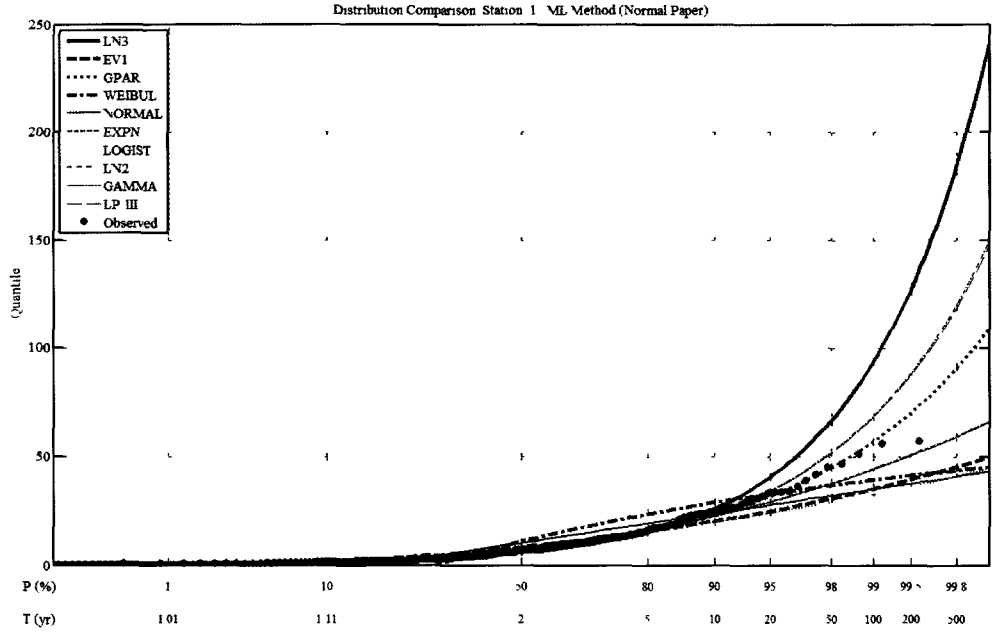

Figure 52: Distribution for Month of July

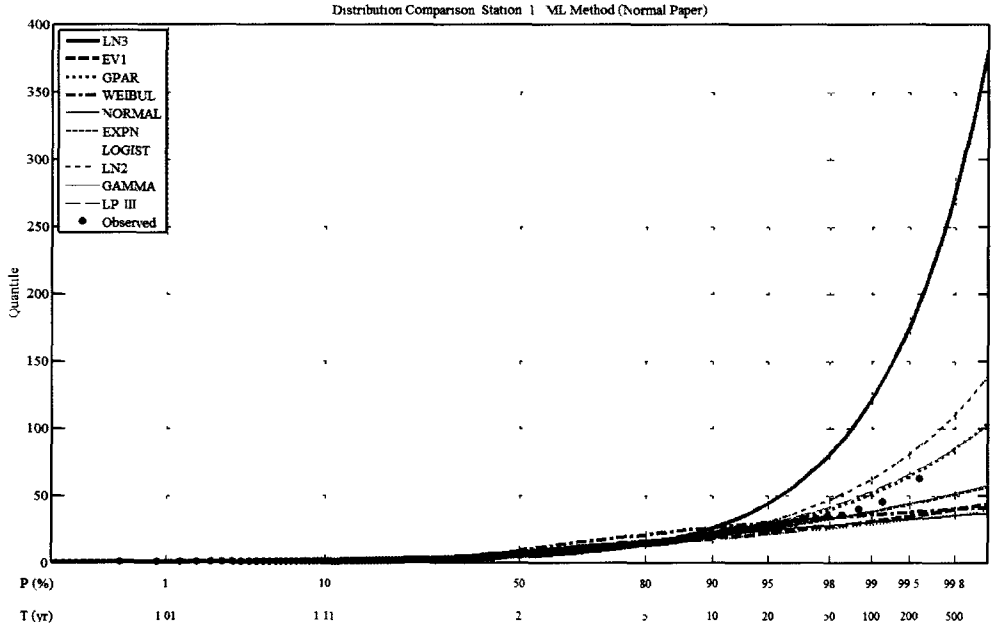

Figure 53: Distribution for Month of August

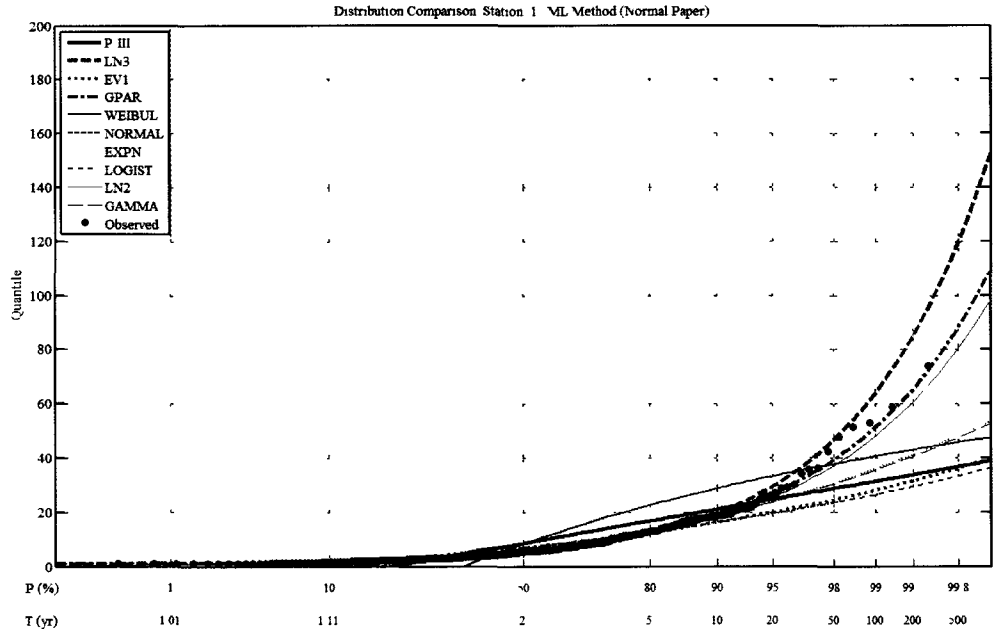

Figure 54: Distribution for Month of September

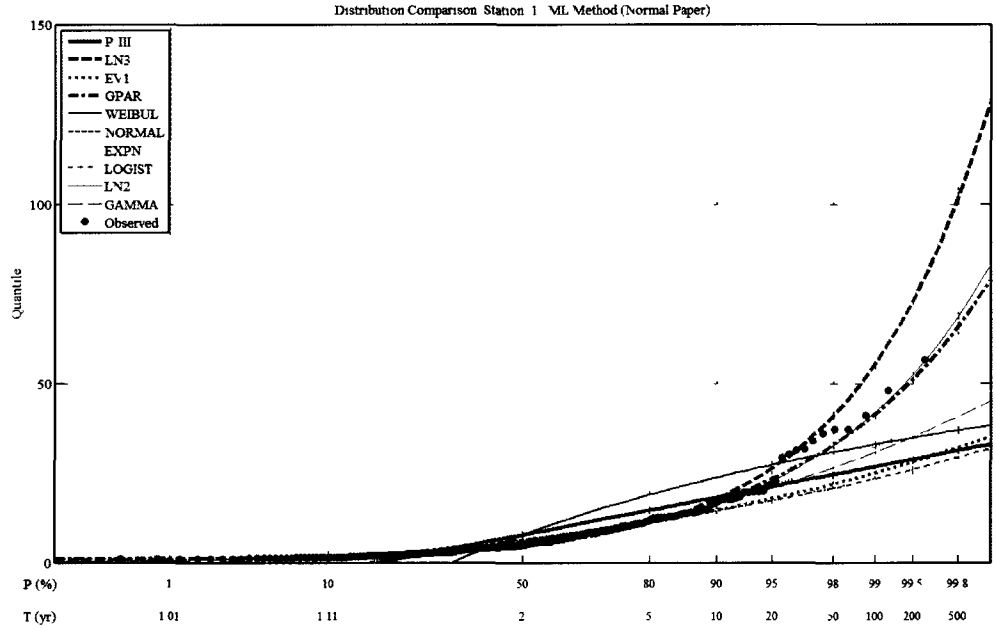

Figure 55: Distribution for Month of October

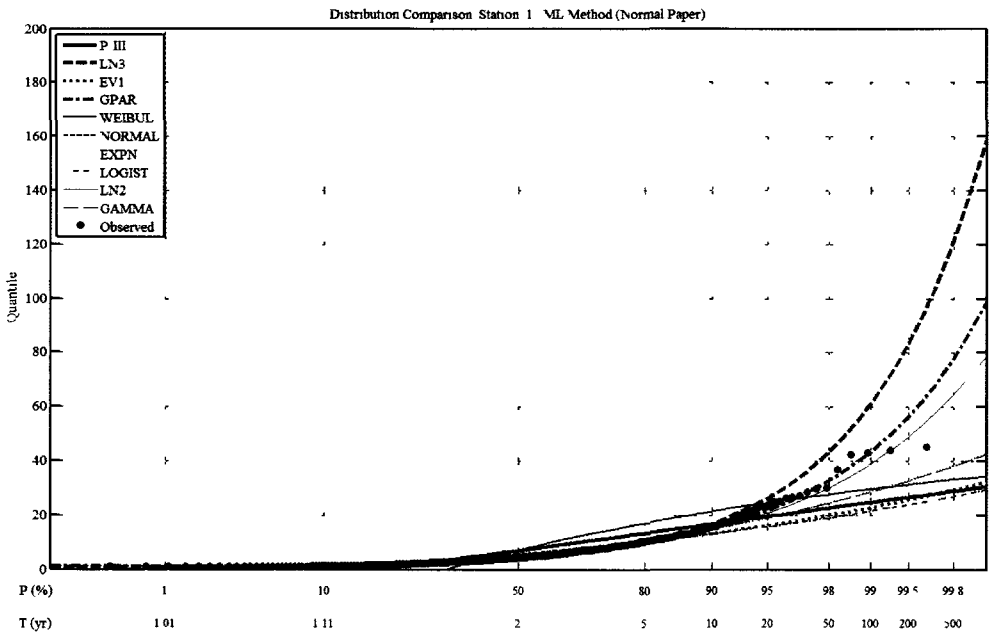

Figure 56: Distribution for Month of November

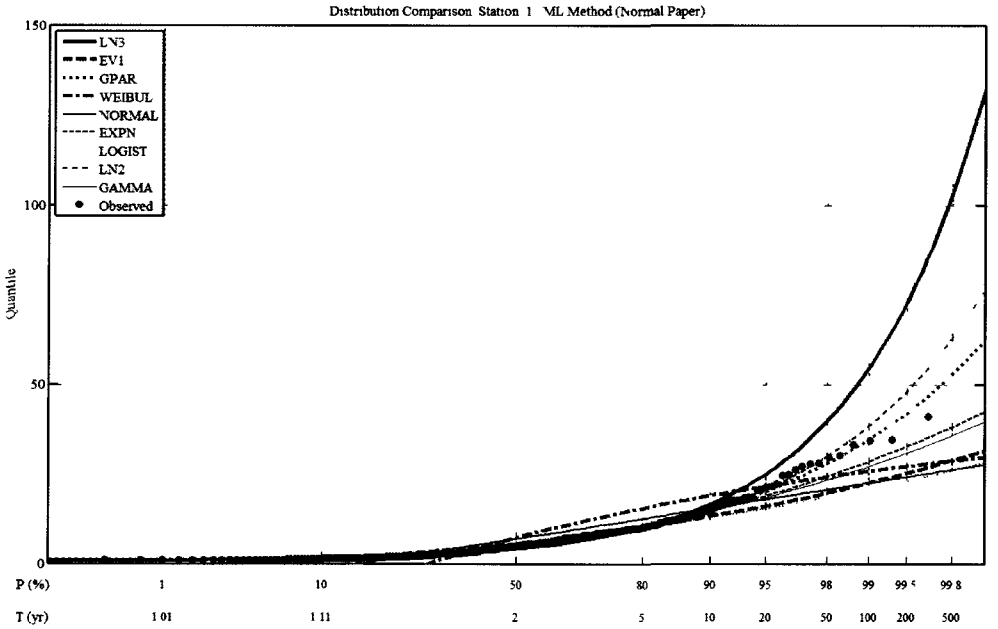

Figure 57: Distribution for Month of December